International Committee for Future Accelerators

Sponsored by the Particles and Fields Commission of IUPAP

Beam Dynamics Newsletter

No. 39

Issue Editor:
K. J. Kim

Editor in Chief:
W. Chou

April 2006

Contents

4

8

1   Foreword

1.1   From the ICFA Chairman: Going Global – A View from ICFA

Albrecht Wagner, DESY
mail to: Albrecht.wagner@desy.de

ICFA, the International Committee for Future Accelerators, was created in 1976 by the International Union of Pure and Applied Physics to facilitate international collaboration in the construction and use of accelerators for high-energy physics. Its goals, as stated in 1985, are as follows:

- To promote international collaboration in all phases of the construction and exploitation of very high-energy accelerators.

- To organize regular world-inclusive meetings for the exchange of information on future plans for regional facilities and for the formulation of advice on joint studies and uses.

- To organize workshops for the study of problems related to super high-energy accelerator complexes and their international exploitation and to foster research and development of necessary technology.

ICFA is an organization in which discussions take place on the international aspects of particle physics, in particular the large accelerators that are at the heart of this field. It has no means of ensuring that any of its resolutions are carried out, but because of its broad international representation, it can act as the "conscience" of the field and its recommendations can also influence national or regional activities.

Over the past years ICFA has undertaken three major activities, which correspond to the three goals of ICFA: *ICFA Meetings* (presently about twice a year); *ICFA Seminars* (every three years), which focus on Future Perspectives in High-Energy Physics; and *ICFA Panels* on specific technical topics (such as the panel on Beam Dynamics chaired presently by Weiren Chou of Fermilab, which has the mission to encourage and promote international collaboration on beam dynamics studies for present and future accelerators; this panel publishes the Newsletter you are reading).

During the past three years Jonathan Dorfan of SLAC has been leading ICFA. Under his chairmanship and ICFA's guidance, major steps were taken to prepare the future of the field. While the Large Hadron Collider is taking shape at CERN, scientists are looking even further ahead. A worldwide consensus emerged that the next major project of the field would be an electron-positron linear collider. The LHC started as a European project and became more and more international, with major contributions from North America and Asia. It was clear from the beginning that due to its size, cost, and complexity, the linear collider—now called the International Linear Collider or ILC—would have to be realised as a truly global project. This led to unprecedented

steps under the guidance of ICFA: a choice of technology in 2004; the formation of an ILC Steering Committee; the appointment of a Director of the Global Design Effort, Barry Barish of Caltech; and the start of the Global Design Effort itself. This is the first step towards a Reference Design and its cost, to be completed by the end of 2006. The Reference Design will then be the starting point for a Technical Design as well as for intensified political discussions among funding agencies in Asia, the Americas, and Europe.

As the new chair of ICFA, I view this impressive track record of the past three years as guidance for the years to come, during which the field of particle physics faces both outstanding scientific opportunities and challenges. The LHC will provide new insights into nature and its fundamental properties and principles. It will show us the way the field might develop over the coming decades. At the same time, during the next few years, experimental particle physics will undergo an alarming concentration: most colliders presently providing data will stop. This will happen in Asia, Europe, and the United States. It is not for lack of ideas that this is occurring. It reflects the fact that most of the answers to the burning questions of today lie at the energy frontier, and new, expensive facilities are required to explore that frontier.

ICFA asks itself the question how to keep our field vital in times of such concentration and in view of the immense cost of new projects. One obvious way is a further strengthening of global collaboration. Can ICFA help guide this process and try to minimize unnecessary duplication of facilities? So far, ICFA has only begun to discuss these matters; it has had an initial discussion about the pros and cons of a global road map for the field. ICFA has decided to wait for the outcome of regional road map studies presently underway in Europe and the United States and then will review the matter.

Another aspect of 'Going Global' discussed at the recent ICFA meeting concerned the three regional accelerator conferences series APAC, EPAC, and PAC. ICFA noted that each of these series is becoming effectively international, with almost one-half of the attendees from outside the region where the conference is organized and held, and similarly for the conference speakers. Each conference is the major world accelerator conference in its time period for the accelerators used in particle physics and other disciplines such as light sources and neutron sources.

In view of increasing international cooperation, ICFA felt that it would be very desirable to have only one such major conference each year, which would be the international gathering that year for the accelerator field. ICFA endorsed the idea to move from regional PAC conferences to the concept of a yearly International Particle Accelerator Conference (IPAC), rotating around the world. ICFA has therefore asked the regional Organizing Committees to discuss the matter and make a proposal on how to implement this International Conference.

ICFA's effectiveness stems from "the sheer force of good will and good sense," Jonathan Dorfan said. Strengthening both will help us to tackle the huge challenges ahead of us.

1.2   From the Beam Dynamics Panel Chairman

Weiren Chou, Fermilab
mail to: chou@fnal.gov

Albrecht Wagner, Director General of DESY and new ICFA Chair, wrote an article "*Going Global – a View from ICFA*," published in this issue of the Newsletter. He emphasized the importance of international collaboration in our field, and in particular, for the two energy frontier machines, the LHC and ILC, one under construction and the other on the drawing board. He also endorsed the idea of moving from the three regional particle accelerator conferences – PAC, APAC and EPAC – to the concept of a yearly International Particle Accelerator Conference (IPAC), rotating around the world. This is an important topic for discussion in our community.

There was a joint ICFA – laboratory directors meeting from February 9 to 10, 2006, at CERN. The meeting heard a number of reports from the ICFA chair, several ICFA panel chairs, and about 20 lab directors from around the world. The meeting minutes will be posted on the ICFA web site. (http://www.fnal.gov/directorate/icfa/index.html) The LHC is on schedule for having the first beam (in an octant of the ring) by the end of this year and first collisions in July 2007. The ILC GDE will finish a Reference Design, including an engineering cost estimate, in 2006. Discussion about the future of ICFA will resume when the two regional strategic studies – EPP2010 in the U.S. and the CERN Council Strategy Group – are completed. The meeting also approved the 40th ICFA Advanced Beam Dynamics Workshop on e^+e^- *Factories*, which will take place September 15-17, 2006 at the Budker Institute of Nuclear Physics (BINP), Novosibirsk, Russia.

The International Accelerator School for Linear Colliders, which this panel is helping to organize and which will be held in Sokendai, Hayama, Japan from May 19 to 27, 2006 (http://www.linearcollider.org/school/), is making good progress. Readers are referred to Section 2 for the present status of the school.

Thanks to Eberhard Keil, past-chair of this panel, two early issues of this Newsletter, nos. 5 and 6, were found at the CERN library. Alessandra Lombardi scanned them and put them into the newsletter archive (http://icfa-usa.jlab.org/archive/newsletter.shtml). We have now a complete collection of all published ICFA Beam Dynamics Newsletters except the first issue, which is still missing.

The editor of this issue is Prof. Kwang-Je Kim, a panel member and a senior scientist at Argonne National Laboratory in the U.S. I'd like to express my gratitude to him for having collected a number of nice articles and producing a well-organized, fine Newsletter.

1.3   From the Editor

Kwang-Je Kim
Argonne National Laboratory, Argonne, IL 60439, USA
mail to: kwangje@aps.anl.gov

The theme papers in this issue are from the Workshop on Pushing the Limits of RF Superconductivity held at Argonne National Laboratory on September 22-24, 2004. The workshop was special because, although it was planned well before, it took place just a few days after the International Technology Review Panel made its historic recommendation that the superconducting RF technology be the basis of the International Linear Collider (ILC).

The interest in SCRF goes beyond the ILC – the technology is the basis for other major accelerator projects such as the Spallation Neutron Source and the Rare Isotope Accelerator, and future light sources such as energy recovery linacs and x-ray free-electron lasers. Pushing the limits in accelerating gradient and Q is critically important for all these accelerators in reducing their size, construction cost, and operating budgets – in short, in making them affordable.

I believe that it is worthwhile to collect these papers by leading experts in the theme section of this Newsletter due to the importance of the topic and because the proceedings of the Workshop containing the original versions of these papers was not widely circulated. In addition, a majority of the papers here have been revised to incorporate further developments since the Workshop at Argonne. I thank the authors of these papers for their additional efforts in updating their papers.

2   International Linear Collider (ILC)

2.1   International Accelerator School for Linear Colliders

Barry Barish, Weiren Chou and Shin-ichi Kurokawa
mail to: barish@ligo.caltech.edu, chou@fnal.gov, shin-ichi.kurokawa@kek.jp

In the last issue (No. 38) of this Newsletter, we announced the *International Accelerator School for Linear Colliders*, which will be held in Sokendai, Hayama, Japan from May 19 to 27, 2006 (http://www.linearcollider.org/school/). The School has received an overwhelming response from all over the world. More than 500 people from 44 countries applied by the application deadline of February 15, 2006. However, the school can only accommodate a maximum of 80 students. This made student selection a difficult job for the Curriculum Committee.

Each applicant was required to submit a CV and a recommendation letter. The committee members spent many hours reading the hundreds of applications. The great majority of the applicants could certainly have been successful in the school, and most

candidates presented strong credentials. The committee was, therefore, faced with the necessity of choosing from among a great many more talented and highly qualified students than it had room to admit. After several weeks of intensive work and deliberations, the committee decided to admit 20 students from America, 20 from Europe and 36 from Asia. The Local Committee will appoint four scientific secretaries who will also attend the class, bringing the total attendance to 80. Most of the students are from countries that are strong in high-energy physics, but several students from such countries as Mongolia and Vietnam will also be attending. The majority of attendees are either graduate students or postdoctoral fellows. They will be "new blood" in our community.

KEK scientists created a wonderful online application system. Everything from application form to CV and recommendation letter was submitted via the Internet and automatically recorded into a database. All applicants' information was made accessible to the committee members electronically. This greatly reduced the committee's workload.

Acceptance letters were sent out in the first week of March. The list of students can be found on the school web site. We are confident these students will eventually make significant contributions to linear colliders. Regret letters were sent out in the third week of March. The School very much appreciates the interest the applicants have shown and hopes that those who cannot attend the school will continue to be interested in linear colliders and be able to attend possible schools in the future.

All 21 lecturers who will teach at the School have been confirmed. The list is attached below. This is a strong team with a good balance between young and senior physicists. It also has a nice geographical distribution among the three regions—Asia, Europe and North America—and maintains a balance between various institutions.

With topics ranging from electron and positron sources, damping ring and linear collider basics, to superconducting and warm RF technology, detectors and conventional facilities, students who attend the school will receive a comprehensive education in linear colliders. Lecturers will be responsible for:
- preparing teaching materials in the form of PowerPoint files and posting them online one month before the school starts
- attending the school and giving the lecture
- assigning homework to the students (1-2 problems per lecture)
- being available at the tutorial and homework time in the evening
- grading homework

At the end of the school, lecturers will select the top students, who will be honored during an awards ceremony on May 25, 2006.

All lectures will be posted on the school web site. The use of video streaming (i.e., synchronized video and slide show) is being considered. Then anyone who cannot be in the classroom could still "attend the class" via a computer.

<u>List of School Lecturers</u>

Lecture	Topic	Lecturer
1	Introduction I	Fumihiko Takasaki (KEK)
2	Introduction II	Tor Raubenheimer (SLAC)
3	Sources	Masao Kuriki (KEK)
4	Bunch compressors	Eun-San Kim (PAL)
5	Damping ring basics	Susanna Guiducci (INFN-LNF)
6	Damping ring design	Andy Wolski (LBL)
7	ILC linac basics	Chris Adolphsen (SLAC)
8	ILC linac beam dynamics	Kiyoshi Kubo (KEK)
9	High power RF	Stefan Choroba (DESY)
10	SRF basics	Shuichi Noguchi (KEK)
11	SRF cavity technology	Peter Kneisel (Jlab)
12	ILC cryomodule	Carlo Pagani (INFN-Milano)
13	Room-temperature RF	Hans Braun (CERN)
14	Beam delivery	Andrei Seryi (SLAC)
15	Beam-beam	Daniel Schulte (CERN)
16	Instrumentation & feedback	Marc Ross (SLAC)
17	Conventional facilities	Vic Kuchler (Fermilab)
18	Operations	Pantaleo Raimondi (INFN-LNF)
19	Detectors	Hitoshi Yamamoto (Tohoku Univ.)
20	Physics	Rolf-Dieter Heuer (DESY)
Special Lecture	Accelerator Test Facility (ATF)	Organized by Junji Urakawa (KEK)

3 Pushing the Limits of RF Superconductivity

3.1 R&D Paths towards Achieving Ultimate Capabilities

Peter Kneisel
Jefferson Lab, Newport News, VA 23606, USA
mail to: kneisel@jlab.org

3.1.1 Introduction

Superconducting niobium cavities for particle accelerator application are performing nowadays better than ever and a series of procedures have been established–if applied properly–which will result in multi-cell cavity gradients of up to E_{acc} = 35 MV/m, the design goal for the International Linear Collider (ILC). In several cases gradients above 40 MV/m have been measured in single cell tests. These gradients are close to or at the critical magnetic field value for niobium–at least what is believed to be the fundamental limitation of the material. However, there are still some open questions, whether the value for the superheated magnetic field of ~ 180 mT is the final answer.

3.1.2 Fundamental Limits

There are two fundamental limitations for a superconducting material applied to the fabrication of accelerating cavities:

- the surface resistance as predicted by the microscopic BCS theory
- a critical RF magnetic field above which the superconducting phase is destroyed

Even though in many cases non-resonant electron loading (field emission) limits the performance of superconducting niobium cavities, this phenomenon is not a fundamental limitation. In RF cavities surface electric fields as high as $E_{peak} \sim 145$ MV/m have been measured in cw operation and in a pulsed mode $E_{peak} \sim 200$ MV/m has been achieved [1]. In DC field emission experiments surface fields exceeding 2300 MV/m have been reached [2].

Multipacting, even though sometimes an annoying limitation in cavity performance, is no fundamental limit and can be avoided by proper cavity design and clean surface preparation.

3.1.2.1 *BCS Surface Resistance*

The BCS surface resistance is given by eq. (1)

$$R_{BCS} = A(\lambda_L, \xi_o, l) \times f^\alpha \times 1/T \times e^{-\Delta/kT} \quad \text{for} \quad T < T_c/2 \tag{1}$$

λ_L is the London penetration depth, l is the mean free path, ξ_o is the coherence length, Δ is the energy gap and T_C is the critical temperature. The value for α varies between 1.7 and 1.9. In Figure 1 the BCS surface resistance is shown as a function of frequency for typical material parameters of niobium at 2K. As can be seen in Figure 2, the surface resistance has a minimum at a mean free path of ~ 20 nm.
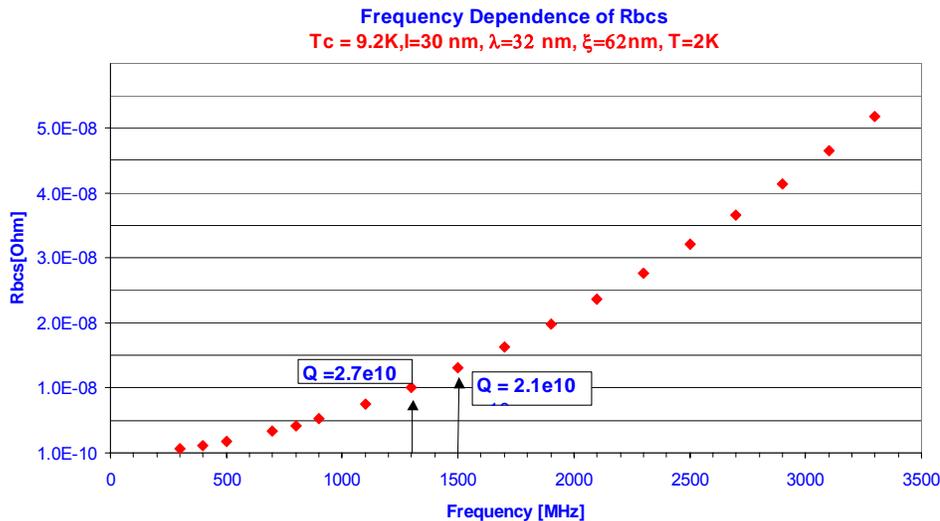
Figure 1: Frequency dependence of the BCS surface resistance for niobium at 2K. For a typical accelerating cavity the corresponding Q-values are $Q(2K) = 2.7 \times 10^{10}$ at 1300 MHz and $Q(2K) = 2.1 \times 10^{10}$ at 1500 MHz; calculations done with program from ref. [3].
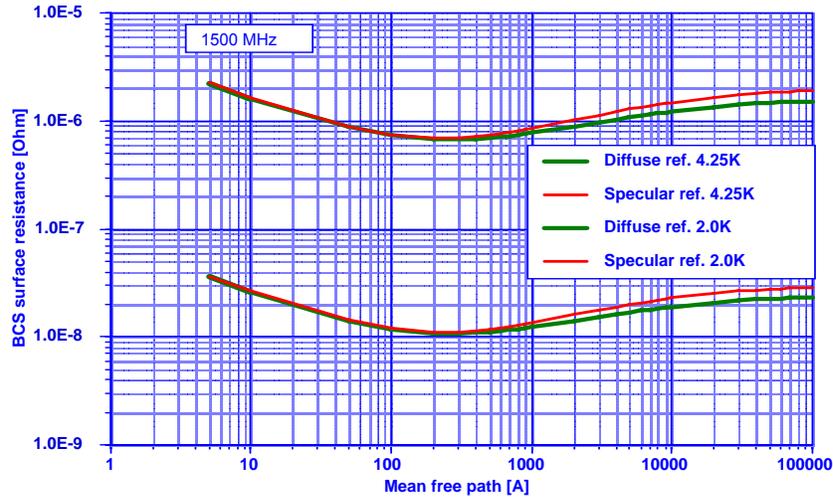
Figure 2: Dependence of the BCS surface resistance on mean free path for niobium at a frequency of 1500 MHz; calculations done with program from ref. [3].

In reality the achievable surface resistance at low temperatures (T < 2K) is limited by the "residual surface resistance," which has typically values ranging from 2 nΩ<R_{res}<15 nΩ. Many contributions to this residual resistance have been identified over the years ranging from foreign material inclusions and surface defects such as delaminations, scratches and chemical residue to insufficiently shielded external magnetic fields or localized states in the highly perturbed metal/oxide interface and weak links as internal surfaces. Figure 3 shows an example of an experimentally obtained R(T) dependence for a 1.5 GHz niobium cavity.
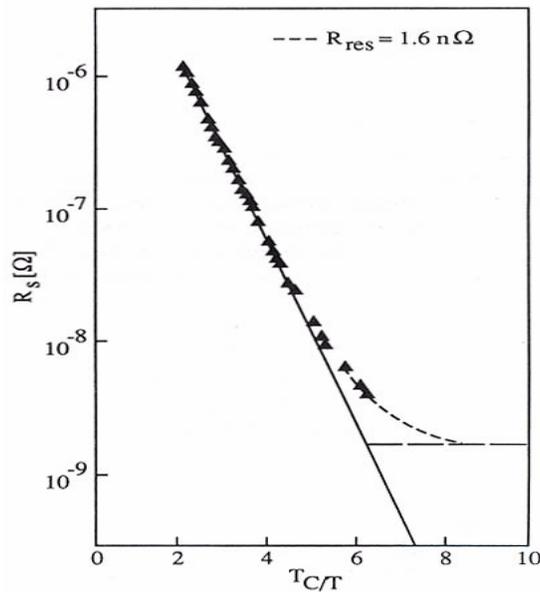
Figure 3: Experimentally achieved temperature dependence of the surface resistance of a 1500-MHz niobium cavity; a residual resistance of R_{res} = 1.6 nΩ was fitted to the data.

3.1.2.2   *Critical Magnetic Field*

It is still not clear which critical field is the fundamental limitation in an RF environment. Analysis of existing data combined with theoretical predictions seem to point at the superheating critical field as the fundamental limit – in the case of niobium, this has a value of ~ 180 mT [4]. A more detailed analysis of multiscale breakdown mechanisms in RF cavities has been presented by A. Gurevich [5].

In order to theoretically explain observed field dependent non-linearities in the surface resistance as shown schematically in Figure 4, it has been concluded that in the future a theory of nonlinear surface resistance needs to be developed, that can be used at high RF amplitudes H_{RF}. It has to take into account "current pairbreaking and nonequilibrium superconductivity in strong RF fields as well as RF dissipation due to vortex penetration through oscillating surface barriers enhanced by the grain boundary network" [5].
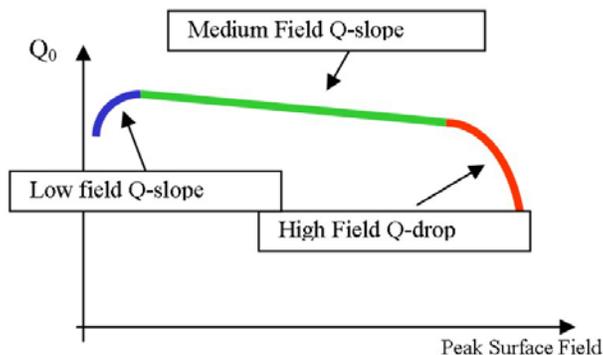
Figure 4: Nonlinear Q vs E behavior (schematic).

3.1.3   Issues

The issues discussed in this section are all related to the application of RF superconducting technology to particle accelerators and are therefore less "academic" than "basic research." Nevertheless, there are many questions open to gain a "basic" understanding of the physics behind the phenomena discussed below; it is believed that addressing those questions is better suited for R&D efforts in a University environment with the appropriate knowledge and experience than in the operations environment of an accelerator laboratory.

3.1.3.1   *Issue #1*

As shown schematically in Figure 4, a highly nonlinear dependence of the Q-value (surface resistance) on RF field amplitude is typically observed in niobium cavities. Even though there exists a series of theoretical explanations, no single theory explains all available data [6-8]. Especially disturbing for accelerator application is the dramatic Q-drop at high gradients, which not only limits the achievable gradients but also greatly increases the cryogenic load. There exists a remedy to overcome this Q-drop, namely the prolonged "in-situ" baking of the cavities at ~120ºC. A beneficial improvement in Q-value and also in gradient has been observed especially for electropolished cavities; it is not uncommon to see such improvements on chemically polished cavities as well [9].

What is needed is a universal explanation for the occurrence of this Q-drop, for the variation in the on-set value from cavity to cavity and for its disappearance after "in-situ" baking. How important is the oxide structure on the surface? Is the Q-drop a magnetic or electric field effect? Do grain boundaries play a role, since they are energetically favored by impurity atoms for segregation? Does hydrogen, known to be a problem for Q-disease, play a role in the Q-drop?

Q-drops of this nature were not observed previously with less pure material [10].

3.1.3.2   *Issue #2*

Issue #2 is the determination of the fundamentally limiting magnetic field in RF applications in general. It is related to issue #1 in the sense that, only in a few rare cases, when high field Q-drop could be overcome, have magnetic surface fields as high as ~ 180 mT been achieved in niobium cavities. As pointed out in [4], this field corresponds to the superheating critical field, which is proportional to $1/\kappa$, where κ is the Ginzburg-Landau parameter. If this is true, then the case for alloy superconductors such as e.g., Nb_3 Sn with large κ values becomes quite weak for application at high RF fields.

3.1.3.3   *Issue #3*

Field emission loading caused by particulate contamination is often a severe limitation in cavities and is difficult to control in complex assemblies such as cavity strings/cryomodules. However, in order to achieve the potential of the cavity material, the contamination level in these assemblies has to be reduced/eliminated and improved surface cleaning and assembly procedures need to be developed to avoid recontamination of the sensitive cavity surfaces.

3.1.3.4   *Issue #4*

Bulk niobium of high purity has been the choice for accelerator cavities for a long time and the best cavity performances have been achieved with this material.

Thin film deposition of niobium by sputtering has been applied successfully to the 352 MHz cavities operating at 4.2 K and at relative low gradients for the LEP machine at CERN. Improved deposition techniques such as energetic deposition [11,12], which hold the promise of improved performance in cavities, are under development at different laboratories.

Compound materials such as Nb_3 Sn, NbN, NbTiN, MgB_2 and others are of some interest because of their high critical temperatures and potentially high critical magnetic fields.

These developments are still in their "infancy" and for potential application in accelerating cavities a great deal of work has to be done. The pulsed power experiments as developed by I. Campisi, which are to be carried out at SLAC [13], seem to be an excellent tool to explore the limitations of these materials.

3.1.4   Some Suggestions

For several decades correlations of cavity performance with surface features of the niobium surfaces have been sought [14]. In addition to investigations of the oxide structure with "conventional" surface analytical tools such as AES, SEM, SIMS, and

XPS a variety of "sample" cavities (TE_{011}, Tri-axial, Quadrupole, …) have been designed with the intention of RF testing with the cavities samples, which subsequently could undergo surface studies. None of these attempts have been very successful. However, other methods such as penetration depth, magnetization, pinning and susceptibility, which employ conduction electrons as in RF tests, have been quite successful in shedding some light into material behaviour. More recently [15], ac susceptibility measurements have been used to characterize volume and surface properties of RRR = 300 niobium, that had been treated in the same way as niobium RF cavities, namely buffered chemical polishing, electropolishing and "in-situ" baking. As a result it was found that surface superconductivity (H_{C3}) is increased by baking and that the highest values of H_{C3} were obtained for electropolished surfaces after "in-situ" baking.

In 1973 a coaxial TE_{011} cavity for measurements of metallurgical properties and RF breakdown fields was proposed [16] as shown in Figure 5, but to the knowledge of the author has never been built. A cavity like this looks like an ideal tool for correlating RF performance with magnetization/susceptibility investigations and additionally "classic" surface studies. This cavity could also be used to investigate RF performance of different materials.
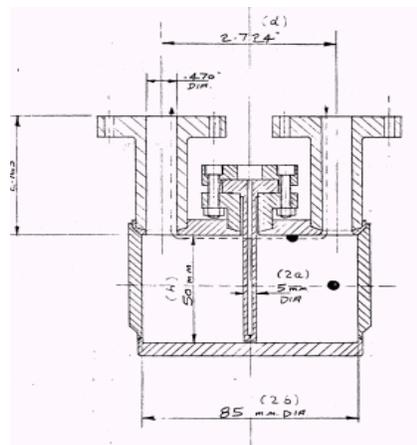
Figure 5: Coaxial TE_{011} sample cavity [16].

In addition, it has the advantage of lacking electric field related effects because it is operating in the TE_{011} mode.

In 1973 the Siemens Research Lab reported that in a TE_{011} X-band cavity made from reactor grade niobium a record magnetic surface field of 159 mT was obtained after an electropolishing, oxipolishing and anodizing surface treatment [10]. This cavity did not show a high field Q-drop, even though the achieved surface magnetic fields are much above the presently observed on-set values for this phenomenon. It might be desirable to manufacture such a cavity again with the high purity material available now and to repeat these surface treatments. Such a cavity could also serve as a tool—either in cw or pulsed operation—to settle the uncertainty about the fundamentally limiting magnetic field.

As mentioned above, the experiments in preparation at SLAC with short pulse power are aimed at answering the same questions.

The high field Q-drop, and its understanding and elimination, is one of the "hottest research" topics at the present time. Of the various open questions mentioned in "Issue #1" the possible influence of grain boundaries and/or hydrogen preferably trapped at grain boundaries can be investigated with cavities made from different grain size material. An extreme approach is being taken at JLab, were a single cell cavity has been fabricated from large grain niobium sheets as shown in Figure 6. This cavity is presently under investigation.

Figure 6: Large grain niobium sheet for cavity fabrication; the center represents a single crystal.

Grain boundaries are "weak links," especially if they are "filled" with oxides or other segregated impurities. It seems to be appropriate to use/develop experimental tools such as tunnel junction/Josephson junction type experiments or magneto-optical methods [17] to investigate them. Hydrogen in grain boundaries might be detected by a sensitive, high spatial resolution Squid system, which would detect the hydrogen magnetic moment.

Such a high resolution Squid system would also be very valuable for defect scanning of niobium sheets used for the fabrication of cavities. Presently such pre-screening is carried out by eddy current or Squid scanning systems developed at DESY; however, these systems have limited resolution (defect size > 50 μm). As the performances of cavities improve and breakdown fields get closer to fundamental limits, better resolution is needed to detect smaller defects. It would also be a further progressive step, if such a system could be employed on a curved surface such as a cavity half cell after deep drawing or even a dumbbell.

It is well known that large amounts of dissolved hydrogen cause "Q-disease" in niobium cavities. Therefore, as a matter of course, cavities are preventively degassed at T > 600C for several hours after initial bulk material removal. Additional chemical treatment by buffered chemical polishing (BCP) as in the case of the SNS or JLab upgrade cavities is most likely increasing the hydrogen concentration in the surface and possibly at grain boundaries and its influence on cavity performance is uncertain.

It has been suggested [18] that this hydrogen take-up can be avoided by immediately rinsing the chemically treated surfaces with an oxidizing agent such as nitric acid: Material removal from a niobium surface takes place only in the presence of an oxidant such as nitric acid in combination with hydrofluoric acid, which removes the generated oxides. This reaction is highly exothermic and reaction energy is kept in "check" by buffering the solution and by cooling and agitating it. However, when the acid is removed, the reaction in the viscose surface layer continues without appropriate removal of the reaction energy. A highly activated niobium surface remains, which

reacts in contact with water during rinsing by setting free large amounts of hydrogen, which may be dissolved in the material. This reaction can be avoided, if the highly activated niobium surface is brought immediately in contact with nitric acid and instead of hydrogen, gases such as NO and NO_2 are evolved.

It might be worthwhile *to try this rinsing method.*

Temperature mapping is one of the most successful methods ever employed to gain a better understanding of processes taking place in a superconducting cavity during operation. Temperature maps have given information about defect locations, electron trajectories and location of field emitters, loss distributions and global heating. However, most of these investigations have been made on single cell cavities and are not routinely applied on multi-cell cavities as a QA/production tool to learn about the problems and shortcomings of, e.g., a particular surface treatment process. It would be very desirable to take temperature maps during every vertical test of multicell cavities and get a "live" picture of multipacting, processing at higher fields in the FE regime, loss distributions and Q-drop. Such information could then be fed back into surface processing techniques such as BCP, high pressure rinsing and its effectiveness depending on nozzle configuration or spray pattern, electropolishing or assembly techniques. If, for example, field emission occurs always in a particular cell or the losses are high in a particular location in a cavity, a different rinsing technique or method of drying (horizontal/vertical) could be found.

Unfortunately, T-mapping systems as presently built from individual C-resistors are quite expensive (it takes about 600 thermometers of $10/unit for a single cell) and also time consuming to install on a cavity. For less expensive mapping systems, one could conceivably take advantage of thin film technology and could evaporate sensors and leads on a flexible substrate, which then could be wrapped around a cavity at room temperature with a contact agent such as Apiezon grease. The routine use of such a system during vertical cavity tests would definitely improve the information gained from these experiments.

Finally it should be mentioned that further improvements in cleaning of sensitive cavity surfaces are needed with the goal of eliminating field emission loading. Among the many methods for surface cleaning [19,20] high pressure ultrapure water rinsing is the most successful. However, there are still many "unknowns" in this process such as: optimal flow rate and pressure at the surface to be cleaned, optimized HPR nozzle configurations (material, shape, and pattern), flow pattern inside cavity, amount of water to be cycled through the cavity. At DESY, very extensive high pressure rinsing (up to 8 times for one cavity) has been applied successfully to 9-cell TESLA cavities. Stringent control of the cleanliness of the ultra pure water with respect to particle count, TOC level and Si content is essential for success. If one could be as successful with many fewer rinses, costs and elapsed times for cleaning would significantly decrease. This is particularly important for large future projects such as the X-FEL and the ILC.

A combination of HPR and megasonic agitation, which is most successful for smaller particle sizes, might be a further improvement.

CO_2 snow cleaning seems to be an attractive method and is actively pursued at DESY as a possible "in situ" method for horizontal configurations. This might also be true for UV – Ozone cleaning, but very little is known about this process for cavities [21].

3.1.5 Summary and Conclusions

Obviously there is a lot of R&D necessary to bring bulk niobium cavities to their ultimate performance allowed by the fundamental limits of the material. This R&D can be conducted as an effort to gain a "basic" understanding of the limiting physics phenomena—most prominently the non-linear behaviour of the surface resistance in high electromagnetic fields ("Q-slope," "Q-drop")—or it can be conducted as "R&D in support of projects." In both cases it is an effort that needs some "staying power," and it cannot be a short-lived enterprise.

In more specific terms the near term R&D should try to solve the physics of the
- nonlinear surface resistance, and
- fundamentally limiting magnetic field.

Control of contamination is essential for future large scale applications and work has to be done in this area.

The development of other materials for application in accelerators such as Nb on copper, Nb_3Sn, NbTiN, MgB_2… hinges on the question of the limiting H-field in an RF environment. If $H_{sh} \sim 1/\kappa$ is the limit, then compound superconductors with large κ-values are no competition for bulk niobium as material for high gradient RF cavities. They might be useful for lower field applications in low frequency cavities and for operations at 4.2K.

3.1.6 Acknowledgement

3.1.7 References

1. J. Delayen and K. W. Shepard., IEEE Trans. Magn. MAG-27, 1928 (1991).
2. T. Habermann et al., Proc. of the 8th Workshop on RF Superconductivity, Abano Terme, Italy, 1997, p. 972.
3. J. Halbritter, KFK-Ext.Report 3/70-6, Kernforschungszentrum Karlsruhe (1970).
4. K. Saito, Proceedings of the Workshop on Pushing the Limits of RF Superconductivity, Argonne report ANL-05/10, March 2005, p. 140.
5. A. Gurevich, Proceedings of the Workshop on Pushing the Limits of RF Superconductivity, Argonne report ANL-05/10, March 2005, p. 17.
6. B. Visentin, Proc. of the 11th Workshop on RF Superconductivity, Lübeck/Travemünde, Germany, 2003, paper TuO01 (http://srf2003.desy.de/) and these proceedings.
7. G. Ciovati et al., Proc. of the 11th Workshop on RF Superconductivity, Lübeck/Travemünde, Germany, 2003, paper WeO14 (http://srf2003.desy.de/) and these proceedings.
8. L. Lilje, Proceedings of the Workshop on Pushing the Limits of RF Superconductivity, Argonne report ANL-05/10, March 2005, p. 43.
9. G. Ciovati, P. Kneisel, Proceedings of the Workshop on Pushing the Limits of RF Superconductivity, Argonne report ANL-05/10, March 2005, p. 74.
10. K. Schnitzke et al., Phys. Lett. A 45(3), 241 (1973).
11 V. Palmieri, Proceedings of the Workshop on Pushing the Limits of RF Superconductivity, Argonne report ANL-05/10, March 2005, p. 158.
12. G. Wu and H.L. Phillips, Proceedings of the Workshop on Pushing the Limits of RF Superconductivity, Argonne report ANL-05/10, March 2005, p. 26.

13. I. Campisi, Proceedings of the Workshop on Pushing the Limits of RF Superconductivity, Argonne report ANL-05/10, March 2005, p. 189.
14. P. Kneisel, Proc. of the 11th Workshop on RF Superconductivity, Lübeck/Travemünde, Germany, 2003, paper TuO02 (http://srf2003.desy.de/).
15. S. Casalbuoni et al., Proc. of the 11th Workshop on RF Superconductivity, Lübeck/Travemünde, Germany, 2003, paper WeO13 (http://srf2003.desy.de/).
16. W. Bauer et al., BNL Report AADD73, 11 (1973).
17. P. Lee et al., Proceedings of the Workshop on Pushing the Limits of RF Superconductivity, Argonne report ANL-05/10, March 2005, p. 281.
18. W. G. Koerber, Report DESY M-91-07 (1991).
19. P. Kneisel, B. Lewis, Proc. of the 7th Workshop on RF Superconductivity, Gif sur Yvette, France, 1995, p. 97.
20. D. Reschke, Proceedings of the Workshop on Pushing the Limits of RF Superconductivity, Argonne report ANL-05/10, March 2005, p. 30.
21. Viet Ngyen Tuong, Proc. of the 2nd Workshop on RF Superconductivity, CERN, 1984, p. 91.

3.2   Overview of Surface Measurements: What Do Surface Studies Tell Us about Q-Slope?

C. Z. Antoine

CEA, DSM/DAPNIA/Service des Accélérateurs, de la Cryogénie et du Magnétisme
CE-SACLAY, F-91 191 Giv-sur-Yvette Cedex, France
mail to: clairant@dapnia.cea.fr

3.2.1   Abstract

For MHz-GHz superconducting RF applications on Niobium, dissipation occurs in the first tens of nanometer of the material. Moreover, the superconducting matrix is covered with a dielectric oxide layer of some nanometer, which is at first order transparent to RF, but which might have a strong influence on the underlying superconductor. Exploration of this thin layer not only requires very high depth resolution, but should also provide some chemical information in order to tell the oxide contribution from the more inner one. It goes without saying that no existing technique is able to provide easily at the same time all the required information, and one has to compare several different techniques to be able to establish a correct image of the real situation near the surface. Moreover one has to keep in mind the limitations and specialties of each technique in order to interpret correctly observations made at such a small scale. We will try to show the advantages and the limitations of the most common techniques and review the main features of surface and interface behaviors of niobium.

3.2.2   Introduction

Many papers exist in the literatures that deal with surface characterization of niobium, and an exhaustive review of them can be found in [1]. In this paper we shall concentrate on different kind of surface analysis that are relevant to explain the high field Q-slope of RF cavities, i.e. thermal dissipation that occurs at high accelerating gradient in absence of field emission. In particular we will concentrate on the effect of low temperature baking (LTB) and the ensuing modifications of the surface.

Indeed baking at temperatures as low as ~ 120°C, ~ 48 h, should only give rise to slight modifications of the very surface. Baking has a dramatic effect on cavities, while superconducting parameters are only slightly affected [2,3]. This suggests that the dissipations originate from a depth even inferior to the penetration depth. This point is further supported by experimental evidences described hereafter. Exploration of the surface with nm resolution cannot be achieved with standard surface analysis. We will try to show the origin of the limitations of those techniques, and in what conditions we can get meaningful results.

3.2.3   Surface Issues

Several types of surface modifications can occur with baking:
- Modification of adsorbed layers; H_2O, hydro-carbides… Water should evaporate, while hydrocarbides [4,5] are progressively reduced to graphitic carbon. At higher temperature (T > 175°C), carbon reacts with niobium to forms niobium carbide, a very stable compound that can't be further destroyed, even upon melting of the niobium.
- Modification of the oxide layer. Many experimental evidences show that LTB under vacuum induces a thinning of the oxide layer, along with reducing of its valence[1]. Released oxygen is injected into the bulk where it forms a solid solution of interstitial oxygen, sometimes referred as "suboxide clusters," although it should not be considered as an independent phase. On the contrary, in the case of baking in air, oxide layer grows thicker, still in competition with oxygen injection to the metal.
- Diffusion of light species (interstitials): H, C, F…O. The diffusion coefficient of H is about 10^{-5}-10^{-6} cm^2/s around room temperature, which means that it moves nearly freely within Nb. Meanwhile, due to mechanical interaction with the surface, it tends to segregate near the surface. Oxygen moves ~ 10^{16} slower, while another factor 100 is expected for carbon [6]. Displacement of oxygen only becomes noticeable at baking temperature (several 10 nm/24 h), whereas it stays about 1 Å/24 h at room temperature.
- Hydrogen case. It should diffuse uniformly inside the material upon baking and diffuse back to the surface and form segregates again, within hours or days upon cooling and staying at room temperature. Meanwhile, there is some experimental evidence that the segregation doesn't occur within several days [3], but it was shown to reappear after 12-18 months [7,8]. The fact that cavities don't loose the baking benefit after even "years" [9,10], makes us think that hydrogen is not in cause, but this point might need further exploration.

Several experiments on cavities allow discarding some of these causes. As we will see afterwards, in those cases surface analysis can provide further support and/or explanation.

---

[1]   It should be noted that the advent of dangling bonds and displaced atoms inside the oxide enhances the number of localized states within the insulating gap of the oxide. The density of localized states will eventually increase until all these states overlap and form the conduction band of the metallic forms of niobium monoxide.

3.2.3.1 *Experiments on Cavities*

Reported experiments on cavities allow discarding adsorbed species as well as oxide layer modification as an origin of the Q-slope:

- Exposure to air + HPR: the effect of baking is preserved upon exposure to air, even after several months/years, and several High Pressure Rinsing cycles [7,8]. In both cases, the oxide layer as well as adsorbed species were regenerated on the niobium surface and are similar to what was on cavity surface before baking. This means that the disappearance of the Q-drop did not arise neither from the evolution of the adsorbed layers nor from the modification of the oxide layer.
- Baking in air: give similar results as baking under vacuum [2]. As we have seen before, in one case the oxide layer is slightly destroyed, while in the other case the oxide layer thickens. Modification of the oxide layer itself is then again not a possible cause.
- Treatment with fluorhydric acid: HF is known to dissolve most of the oxide layer. A fresh oxide layer grows afterwards on the niobium during rinsing. The baking effect is not reversed by HF rinsing [10]. This also rules out any direct effect from the oxide layer.
- Oxipolishing: it was shown in [11] that oxipolishing (i.e., thick anodization followed by oxide dissolution in HF) progressively reverse the benefit of baking. This procedure allows a very controlled dissolution of the niobium surface (with some nm steps). Successive oxipolishing and RF testing cavity show that the affected surface layer with altered material parameters has a thickness <300 nm. Recent results from DESY and Cornell seem to confirm those results, although some confusion might arise from the fact that the thickness of the anodized layer not only depends on the applied voltage, but also on the electrolyte composition of the anodizing solution [12].

3.2.3.2 *Diffusing Species*

Surface physics as well as reported experiments on cavities lead us to conclude that diffusing species are the most probable suspects, and among them, oxygen, the main impurity inside niobium, is the most likely to be involved.

Moreover, susceptibility measurements have shown that baking doesn't change bulk properties while it affects the surface critical field. It was reported that $Bc2surf > B_{c2}^{bulk}$, and B_{c2}^{surf} is higher for electropolished samples than for chemically polished samples, and that baking increases further the surface critical magnetic field for both [13,14]. This increase in surface H_{C2} with baking seems to go hand in hand with an increase of the paramagnetic moment, possibly another hint toward increased O contamination.

We need therefore monitoring carefully oxygen repartition under the surface, along with possible interaction with other species. We need to explore the surface behavior with a resolution below the penetration depth. Indeed, RF measurements at 2K usually probe ~ 50-100 nm, and RF measurements at 10 K probe ~1 μm. We have seen that in standard baking condition, the superconducting parameters are only slightly affected: we cannot measure strongly localized modifications of the SC parameters with cavities or usual RF parameters.

3.2.3.3 *What Surface Technique?*

It is important to note that there is no "miraculous" surface analysis tool that can provide information of interest with such a high resolution as we require, especially in the case where the surface is covered by hydrocarbons and an oxide layer. Any picture of the near surface niobium must be inferred from the combined results of several different techniques, keeping in mind the physical limitations of each one.

3.2.3.3.1 Photoemission

Among surface experiments, photoemission (also known as ESCA or XPS) has a particular place. It constitutes a unique way to get info from the matrix under the oxide because it allows differentiating the oxide signal from the metal one. The principle of this technique is the following: the sample is irradiated with X-rays. Core electrons of the atoms are ejected with a kinetic energy E_k related to its binding energy: $E_B = h\nu - E_k$. E_B(the binding energy) is characteristic for each element and is influenced by the electronegativity of bonded neighbors. Thus we also get chemical environment information, although it is limited to the closest neighboring atoms, and it is only a local indication of stoechiometry. The escape depth of the electrons depends on the initial energy of the X-rays, and on the orientation of the detector. Variation of incident energy and/or detection angles allows reconstructing the depth profile. Profiling by ion sputtering shall be discarded as it is known to destroy the oxide layer through preferential oxygen sputtering [15]. In this case, the observed species (suboxides) are generally generated by the sputtering process itself. Note that Auger is similar in principle, although the excitation source is electrons instead of X-rays.

The XPS technique has been extensively used to study niobium oxides and has already given a lot of information. It has meanwhile several drawbacks:

- It is a superficial technique; most of the signal comes from the oxide layer and masks the signal originating from the metal underneath.
- Its sensitivity is poor: elements present at less than 0.1-0.5 at% will not be detected.
- Conventional XPS has a low energy resolution: ~1 eV (peak separation), although it is often claimed to be better.
- The deconvolution of signals can easily lead to misinterpretation for fractions inferior to ~10%: the fact that a species is found by deconvolution is not sufficient a proof of its physical existence. For example, NbO is generally inferred from the asymmetry of the metal signal, but one can also fit most of the spectra without an NbO signal, by simply increasing the degree of asymmetry of the metal signal [16,17].
- Due to preferential sputtering of oxygen, ion sputtering profiling can not be used to monitor the oxygen content of the surface

Conventional XPS is not precise enough to study interstitial oxygen repartition and even low concentration sub-oxide fractions. Some misinterpretations can be found in literature, either because the statistical signification of the results has not been checked, or because erroneous conclusion on the physical meaning of the observed signal: e.g., local stoechiometry being considered as one defined species.

For low concentration species, additional experimental data are necessary to fully establish their existence. For instance one can use statistical tools like Main Components Analysis (MCA) to check how many species have a significant statistical

weight [18]. Or use a better light source (e.g., synchrotron radiation) and an appropriate monochromator to gain in energy resolution [19-21].

The variation of EB with Nb valence is quasi linear (see [21] and reference therein). For instance, the species Nb_2O is often referenced in the literature as a peak at E_B 203.1 eV upon deconvolution. By the way this species does not exist as a phase because the lowest known suboxide of Nb is NbO at 204.5 eV. On the other hand the signal at 203.1 eV was shown to be an interface signal, i.e. a row of Nb atoms having a niobium matrix on one side and an oxide (namely NbO) on the other side. As it is only 1-2 monolayers thick Nb_2O cannot be considered as a separate phase.

Figure 1a) shows a conventional XPS spectrum. Intermediate species like NbO, and O dissolved in the Nb matrix cannot be determined accurately against the base line.

Figure 1b) shows the spectrum of a Nb sample covered with 1-2 monolayers of NbO. In this case, deconvolution of the signal is done simultaneously on a set of nine spectra (three different incident energies and three different detector angles for the same sample). In this case, the signal treatment requires a lot of time, but is far more reliable than conventional deconvolution on one single spectrum.
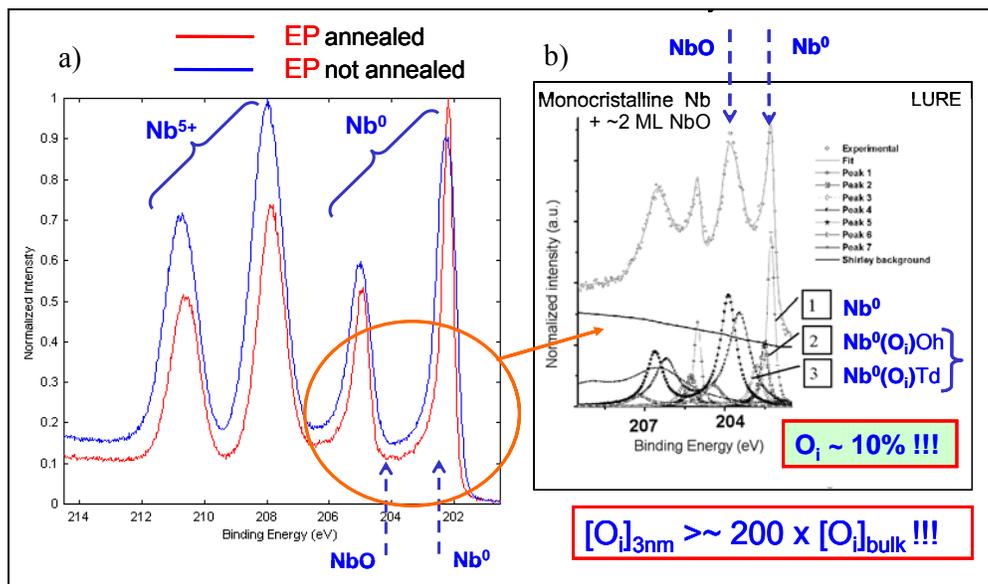
Figure 1. a) Conventional XPS spectrum of electropolished samples. Intermediate species like NbO, and O dissolved in the Nb matrix cannot be determined accurately. b) Spectrum of a heat treated Nb sample covered with only 1-2 mono layers of NbO. Deconvolution of the signal is done simultaneously on a set of nine spectra (three different incident energies and three different detector angles for the same sample) from [19].

The stoechiometry Nb_4O and Nb_6O does not refer to a defined suboxide, but to the configuration of interstitial oxygen in the metal. Indeed, oxygen atoms form a solid solution in the niobium matrix, occupying specific sites of the BCC lattice: namely the tetrahedral and octahedral sites, the latter being more favorable. The distribution can be random (lattice gas distribution) or distributed along specific defects like dislocations or grain boundaries, depending on the temperature condition and the local defects distribution. In the latter case it might be considered as a "cluster," as claimed by

Halbritter. But although oxygen distorts slightly the Nb lattice, it is not a precipitate and neither a distinct phase: we still have the usual BCC lattice. Moreover, X-ray diffraction seems to indicate that oxygen is in the form of isolated atoms rather than clusters (see next section).

In the case described in Figure 1b) the total amount of dissolved oxygen (octahedral and tetrahedral sites) in the vicinity of the surface is about 10 at%, i.e., about 200 times the bulk content of the sample. It is commonly admitted that there is a competition between oxidation and interstitial oxygen production during any process of niobium oxidation. In [22], amounts as large as $\sim$ 70 at% of O_i have been found under the oxide layer during the oxidation of thin Nb films in the air and at modest temperature (≤ 240°C). Segregation of oxygen at the interface has been observed by several different means but actual concentration is rather difficult to evaluate with precision with classical tools. From the above figures we know we could expect several 10 at%, but we now need to measure it accurately, in conditions close to the wet oxidation that is applied to cavities during surface treatments. Although this is feasible in theory with photoemission, we can use X-ray diffraction in order to have a better sensitivity.

3.2.3.3.2 X-ray Diffraction

Several X-ray techniques can be used to characterize Nb surfaces (see e.g., [22]). Reflectometry gives information on oxide thickness, electronic density, and surface and interface roughness. Grazing incidence diffraction and in particular diffuse scattering provide in depth information on the lattice structure. Variation of incident angles as well as detection angles allows reconstructing the depth profile. The crystal truncation rod (CTR) method allows getting information on the first monolayers of the surface, by comparing the actual signal (between two Bragg peaks) to the theoretical one expected for an infinite crystal. In the two last techniques, the expected signals are so small that only the use of synchrotron sources allows getting significant signal.

Figure 2 shows the principle of diffuse scattering measurement. Deformation induced on the lattice by interstitial oxygen gives rise to additional diffracting patterns that are measured out of the diffraction plane (Y,Z).
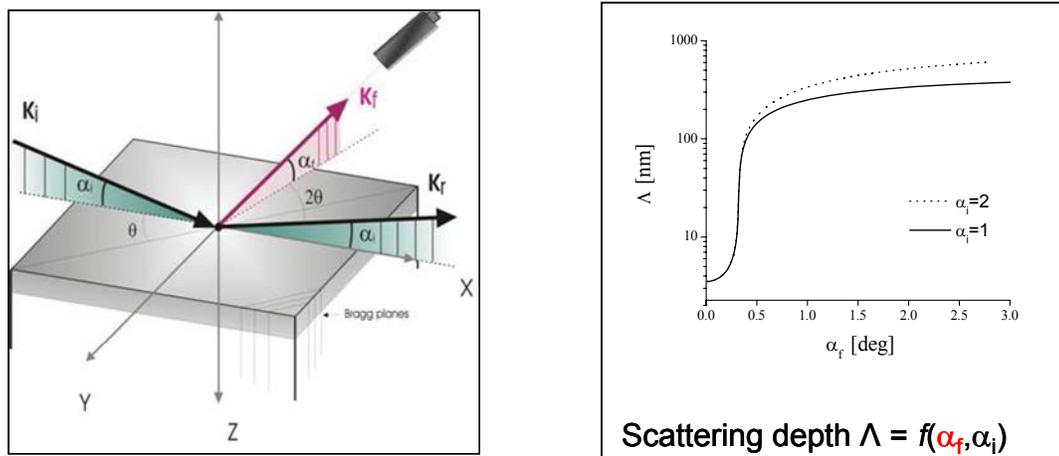
Figure 2: Principle of diffuse scattering, for each θ, the signal at a fixed α_i is registered for a range of α_f. The experiment can be done for various α_i so that the probed depth changes. Bragg peaks due to diffuse scattering are measured this way.

The deformation induced by isolated oxygen atom on the Nb lattice is well documented. It is analogous for a wide range of "interstitial alloys" of BCC metals like NbO_x, NbN_x, TaO_x, TaN_x… Bulk NbO_x has been studied in detail by neutron diffraction with x ranging between 0.9 at% and 2 at% [23]. The presence of an oxygen atom in an octahedral interstitial site induces a local trigonal distortion, called the "ω phase," which induces a distinct diffuse scattering peak. Comparison with theory shows that this distortion is due to **isolated Nb** and that the deformation does not exceed the third nearest neighboring Nb atoms.

Diffuse scattering at grazing angles, combined with detection angle variation should allow us to measure the concentration of interstitial oxygen near the metal-oxide interface, and hopefully to reconstruct a depth profile. Preliminary results on a monocrystalline bulk sample have already exhibited the **characteristic O_i diffuse scattering peak** [24]. Depth profile is more delicate as other factors than depth distribution might interfere with the intensity of the signal. Examining of results is underway. We shall further check the evolution of this peak with various heat treatments.

3.2.3.3.3 Chemical Polishing (BCP) versus Electropolishing (EP)

From the Q-drop point of view, before baking, BCP and EP seem to be very alike [2]. Meanwhile it is interesting to know what the differences are from the surface point of view. After BCP + rinsing and HPR, the oxide thickness reaches ~ 5 nm within some hours, and is probably serrated, i.e. the thickness is not uniform. Note that those results seem to contradict [25], where it is claimed that the growth of Nb_2O_5 saturates at 6 nm within minutes in presence of water. But the difference of purity (RRR ~ 100 vs. RRR ~ 300 to 400) can easily explain those differences: purer niobium is indeed expected to react somewhat slower.

After EP, a lot of discrepancies can be found in the literature. But the thickness of EP oxide depends on the time it was kept in the EP bath with and without bias: if the applied bias is about 10 Volt, ~ 20 nm of oxide are expected on Nb, which will readily dissolve into the EP bath because of the presence of HF. If the sample is withdrawn quickly, a thick oxide is expected. On the other hand if the sample is kept in the bath for some minutes, a thin oxide will be found. In this last case, XPS measurements have been done: 1 hour after EP, even after rinsing + HPR, the oxide thickness is only 2.5 nm, not serrated. It grows eventually to 5 nm within one week. This indicates some difference in nature of the oxide: although it is still Nb_2O_5, some differences appear in structure and ordering, as well as in impurity incorporation (ppm level) [17]. Meanwhile, there are some indications that EP contains more oxygen than BCP (also carbon). Those results have been found with profiling technique (ion sputtering) and therefore have to be considered carefully. Figure 3 show the comparison of an EP sample and a BCP sample by SIMS and similar trends have also been observed by AES [26]. Indirect confirmation arises from the magnetization experiment cited above [13,14]: EP samples seem to present a degraded surface BC2 as compared to BCP. Baking (which induce O_i diffusion in the penetration depth) also further increases B_{C2}.
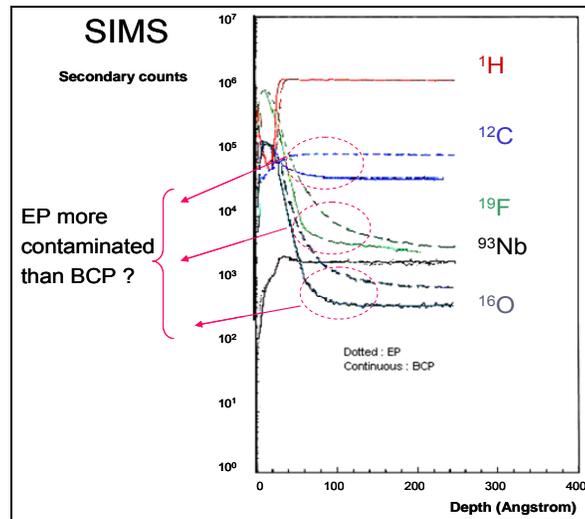
Figure 3: SIMS profiles of an electropolished (dotted) and a chemically polished Nb sample.

3.2.3.3.4 The Interstitial Oxygen Scenario and Local Measurement of the Superconducting Gap Δ

Among several other models, the influence of interstitial O has much experimental support. Other diffusing species might be involved but with lesser influence. For instance F is found in abundance under the oxide layer, especially in the case of HF rinsing of the surface [27]. Meanwhile no difference can be noticed on cavities before and after HF treatment [28]. Carbon is also likely to have an influence when heat treatment is done above 175°C, as it reacts with niobium and forms carbides. This reaction might be at the origin of the permanent degradation observed on cavities when the heat treatment has been done at high temperature [3,29]. Meanwhile it is important to determine not only the oxygen repartition in the surface of the superconductor, but also how this oxygen influences the superconducting properties. If a severely contaminated layer (~ 2 nm) exists near the surface, it will be too thin to influence mean values as measured within the penetration depth. But locally the superconducting properties might be affected [30]. For instance, the superconducting gap might be decreased, in the very area where the field is the highest. A 10-15% decrease of Δ might affect the surface resistance of a factor 10 in the first 2 nm of the surface. Upon baking this thin layer gets diluted within the whole penetration depth. Thus more material is affected, but to a lesser extent. (See Figure 4.)

Measuring Δ in the vicinity of the surface should be possible with photo emission, provided that one has a very high energy resolution. A dedicated cryogenic facility has been developed at Tokyo University, with an incident laser beam as an excitation source, sub MeV energy resolution, and angle resolution that allows reconstructing depth profiles [31]. Measurement of the electronic density inside the conduction band around the Fermi level above and under Tc show the appearance of Δ. ̃Measurements on EP and BCP samples, with and without baking are now underway and should be published soon [32].
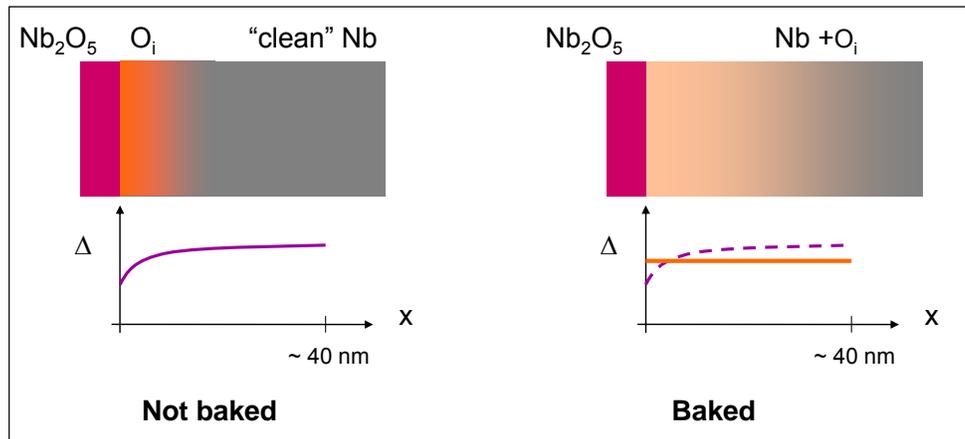
Figure 4: Schematic behaviour of Δ in the case of unbaked and baked Nb.

3.2.4 Surface Morphology

Among the different existing models, surface morphology has also been evoked as a possible source of the Q-drop [33]. This explanation is difficult to further support since EP and BCP cavities exhibit the same kind of Q-slope, although the surface morphology is really different. Meanwhile, this model might apply very nicely to another dissipation related phenomena: the quench. Indeed with a replica technique, we were able to measure the local morphology in the vicinity of the quench site as well as elsewhere inside cavities [34,35]. The field enhancement factor and related dissipated power has been calculated according to the measured profile as shown in Figure 5.
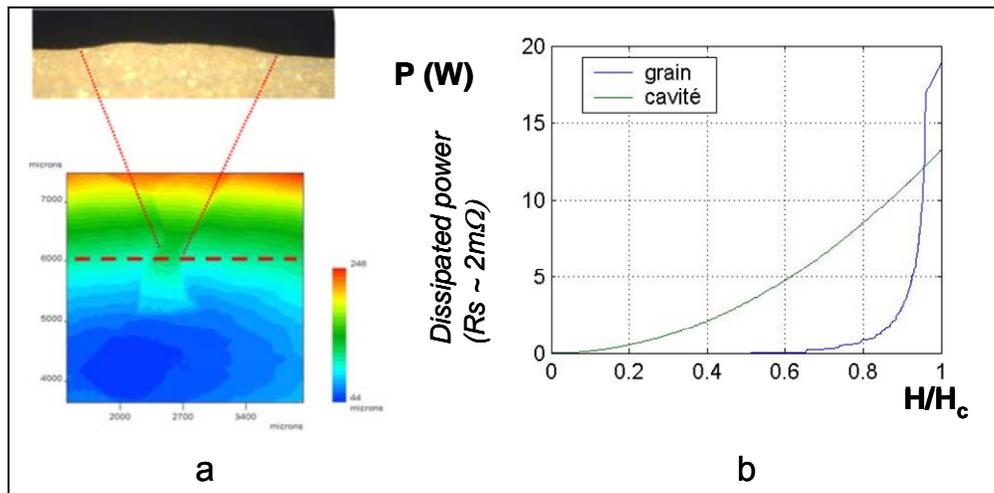
Figure 5: a) Contour line (down) and cut (up) of a replica of the inner cavity surface at the quench location. b): 2D model, contribution to dissipated power from the "defect free" cavity (green) and from the defect (blue). Thermal calculation show that normal conducting edges of the grain can be thermally stabilized at $H_{local} > H_c$, but $T<T_c$. By further increasing the magnetic field, change less than 1 mW lead to thermal instability.

It shows that the contribution of the grain is more "abrupt" than the general heating of the cavity. Moreover, thermal calculations show that normal conducting edges of the grain can be thermally stabilized at $H_{local} > H_c$, but $T<T_c$. By further increasing the magnetic field, change less than 1 mW lead to thermal instability [36]. This scenario better describes a quench phenomenon than the observed Q-slope.

3.2.5   Conclusion

The understanding of RF dissipation in the London penetration depth now requires probing the surface with a resolution better than 1 nm. This cannot be achieved with conventional equipment, and requires access to most advanced techniques. Collaboration and support from experts in surface science or solid state physics is also necessary as those techniques usually don't give rise to straight forward interpretation. Although difficult, experimental ways exist to determine the local surface composition as well as some local superconducting parameters, and we hope to be able to start a new step toward understanding of RF superconductivity.

3.2.6   References

1.   P. Kneisel, "Surface characterization of bulk Nb: what has been done, what has been learnt?" Proc. of the 11th Workshop on RF Superconductivity, Lübeck/Travemünde, Germany, 2003, paper TuO02 (http://srf2003.desy.de/).
2.   B. Visentin, "Q-Slope at high gradients: review of experiments and theories," Proc. of the 11th Workshop on RF Superconductivity, Lübeck/Travemünde, Germany, 2003, paper TuO01 (http://srf2003.desy.de/).
3.   G. Ciovati, "Effect of low temperature baking on Niobium cavities," Proc. of the 11th Workshop on RF Superconductivity, Lübeck/Travemünde, Germany, 2003, paper WeO14.
4.   Q. Ma and R. Rosenberg, "Thermal and electron-beam irradiation effect on the surfaces of Nb for RF cavity production," Proc. of the 10th Workshop on RF Superconductivity, Tsukuba, Japan, 2001, pp. 368-372.
5.   K. Kowalski et al., "'In situ' XPS investigation of the baking effect on the surface oxide structure formed on niobium sheets used for superconducting RF cavity production," Proc. of the 11th Workshop on RF Superconductivity, Travemünde, Germany, 2003, paper ThP09.
6.   G. Horz et al., "Group VA Metals (2), niobium, Thermodynamics, kinetics and properties," Gases and Carbon in Metals, Fachinformationszentrum Energie: Karlsruhe, 1981, p. 117.
7.   S. Isagawa, "Influence of H on Nb superconducting cavities," *J. Appl. Phys.* **51**(11), 6010-6017 (1980).
8.   C.Z. Antoine et al., "The Role of Atomic Hydrogen in Q-Degradation of Niobium Superconducting Cavities: Analytical Point of View," Proc. of 5th Workshop on RF Superconductivity, DESY, Hamburg, Germany, 1991, pp. 616-634.
9.   L. Lilje et al., "Achievement of 35 MV/m in the Superconducting Nine-Cell Cavities for TESLA," TESLA Report 2004-05, DESY, Hamburg, 2004.
10. B. Visentin, Proceedings of the Workshop on Pushing the Limits of RF Superconductivity, Argonne report ANL-05/10, March 2005, p. 94.
11. P. Kneisel, "Preliminary experience with 'in-situ' baking of niobium cavities," Proc. of the 9th Workshop on RF Superconductivity, Santa Fe, NM, USA, LA-13782-C, 2000, pp. 328-335.
12. L. Lilje and H. Padamsee, Proceedings of the Workshop on Pushing the Limits of RF Superconductivity, Argonne report ANL-05/10, March 2005, p. 242 and p. 291.

13. S. Casalbuoni, L.V. Sawilski, and J. Kötzler, "Superconductivity above H_{c2} as a probe for Niobium RF-cavity surfaces," Proc. of 11th Workshop on RF Superconductivity, Lübeck/Travemünde, Germany, 2003, paper WeO13 (http://srf2003.desy.de/).

14. B. Steffen et al., "Suceptibility measurements on surface treated niobium samples," Proc. of the 11th Workshop on RF Superconductivity, Lübeck/Travemünde, Germany, 2003, paper MoP49 (http://srf2003.desy.de/).

15. T. Choudhury et al., "Reduction of oxides of iron, cobalt, titanium and niobium by low-energy ion bombardement," *J. Phys. D: Appl. Phys.* **22**, 1185-1195 (1989).

16. D.B.M.P. Seah, "Auger, X-Ray Photoelectron Spectroscopy," in *Practical Surface Analysis*, J.W. Son, Editor, 1990.

17. C.Z. Antoine et al., "Morphological and Chemical studies of Nb Samples after Various Surface Treatment," Proc. of the 9th Workshop on RF Superconductivity, Santa Fe, New Mexico, USA, LA-13782-C, 2000, pp. 295-303.

18. A. Chincarini et al., "Statistical approach to XPS analysis: Application to niobium surface treatment," Proc. of the 10th Workshop on RF Superconductivity, Tsukuba, Japan, 2001, paper PR010 (http://conference.kek.jp/SRF2001/).

19. I. Arfaoui et al., "Evidence for a large enrichment of interstitial oxygen atoms in the nanometer-thick metal layer at the NbO/Nb (110) interface," *J. Appl. Phys.* **91**(11), 9319-9323 (2002).

20. I. Arfaoui, J. Cousty, and C. Guillot, "A model of the NbOx~1 nanocrystals tiling a Nb(110) surface annealed in UHV," *Surface Science* **557**, 119-128 (2004).

21. I. Arfaoui, "Stoechiométrie, structure et tenue en champ électrique d'un film ultramince de NbOx~1 sur Nb (110)," Physique des Surfaces et Science des Matériaux, Ecole Centrale de Paris, 2001.

22. O. Hellwig, "Oxidation of Epitaxial Nb(110) Films: Oxygen Dissolution and Oxide Formation," Fakultät für Physik und Astronomie, Ruhr-Universität Bochum: Bochum. 2000.

23. H. Dosch, A.V. Schwerin, and J. Peisl, "Point-defect induced nucleation of the w-phase," *Physical Review B* **34**(3), 1654-1660 (1986).

24. M. Delheusy et al., to be published.

25. M. Grundner and J. Halbritter, "On the natural Nb_2O_5 growth on Nb at room temperature," *Surface Science* **136**, 144-154 (1984).

26. K. Asano et al., "XPS and AES studies of thin oxide layers on Nb for superconducting RF cavities," KEK-Report-88-2, KEK, 1988.

27. Measured with SIMS, unpublished results.

28. B. Visentin, Proceedings of the Workshop on Pushing the Limits of RF Superconductivity, Argonne report ANL-05/10, March 2005, p. 94.

29. B. Visentin et al., "A non-electropolished niobium cavity reached 40 MV/m at Saclay," Proc. of the 2002 European Particle Accelerator Conference, Paris, France, 2002, pp. 2292-2294.

30. A. Gurevich, personal communication.

31. T. Kiss et al., "Direct measurement of bulk superconducting electronic state with sub-MeV resolution," Proc. of SNS 2004, Sitges, Spain, 2004, *J. Phys. Chem. Solids*, to be published.

32. T. Kiss and C.Z. Antoine, to be published.

33. J. Knobloch et al., "High-Field Q Slope in Superconducting Cavities Due to Magnetic Field Enhancement at Grain Boundaries," Proc. of the 9th Workshop on RF Superconductivity, Santa Fe, New Mexico, USA, 1999, LA-13782-C, 2000, pp. 77-91.

34. S. Berry, C. Antoine, and M. Desmons, "Surface morphology at the quench site," Proc. of the 2004 European Particle Accelerator Conference, Lucerne, Switzerland, 2004, pp. 1000-1002.

35. S. Berry et al., "Topologic analysis of samples and cavities: a new tool for morphologic inspection of quench site," Proc. of the 11th Workshop on RF Superconductivity, Lübeck/Travemünde, Germany, 2003, paper ThP04 (http://srf2003.desy.de/).
36. M. Desmons, S. Berry and C.Z. Antoine, to be published.

3.3   Thermal RF Breakdown of Superconducting Cavities

Alex Gurevich

Applied Superconductivity Center, Univ. of Wisconsin, Madison, WI 53706, USA

mail to: gurevich@engr.wisc.edu

3.3.1   Abstract

A brief overview of multiscale mechanisms of RF superconductivity breakdown is given. We start with the BCS surface resistance R_s in the clean limit and then address nonlinear corrections to the isothermal R_s quadratic in the RF peak magnetic field. Then an analytic thermal breakdown model is developed with the account for both linear and nonlinear surface resistance. The model is applied to describe RF breakdown of clean Nb cavities.

3.3.2   Introduction

Surface resistance R_s of superconducting cavities exposed to a high-amplitude RF field is controlled by multiple mechanisms, which can manifest themselves on very different length scales. On fundamental nano-scales set by the superconducting coherence length $\xi \sim 32\text{-}38$ nm, and the magnetic London penetration depth $\lambda \sim 40$ nm for Nb at 0K, the dissipated power $P = R_s H_0^2/2$ is due to RF absorption by thermally-activated normal electrons, which then transfer the RF power to the lattice via impurity and electron-phonon scattering. The BCS surface impedance $Z = R + iX$ describes the electromagnetic linear response to low-amplitude ($H_0 \ll H_c$) RF field $H(t) = H_0\cos\omega t$, for which the surface resistance $R_s = \omega^2\exp(-\Delta/T)A/T$, is independent of the RF field H_0 much smaller than the thermodynamic critical field H_c [1,2]. Here Δ is the superconducting gap, and the factor A determined by particular scattering mechanisms depends weakly on ω at low frequencies $f = \omega/2\pi = 1\text{-}3$ GHz characteristic of superconducting cavities for which $\omega \ll \Delta = 1.9T_c \sim 400$ GHz [3]. However, high-performance Nb cavities can already operate at high accelerating fields $E_{acc} \sim 30\text{-}40$ MV/m and peak magnetic fields $H_0 \sim 100\text{-}200$ mT comparable to $H_c(0) = 200$ mT [4]. In this case the linear BCS impedance cannot be used to describe the RF breakdown, in which instability of the superconducting steady state in RF field occurs due to nonlinear mechanisms of dissipation.

An important mechanism of RF nonlinearity is due to vortex penetration, which could occur at the lower critical field H_{c1}, although the magnetic surface barrier can prevent vortex penetration up to the fields H close to H_c [5]. Once vortices penetrate a superconductor, R_s increases by several orders of magnitude, triggering global thermal quench. Grain boundaries and other surface defects can locally reduce the magnetic surface barrier, so that vortices start penetrating at $H_{gb} < H_c$ (or $H_{gb} < H_{c1}$). In this case dissipation is due to oscillation of vortices in a network of grain boundaries on a small

fraction of the sample surface, so even if the global thermal instability may not occur, grain boundaries can contribute to the reduction of the quality factor Q for RF amplitudes $H_{gb} < H_0 < H_c$ [6].

In this paper we consider the maximum breakdown RF field H_b, which can be achieved in a clean superconductor without defects, so the contribution of grain boundaries will be neglected. We limit ourselves to the RF breakdown of the Meissner state for which the nonlinearity of R_s results from pairbreaking and nonequilibrium effects. Among other things, the latter manifest themselves in local heating, while the strong exponential dependence of $R_s = \omega^2 \exp(-\Delta/T) A/T$ provides a positive feedback between the RF absorption and the local temperature increase, which triggers thermal instability of the nonisothermal Meissner steady state for $H_0 > H_b$. However, unlike previous thermal breakdown models [7,8], the analytical model proposed in this work shows that the RF thermal breakdown can occur at rather weak overheating $T - T_0 \sim$ 0.1-0.2K, sufficient to triggers a thermal runaway. This situation resembles thermomagnetic flux jumps in type-II superconductors with strong pinning [9,10]. This model also includes the BCS nonlinearity due to pairbreaking effects, which can significantly increase the high-field Q-slope at RF amplitudes comparable to H_c. In particular, the high-field Q-slope can significantly increase if the surface has an oxide or intermetallic layers, which locally suppress the gap Δ and the critical field H_c due to proximity effect.

3.3.3   Isothermal BCS Surface Resistance

Here we consider some general properties of the BCS surface resistance, starting with the linear surface resistance R_S which corresponds to the peak magnetic fields $H_0 << H_c$ and then addressing nonlinear corrections to R_s at $H_0 \sim H_c$. Here we consider the case of ideal cooling for which the temperature of the superconductor coincides with the bath temperature.

3.3.3.1   *Linear BCS Surface Resistance*

BSC surface resistance R_s is determined by thermally-activated normal electrons accelerated by RF filed, which only penetrates in the layer of thickness λ at the surface. Depending on the relation between the electron mean free path ℓ and the London penetration depth λ, one can distinguish two different regimes. 1. Dirty RF limit $\ell << \lambda$, for which an incident electron moving toward the surface undergoes multiple impurity scattering in the accelerating surface layer of thickness λ before getting reflected back to the bulk. 2. Clean RF limit $\ell >> \lambda$ for which an incident electron collides with the surface and then gets reflected to the bulk without impurity scattering in the accelerating layer, as depicted in Fig. 1.
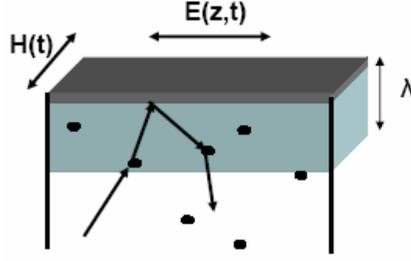
Figure 1: A trajectory of a thermally-activated electron scattered by impurities (black dots) within an accelerating layer of penetrating RF field (shaded) at the surface of a superconductor in a parallel RF magnetic field H(t). A darker layer marks a surface layer which provides additional scattering.

Both for $\ell \ll \lambda$ and for $\ell \gg \lambda$, the dissipated power $P = R_s H_0^2/2$ results from acceleration of thermally activated electrons and holes by RF field, but the mechanisms of RF energy transfer are rather different. In the dirty limit, $\ell \ll \lambda$, the surface resistance is dominated by impurity scattering, in which case $R_s \sim \mu_0^2 \omega^2 \sigma_n \lambda^3 \Delta \ln(\Delta/\omega)\exp(-\Delta/T)/T$ for type-II superconductors ($\lambda > \xi$) is proportional to the residual conductivity $\sigma_n = ne^2\ell/p_F$ in the normal state [2]. Here n is the total electron density, e is the electron charge, and $p_F = (3\pi^2 n)^{1/3}\hbar$ is the Fermi momentum. This case is analogous to the normal skin effect in nonsuperconducting metals. However, for typical mean-free paths $\ell \sim 10^2 - 10^3$ nm of pure Nb in high-performance cavities [4,11], the opposite clean RF limit may be more relevant.

In the clean RF limit $\ell \gg \lambda$, the BCS surface resistance becomes independent of the impurity scattering and thus on the normal state conductivity. As a result, purifying the material does not change R_s, because electrons moving through the accelerating layer get scattered not by impurities but the gradient of the penetrating magnetic field. In this case the BCS surface resistance is given by a formula similar to that for R_s in the dirty limit, except that the Drude conductivity $\sigma_n = ne^2\ell/p_F$ should be replaced by the effective conductivity $\sigma_{eff} \sim ne^2\lambda/p_F$ in which the London penetration depth λ plays the role of the mean-free path [1]. The clean RF limit $\ell \gg \lambda$ in superconductors is analogous to the anomalous skin effect in normal metals [5].

Calculation of R_s for a general scattering mechanism of electrons by the sample surface requires solving a kinetic equation for thermally-activated quasiparticles in a superconductor in a RF field. General formulas for the impedance Z for either specular or diffusive surface scattering are rather complicated [1,2] so here we present R_s for a clean type-II superconductor ($\ell \gg \lambda$, and $\lambda > \xi$) for diffusive scattering from the surface [12].

$$R_{s0} \cong \frac{3\Delta}{2T}\mu_0^2\sigma_{eff}\omega^2\lambda^3 \ln\frac{1.2T\Delta\xi^2}{\omega^2\lambda^2}\exp\left(-\frac{\Delta}{T}\right), \tag{1}$$

where $\sigma_{eff} = ne^2\lambda/p_F$ is the effective conductivity, characteristic of the clean RF case. The surface resistance given by Eq. (1) is independent of the electron mean free path due to impurity scattering. At low temperatures, scattering by phonons does not

contribute to R_s either, because of very large mean free path of electron-phonon collisions, $\ell_{ep} \sim a(\Theta/T)^5$, where a is the lattice spacing, and Θ is the Debye temperature. Thus, σ_{eff} is dominated by electron scattering on the gradient of the RF field, which varies on the scale $\sim \lambda << (\ell, \ell_{ep})$.

3.3.3.2 *Nonlinear BCS Surface Resistance*

For $H_0 \sim H_c$, the BCS surface resistance R_s becomes strongly dependent on H_0. This dependence, in principle, could be obtained from nonlinear equations of nonequilibrium superconductivity, which describe self-consistently the distribution function of quasiparticles, the gap and the spatial distribution of RF field [13]. These equations in general case are very complicated and can hardly be solved even numerically.

We consider a nonlinear correction to R_s which results from the pairbreaking effect of supercurrent density $J(x,t) = (H_0/\lambda)e^{-x/\lambda}\cos\omega t$ induced by RF field. The pairbreaking manifests themselves in two different ways. First, there is a direct suppression of the superconducting gap Δ by supercurrent, however as was shown by Bardeen [14], the gap in clean ($\ell >> \xi$) superconductors at T = 0 is *independent* of DC current as long as $J < J_d \sim \phi_0/4\pi\lambda^2\xi$. This result can be used to conclude that Δ in clean high-performance Nb cavities at low temperatures T < 2K is practically independent of the low-frequency RF field with $\omega << \Delta$ and $H_0 < H_c$. The second effect results from the change of the electron energy spectrum in a current-carrying superconductor, $E(k) = E_0(k) + \mathbf{v_s}\mathbf{k_F}$, where $\mathbf{v_s} = \mathbf{J}/en$ is the supercurrent velocity, and $E_0(k)$ is the quasi-particle spectrum at J = 0 [5]. Solving the kinetic equation for the distribution function of quasi-particles in a superconductor in a strong RF field, allows one to calculate the dissipation power P = $R_s H_0^2/2$. For diffusive surface scattering, the nonlinear surface resistance with the account of the first quadratic correction due to RF field is given by [12]:

$$R_s = \left[1 + C\left(\frac{\Delta}{T}\right)^2\left(\frac{H_0}{H_c}\right)^2\right]R_{s0} .$$

(2)

Here R_{s0} is the linear BCS resistance, $\Delta \approx 1.92\ T_c$ (for Nb), and the constant C depends weakly on ω:

$$C = \frac{\pi^2}{384}\left[1 + \frac{\ln 9}{3\ln(4.1T\Delta\xi^2/\lambda^2\omega^2)}\right],$$

(3)

where the contribution of the last term in the brackets for Nb at 2K, and $\omega/2\pi = 2$GHz is less than 8%. As follows from Eq. (2), the nonlinear contribution increases as the temperature decreases. For Nb at 2K, the factor $\gamma = C(\Delta/T)^2 \approx 2$ in Eq. (2) noticeably increases the surface resistance as the RF peak field H_0 approaches H_c. As shown below, the RF nonlinearity in R_s can significantly affect thermal breakdown of superconductivity, decreasing the high-field Q values at $H_0 \sim H_c$ and reducing the breakdown field H_b.

3.3.4   Thermal RF Breakdown

Strong RF fields drive superconductors out of equilibrium. The simplest manifestation of nonequilibrium effects is local heating due to transfer of RF energy absorbed by thermally-activated quasi-particle to the lattice. Because of the strong temperature dependence of the BCS resistance $R_{s0}(T)$, heating can make thermal steady-state equilibrium impossible, giving rise to RF breakdown of superconductivity. We consider here a simple thermal breakdown model for a superconducting slab of thickness d in a parallel RF field, which causes a local temperature increase at the side of the exposed to the RF field. The other side of the slab is cooled by liquid helium, as shown in Fig. 2
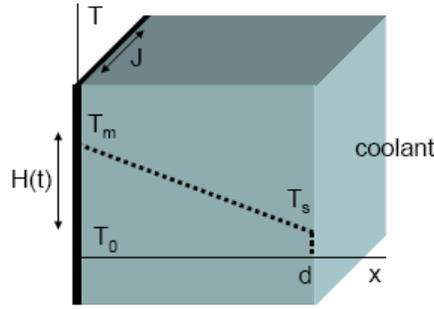
Figure 2: A slab of thickness d in a parallel RF field H(t). The black area on the left side shows the surface layer of thickness λ in which RF heating causes local temperature increase from the bath temperature T_0 to T_m. The temperature profile in the slab is shown with the dotted line. The temperature jump $T_s - T_0$ at the right side of the slab is due to the Kapitza thermal resistance.

Steady-state temperature distribution across the slab is determined by the heat diffusion equation

$$\frac{\partial}{\partial x}\kappa(T)\frac{\partial T}{\partial x} + \frac{1}{2}R_s(T_m, H_0)H_0^2\delta(x) = 0,\qquad(4)$$

where $\kappa(T)$ is the thermal conductivity and the second term describes the RF heating source. The delta function $\delta(x)$ reflects the fact that this source is strongly localized in a narrow layer of thickness $\sim \lambda \ll d$, so the resistance $R_s(T)$ is taken at the surface temperature T_m. The solution $T(x)$ of Eq. (4) depends on T_m and T_s, which are determined from the boundary conditions: $\partial T/\partial x = 0$ at $x = 0$ and $\kappa(T_s)\partial T/\partial x + \alpha(T_s,T_0)(T_s - T_0) = 0$ at $x = d$, where $\alpha(T_s,T_0)$ is the heat transfer coefficient between the superconductor and the coolant. The boundary conditions give the following equations for T_m and T_s:

$$\alpha(T_s,T_0)d(T_s - T_0) = \int_{T_s}^{T_m}\kappa(T)dT,\qquad \frac{1}{2}R(T_m,H_0)H_0^2 = \alpha(T_s,T_0)(T_s - T_0).\qquad(5)$$

Here the first relation is obtained by integrating the constant heat flux $q = -\kappa(T)\partial T/\partial x$ from $x = 0$ to $x = d$, and then taking $q = \alpha(T_s - T_0)$ at $x = d$. The second relation in Eq.

(5) is the conservation law: the RF heat release on one side of the slab equals the heat flux to the coolant from the other side.

The slope of the quality factor $Q = G/R_s(T_m)$ is determined by the dependence of the surface temperature $T_m(H_0)$ on the RF amplitude H_0. Here the function $T_m(H_0)$ can be directly obtained by numerically solving Eqs. (5) for any materials relations $R_s(T)$, $\kappa(T)$, and $\alpha(T)$. This approach appears to be much more efficient than a direct integration of Eq. (4), in which case obtaining $T_m(H_0)$ requires calculation of many temperature profiles $T(x)$ which should also satisfy the particular boundary conditions. For Nb cavities operating at low temperatures ($T < 2K$), there is another significant simplification, which often makes it possible to solve Eqs. (5) analytically and obtain explicit formulas for $Q(H_0)$ and the breakdown field H_b. As shown in the next paragraph, for $T \ll \Delta$, the maximum overheating even at the breakdown field turns out to be rather small: $T_m - T_0 \cong T_0^2/\Delta \ll T_0$ ($T_0^2/\Delta = 0.18K$ for $T_0 = 1.8K$). This allows us to take $\kappa(T)$ and $\alpha(T)$ at $T = T_0$ and replace the integral in Eq. (5) by $(T_m - T_s)\kappa(T_0)$. Solving then the first linear equation (5) for T_s, and substituting the result into the second Eq. (5), we arrive at the following equation for the surface temperature T_m:

$$\frac{H_0^2}{2} R_s(T_m, H_0) = \frac{\kappa\alpha(T_m - T_0)}{\kappa + d\alpha} \; . \tag{6}$$

The right hand side of Eq. (6) is the total heat flux determined by two serial thermal resistances due to thermal conductivity and the Kapitza surface resistance.

For small H_0, Eq. (6) always has a solution $T_m(H_0)$, which corresponds to a stable temperature profile $T(x,T_m)$ across the sample. However, because of the strong exponential temperature dependence of $R_s(T)$, solutions for T_m disappear if the RF field H_0 exceeds a critical value H_b. This means that for $H_0 > H_b$, the steady-state thermal balance (6) between RF heat generation and heat transfer to the coolant becomes impossible and a thermal runaway instability occurs. In the next paragraphs, the quality factor $Q(H_0)$ and the thermal breakdown field H_b are calculated from Eq. (6) for both linear and nonlinear surface resistance. Notice that Eq. (6) does not imply any particular scattering mechanism, so the thermal breakdown model can be equally used both for clean and dirty RF limits.

3.3.4.1 *Linear Surface Resistance*

We first apply Eq. (6) to calculate $Q(H_0)$ and H_b for a weak RF field $H_0 \ll H_c$, taking the conventional form for the linear BCS surface resistance $R_{s0}(T) = A\omega^2\exp(-\Delta/T)T + R_0$, where A is a factor determined by particular mechanisms of scattering, and R_0 is the residual resistance (both A and R_0 are assumed temperature independent). It is convenient to express H_0 in Eq. (6) as a function of T_m:

$$H_0^2 = \frac{2\kappa\alpha T_m(T_m - T_0)}{(\kappa + \alpha d)[A\omega^2\exp(-\Delta/T_m) + R_0 T_m]} \; . \tag{7}$$

The function $H_0(T_m)$ plotted in Fig. 3 for Nb for different ratios of $R_0/R_{BCS}(T_0)$ has a maximum at $T_m = T_b$, which defines the thermal breakdown field H_b above which Eq. (7) has no solutions.
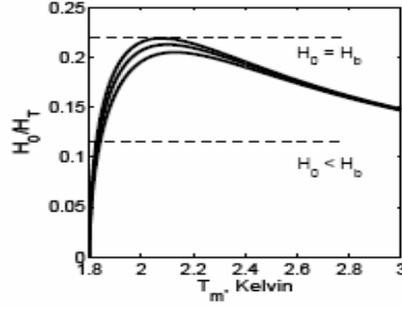
Figure 3: RF peak field H_0 as a function of T_m for Nb ($\Delta = 17.7$K) an $T_0 = 1.8$K and different ratios of $R_0/R_{BCS}(T_0) = 0$, 0.2 and 0.5 (from top to bottom, respectively). The field H_0 is expressed in the units of H_T, where $H_T^2 = 2\kappa\alpha T_0/(\kappa + \alpha d)R_{BCS}(T_0)$. Here $T_m(H_0)$ is the abscissa of the intersection point of the black curve and the horizontal dashed line for a given H_0.

As follows from Fig. 3, the surface temperature $T_m(H_0)$ gradually increases as the peak field H_0 increases up to the critical value H_b at which the dashed line touches the maximum. For $H_0 > H_b$, solutions for T_m disappear, which indicates thermal runaway and superconductivity breakdown. An important result evident from Fig. 3 is that the overeating $T_m - T_0$ is rather weak at all fields, including the thermal breakdown point at which $T_m - T_0 \approx 0.2$ K. To calculate the breakdown field $H_b = \max H_0(T_m)$, we differentiate Eq. (7) with respect to T_m and find the temperature $T_m = T_b$ at which $H_0(T_m)$ is maximum (for simplicity the residual resistance is neglected)

$$T_b - T_0 = \frac{T_0}{4}\left[1 - \frac{3T_0}{\Delta} - \sqrt{\left(1 - \frac{3T_0}{\Delta}\right)^2 - \frac{8T_0^2}{\Delta^2}}\right] \approx \frac{T_0^2}{\Delta}. \tag{8}$$

This result confirms the previous assertion that the overheating remains weak even at the breakdown field. Substituting $T_b - T_0 \approx T_0^2/\Delta$ into Eq. (6) and using $\exp(-\Delta/T_b) \approx \exp(-\Delta/T_0 + 1)$, we obtain

$$H_b^2 \cong \frac{2\alpha\kappa T_0^2}{e(\kappa + d\alpha)\Delta R_{s0}(T_0)}, \tag{9}$$

where $e = 2.718$. We evaluate $B_b = \mu_0 H_b$ for a high purity Nb at 2K, taking $\alpha = 5\times10^3$ W/m^{2}K, $\kappa = 20$ W/mK, $\Delta = 17.7$K, $R_{s0}(2K) = 20$ nΩ, and $d = 3$mm. For this case Eq. (9) gives $B_p \approx 200$ mT, surprisingly close to the critical field of Nb at 0K. This coincidence is certainly spurious, because, unlike the fundamental material parameter H_c, the thermal breakdown field H_b, can be strongly affected by varying T_0, R_{s0}, or thermal parameters α and κ due to change of the purity of the material and conditions of the surface facing the coolant. The thickness d in Eq. (9) is also essential because the term $d\alpha = 15$ W/mK in the denominator of Eq. (9) is comparable to $\kappa = 20$ W/mK. Yet, Eq. (9) shows that for $\kappa \sim d\alpha$ (as in the above example) improving material's purity can be the important way of increasing H_b. However, in both limits $\ell \ll \xi$ and $\ell \gg \xi$, the breakdown field (9) becomes in fact independent of the material purity. Indeed, in the dirty limit ($\ell \ll \xi$), the surface resistance R_{s0} is proportional to σ_n, and $\kappa \ll d\alpha$. In this

case H_b approaches a finite limit for $\ell \to 0$, because $H_b \propto (\kappa/\sigma_n)^{1/2}$ is independent of the mean free path due to the Wiedeman-Frantz law. In the opposite superclean limit ($\ell \gg \xi$), we have $\kappa \gg d\alpha$, and R_{s0} independent of ℓ, as discussed above. Hence $H_b = (2\alpha T_0^2/e\Delta R_{s0})^{1/2}$ is again independent of the material purity.

Shown in Fig. 4 are the quality factors $Q = G/[R_0 + A\omega^2 \exp(-\Delta/T_m)T_m]$ obtained by numerical solution of Eq. (7) for $T_0 = 2.2K$ and different ratios of $R_0/R_{BSC}(T_0)$. The parameters $R_{s0}(2K)$, α, κ and d are the same as above, and G is taken such that $Q = 10^{10}$ for $H_0 = 0$ and $R_0 = 0$.
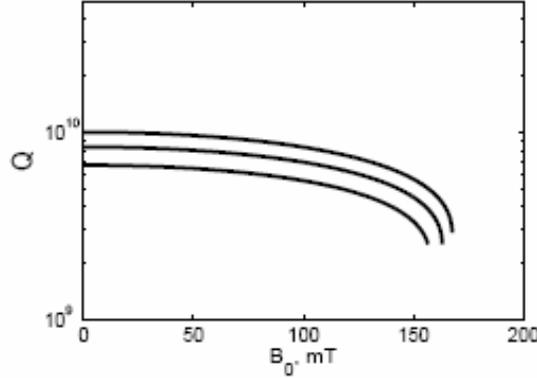
Figure 4. $Q = G/R_s$ versus H_0 for $T_0 = 2.2K$ and different $R_0/R_{BCS}(T_0) = 0$, 0.2 and 0.5 (from top to bottom, respectively).

As follows from Fig. 4, the Q-slope increases as H_0 increases, becoming infinite at H_b, although the threshold value of $Q(H_b)$ remains of the order of $Q(0)$. Indeed, for the parameters used to calculate $Q(H_0)$ in Fig. 4 for $R_0 = 0$, we have $Q(0) \approx 3.3Q(H_b)$. If $T_b - T_0 = T_0^2/\Delta \ll T_0$, then the model presented in this paper gives $Q(0) = eQ(H_b)$. These results are very different from the previous thermal feedback models [7,8], in which the surface resistance $R_s = R_{s0}/(1 - C_0E_{acc}^2)$ and the surface temperature T_m diverge at the thermal breakdown field (here $C_0 \propto \partial R_s/\partial T$). This result is due to the linear expansion $R_s(E_{acc}) = R(T_0) + (T - T_0)\partial R/\partial T$ used in these models under the assumption that $T - T_0$ is small. However, because $T_m - T_0$ diverges at H_b this assumption becomes incorrect, and the approach based on Eqs. (5)-(7) in which no such assumptions are made is more adequate. The behavior of $Q(H_0)$ shown in Fig. 4 looks similar to that observed on high-performance Nb cavities. However, because the calculated H_b turns out to be of the order of H_c, one needs to take into account the nonlinear correction in R_s, as shown below.

3.3.4.2   *Nonlinear Surface Resistance*

The effect of nonlinearity of the surface resistance on the thermal breakdown can be taken into account by using R_s given by Eq. (2) in Eq. (6). This gives the following bi-quadratic equation for H_0:

$$\left[1 + C\left(\frac{\Delta}{T_m}\right)^2 \left(\frac{H_0}{H_c}\right)^2\right] H_0^2 = \frac{2\alpha\kappa(T_m - T_0)T_m}{A\omega^2(\kappa + \alpha d)} \exp\left(\frac{\Delta}{T_m}\right), \qquad (10)$$

where the residual resistance is neglected. The qualitative behavior of $H_0(T_m)$ described by Eq. (10) appears to be very similar to that of the linear model shown in Fig. 3. Likewise, the thermal breakdown occurs at the field H_b which corresponds to the maximum of $H_0(T_m)$ at $T_b \approx T_0 + T_0^2/\Delta$ for $T_0 \ll \Delta$. Substituting this T_b into Eq. (10) and solving the quadratic equation (10) for H_b^2, we obtain the thermal breakdown field with the account of the nonlinear pairbreaking effects:

$$H_b^2 = \frac{T^2 H_c^2}{2C\Delta^2}\left(\sqrt{1 + \frac{4C\Delta^2 H_{b0}^2}{T^2 H_c^2}} - 1\right),\tag{11}$$

where H_{b0} is the linear breakdown field given by Eq. (9). For poorly cooled samples for which $(2\Delta H_{b0}/TH_c)^2 C \ll 1$, Eq. (11) reproduces the linear result (9), otherwise Eq. (11) shows that the nonlinear effects reduce H_b as compared to Eq. (9). This reduction of H_b results from enhanced surface resistance and RF dissipation caused by the nonlinear term in Eq. (2).

Shown in Fig. 5 is the comparison of the behaviors of $Q(H_0)$ predicted by linear ($C = 0$) and nonlinear models at the same values of the parameters.
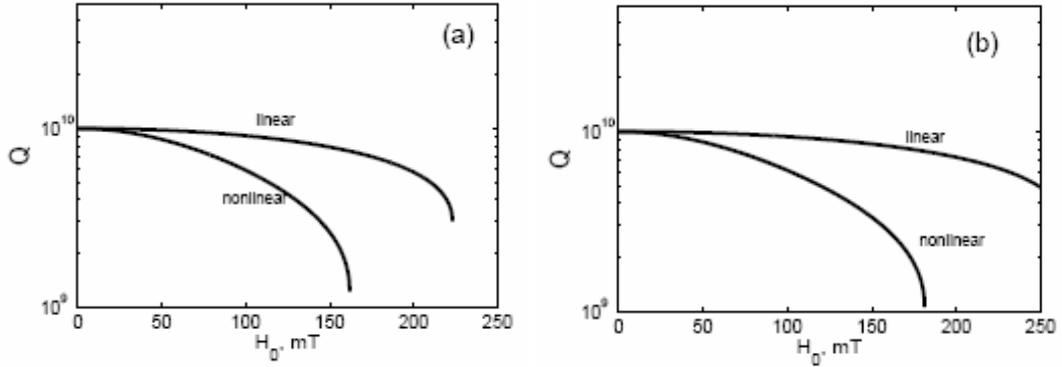
Figure 5: (a) Comparison of the behaviors of $Q(H_0)$ for linear and nonlinear models for the same materials parameters as in Fig. 4 at $T_0 = 2K$ and $R_0 = 0$. (b) Same as in (a), except that the Kapitza coefficient α is doubled, from 0.5 W/cm^{2}K to 1 W/cm^{2}K.

As clearly seen from Fig. 5, the nonlinearity reduces the breakdown field H_b and increases the Q slope. As a result, the ratio $Q(0)/Q(H_b)$ noticeably increases, from ~ 3 for the linear model to ~ 10 for the nonlinear model. The beneficial effect of a lower Kapitza resistance is also apparent.

3.3.5 Discussion

The thermal breakdown model of the Meissner state developed in this work gives a self-consistent description of the $Q(H_0)$ dependence, including the breakdown field H_b. Here the calculated values of H_b turn out to be consistent with those observed on high-performance cavities even without invoking enhanced dissipation on defects, or vortex penetration. The main feature of this model is that even weak overheating caused by RF field can trigger thermal runaway instability. This behavior is somewhat similar to the well known flux jump thermomagnetic instabilities [9] or thermal instabilities of current

flow around defects in superconductors with strong pinning [10]. Although the surface resistance for clean superconductors with $\ell \gg \lambda$ is independent of the mean free path, purifying the material can significantly increase the breakdown field H_b due to increase of thermal conductivity. Furthermore, the pairbreaking nonlinear correction to the surface resistance becomes essential at peak fields H_0 of the order of H_c, resulting in a significant increase of the high-field Q slope. At low H_0, $\ll H_c$, the apparent nonlinear surface resistance, which takes into account both isothermal pairbreaking and heating effects, can be written in the conventional form

$$ R_s = R_{s0}\left[1 + \gamma\left(\frac{H_0}{H_c}\right)^2\right], \qquad \gamma = C\left(\frac{\Delta}{T_0}\right)^2 + \frac{(\kappa + \alpha d)H_c^2}{2\alpha\kappa}\frac{\partial R_{s0}}{\partial T_0} \qquad (12) $$

where the factor γ is the sum of BCS pairbreaking and thermal contributions. However, Eq. (12), which usually describes well the observed quadratic dependence of $R_s(H_0)$ at small H_0 [15], can only be used for H_0 not too close to the thermal breakdown field H_b. For $H_0 \approx H_0$, higher order terms in $R_s(H_0)$ become important so one has to use general Eqs. (2) and (10), which describe self-consistently both thermal and pairbreaking effects for all $H_0 < H_b$.

In this work we took into account only the second order field correction in the isothermal nonlinear surface resistance (2). As H_0 approaches H_c, higher order terms become increasingly important, eventually resulting in the change from the quadratic to a much stronger exponential dependence of R_s on H_0. These effects would further increase the high-field Q slope if H_b turns out to be close to H_c At such high fields other mechanisms of RF nonlinearity become important, most notably networks of grain boundaries and other surface defects which provide easier "gates" for vortex penetration and dissipation channels [6].

All numerical calculations of this work were performed by taking bulk superconducting parameters, thus ignoring a very real possibility that the superconducting gap or the critical field at the surface is different from the bulk values. This is particularly relevant to Nb, which has very complicated oxidized surface covered with layers of multiphase mixture of NbO, NbO_2, and Nb_2O_5 typically 3-10 nm thick [16,17]. These partly metallic phases and the impurity segregation near the surface may cause additional ohmic losses and the proximity effect suppression of Δ and H_c in the crucial surface layer of thickness $\lambda \approx 40$ nm. The gap profile $\Delta(x)$ is particularly important for the BCS surface resistance because of its very strong exponential temperature dependence. For example, even a moderate 10% decrease of Δ on the surface would more than double $R_s \propto \exp(-\Delta/T)$ at 2K. The resulting variations of Δ can have a strong effect on cavity performance [18].

3.3.6 Acknowledgments

3.3.7 References

1.   D.C. Mattis and J. Bardeen, *Phys. Rev.* **111**, 412 (1958).

2. J.P. Turneaure, J. Halbritter, and H.A. Schwettman, *J. Superconductivity*, **4**, 341 (1991).
3. H. Padamsee, J. Knobloch, and T. Hays, *Superconductivity for Accelerators*, John Wiley & Sons, Inc. New York, 1998.
4. B. Visentin, Proc. 11th Workshop on RF Superconductivity, Lübeck/Travemünde, Germany, 2003, paper TuO01 (http://srf2003.desy.de/).
5. M. Tinkham, *Introduction to Superconductivity*, McGraw-Hill, New York, 1985.
6. J. Halbritter, Proc. of the 10th Workshop on RF Superconductivity, Tsukuba, Japan, 2001, paper MA006 (http://conference.kek.jp/SRF2001/).
7. V.G. Kurakin, Proceedings of the 4th European Particle Accelerator Conference, London, England, 1994, p. 2080.
8. E. Haebel, R&D Issues in Superconducting Cavities, TTF meeting, TESLA98-05, 60 (1998).
9. A.V. Gurevich, R.G. Mints, and A.L. Rakhmanov, *Physics of Composite Superconductors*, Begell House, New York 1997; A. Gurevich and R.G. Mints, *Rev. Mod. Phys.* 59, 941-999 (1987).
10. A. Gurevich, *Appl. Phys. Lett.* 78, 1891-1893 (2001).
11. P. Bauer, Review of models of RF surface resistance in high gradient niobium resonators for particle accelerators, Fermi Lab Report, TD-04-014, June 2004.
12. A. Gurevich, unpublished.
13. N.B. Kopnin, *Theory of Nonequilibrium Superconductivity*, Clarendon Press, Oxford, 2001.
14. J. Bardeen, *Rev. Mod. Phys.* 34, 667 (1962).
15. C. Benvenuti, S. Calatroni, I.E. Campisi, P. Darriulat, M.A. Peck, R. Russo, and A.-M. Valente, *Physica* C 316, 153 (1999).
16. C.Z. Antoine et al., Proc. of the 11th Workshop on RF Superconductivity, Lübeck/Travemünde, Germany, 2003, paper ThP05 (http://srf2003.desy.de/).
17. P. Kneisel, Proc. of the 11th Workshop on RF Superconductivity, Lübeck/Travemünde, Germany, 2003, paper TuO02 (http://srf2003.desy.de/).
18. K. Saito and P. Kneisel, Proc. of the 9th Workshop on RF Superconductivity, Santa Fe, New Mexico, USA, 1999, pp. 277-282.

3.4   A Magneto-Optical Investigation of Niobium for Super-conducting RF Cavities

Anatolii Polyanskii[1], Pierre Bauer[2], Peter J. Lee[1], Cristian Boffo[2], Helen Edwards[2],
Alex Gurevich[1], David Larbalestier[1], Alex Squitieri[1]
[1] Applied Superconductivity Center, Univ. of Wisconsin at Madison, USA
[2] Fermilab, Batavia, Illinois, USA
mail to: pbauer@fnal.gov; lee@engr.wisc.edu

3.4.1   Abstract

To gain a better understanding of the superconducting properties of the niobium used in SRF cavities, a combination of magneto-optics and magnetization and surface analysis with electron microscopy were applied to samples of high purity

3.4.2   Introduction

In the framework of the R&D effort in support of the future International Linear Collider (ILC) project, we are studying the superconducting properties of Nb for SRF

cavities using different experimental techniques, such as magneto-optics, magnetization and surface analysis with electron microscopy. Magnetization and magneto-optical (MO) measurements reveal how magnetic vortices penetrate the niobium. This is important since the penetration of small numbers of flux lines into the cavity surface during RF operation is a possible mechanism causing Q-drop or quench. These phenomena are particularly relevant given the recent decision to set the ILC design gradient at ~35 MV/m (or ~150 mT peak surface magnetic field on the cavity surface). The MO imaging of DC flux penetration is the first step towards the understanding of flux penetration in RF fields. The Nb samples were selected to model the material and surface condition found on the side of the cavities exposed to RF fields, such as samples representative of the weld region as well as the rest of the cavity surface. Samples were cut from polycrystalline, rolled sheets as well as from a quasi single crystal disc with large grains cut directly from an ingot as kindly provided by JLab. The following discusses the results of the magnetic characterization of these samples. The data and figures were taken from previous publications submitted to the proceedings of the "Pushing the Limits of RF Superconductivity" workshop at Argonne National Lab in Sept. 2004 [1], and the RF Superconductivity workshop at Cornell University in July 2005 [2,3].

3.4.3 Description of the Samples

Many different types of samples were made from high purity niobium (RRR 300) with small grain substructure after rolling (Wah-Chang) and with large grains directly from the ingot (CBMM). The wrought material (2-3 mm thick), is characterized by a linear intercept grain size of ~ 50 microns. We also included weld-samples, i.e. samples cut from an e-beam weld from two poly-crystalline Wah-Chang plates. The weld samples were characterized by large (~ 1 mm) grains grown during the melting of the material during welding. The weld samples were also characterized by deep grain-boundary grooving. Pictures of all these types of materials are shown in Figs. 1 and 2. The samples were mostly cut from sheet by electro-erosion. In some cases they were machined or cut with a diamond saw. They were subsequently processed in the same way as the inner cavity surfaces, including various etchings and heat treatments. The only (but notable!) exception is that the Wah-Chang sheet material was not mechanically deformed, as the cavity material is during deep drawing. The preparation steps comprised of two BCP (1:1:2) etching stages and high (~ 700-800ºC) as well as low (120ºC) temperature heat treatment. The first etching step removed ~ 100 microns and with it the mechanical defects introduced into the surface by rolling and wire erosion cutting or machining. The high temperature heat treatment served to outgas the hydrogen introduced into the material by the etching and to anneal the previously work-hardened material. The second, light etching step served to remove the surface contamination introduced by the heat treatment. The final, low temperature heat treatment served to emulate the so-called "baking," which is known to improve the high field SRF cavity performance. Rinsing with ultra-pure water and drying with filtered nitrogen, was always performed in a class 1000 clean-room. The samples were transported in polyethylene tubes containing dry nitrogen as buffer gas. The exposure of the samples to external atmosphere, especially following the heat treatment was thus kept to the minimum.
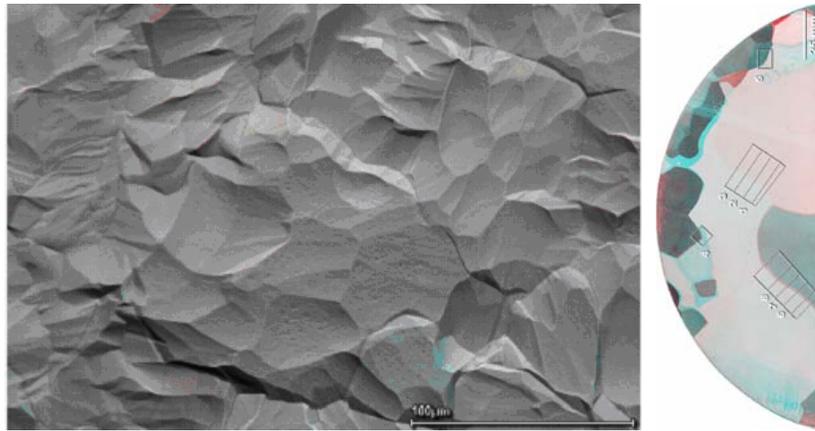
Figure 1: Left: 3D-SEM of polycrystalline Wah-Chang sheet after processing; Right: light microscopy of large grain disc from CBMM.
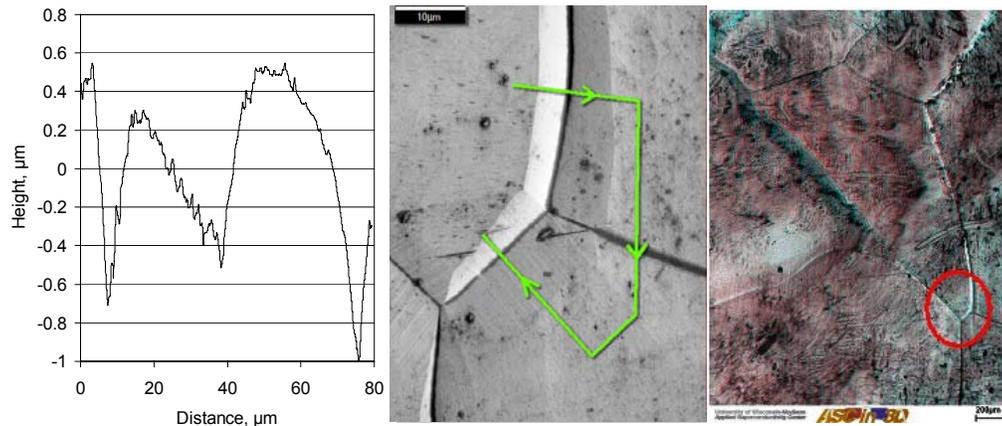
Figure 2: Left: Grain boundary profile along arrowed line in middle figure in weld sample (right figure) obtained with MEX[2]. Middle and Right: 3D SEM zoom into weld sample.

3.4.4   Magnetization Measurements

DC magnetization provides a quantitative measure of the average magnetic and superconducting properties of the bulk-material. Such magnetization measurements were performed at Fermilab by flux integration and at ASC/UW by Vibrating Sample Magnetometry (VSM). For the Fermilab measurements the samples tested were obtained by deforming the sheet material into long, hollow cylinders. This step introduced strong cold working into the material, not unlike in the deep-drawing stage of the fabrication of the cavities. The VSM technique could be used with the same rectangular samples cut from sheet as used in the MO imaging. Magnetization curves obtained at Fermilab are shown in Fig. 3. They clearly reflect the expected type II

---

[2]   Example of profilometric measurement using MEX, demo provided by A. Groeber / Alicona Imaging GmbH.

behavior, with flux penetrating into the bulk at the lower critical field H_{c1}. Pinning of vortices leads to an irreversible magnetization component and hysteresis. The pinning is reduced following the 100 micron BCP etching and heat treatment (5 hrs, 800ºC). This is expected as those treatments remove the mechanically damaged layer on the surface and further anneal the material. Interestingly, the upper critical field H_{c2} is not changed by this treatment. This indicates that the mean free path in the bulk was not affected by the heat treatment (the fact that the RRR also remained unchanged further corroborates this fact). This indicates that most of the pinning actually occurs at the surface. The H_{c2} values found (~ 287 mT) are slightly higher than expected, further indicating enhanced defect and/or contamination density in the surface. The small bump of the magnetization curve just below H_{c2}, especially in the before annealing case, is thought to be due to the enhanced surface H_{c2}.

The lower and upper critical fields were extracted from the curves shown in Fig. 3. The critical fields at 4.2 K are $\mu_0 H_{c1}$~140 mT, $\mu_0 H_{c2}$~285 mT. The measured 4.2 K values were used to calibrate a standard function describing the temperature dependence of the critical fields. Using this function[3] (see Fig. 3, right graph) the critical fields at 6 K become $\mu_0 H_{c1}$~88 mT, $\mu_0 H_{c2}$~177 mT. At 7 K they are $\mu_0 H_{c1}$~59 mT, $\mu_0 H_{c2}$~118 mT. The important parameters derived from the magnetization measurements helped us interpret the magneto-optical measurements. Also shown in Fig. 3 is the MO penetration field, i.e. the field at which flux first penetrates into the samples, for a "regular" MO sample (see Fig. 5).
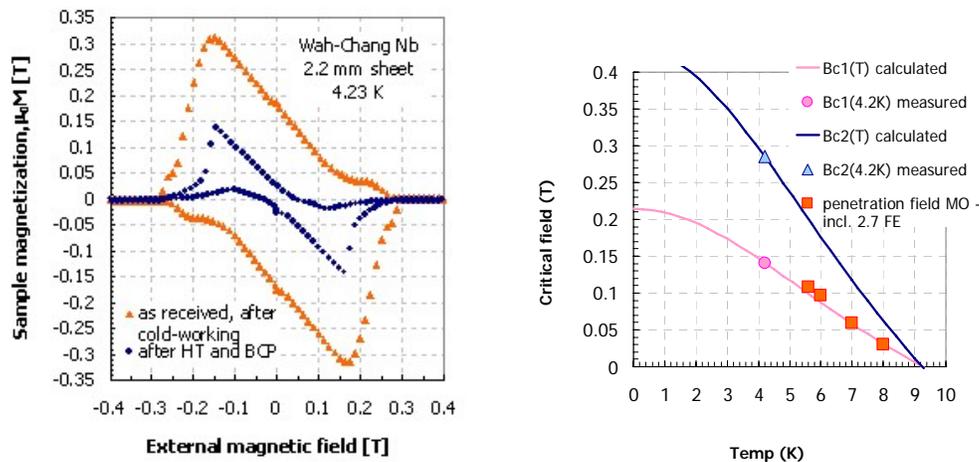
Figure 3: Left: Magnetization measured on samples of niobium for the Fermilab SRF cavities before and after annealing. Right: Calculated extrapolation of critical magnetic fields to higher temperatures. Also shown are the fields at which magnetic flux first penetrates the magneto-optical samples (multiplied by the calculated field enhancement (FE) factors for the MO measurements). The corresponding magneto-optical measurements are shown in Fig. 5.

3.4.5 Magneto-Optical Measurements

The magneto-optical (MO) technique is described in detail in [4]. It uses the strong Faraday effect in YFe garnet to measure the vertical magnetic field component above a

---

[3] $H_c(t) = H_c(0) (1-(T/T_c)^2)/(1+(T/T_c)^2)$, with $T_c = 9.25$K.

sample, in this case of superconducting material. The spatial resolution attained is ~5-10 microns. This is also the depth below the surface to which the technique is sensitive. The ~1 micron thin garnet is placed on the face of the sample to retain the highest possible sensitivity. The technique is able to resolve fields of the order of 1 mT. The sample is typically a 5×5 mm^2 rectangle (~ 2 mm thick). Via indirect cooling with a cold finger containing liquid helium, the sample temperature was held at temperatures between 5.6-7 K. An external solenoid is used to apply a vertical magnetic field on the sample. Figure 4 also shows the calculated vertical field distribution above a perfectly superconducting sample ($H < H_{c1}$). In the so-called Meissner state the superconductor expels all flux with a strong surface current flowing along the thin edges around the sample. In this condition strong field enhancement of up to a factor 2.7 (for a 2-mm-thick sample) was found with a finite element model for the edge mid-points of the $5 \times 5 \times 2$ mm^3 sample. The field enhancement is reduced in the corners, producing the very characteristic field penetration pattern that will appear in the following figures. This enhancement factor needs to be taken into account when choosing the external field strength during a test. Combining DC magnetization with MO measurements for the same samples allows one to eliminate uncertainty related to the geometrical field enhancement. The magnetization measurement also facilitates detection of anomalous (i.e., nonuniform) field penetration.
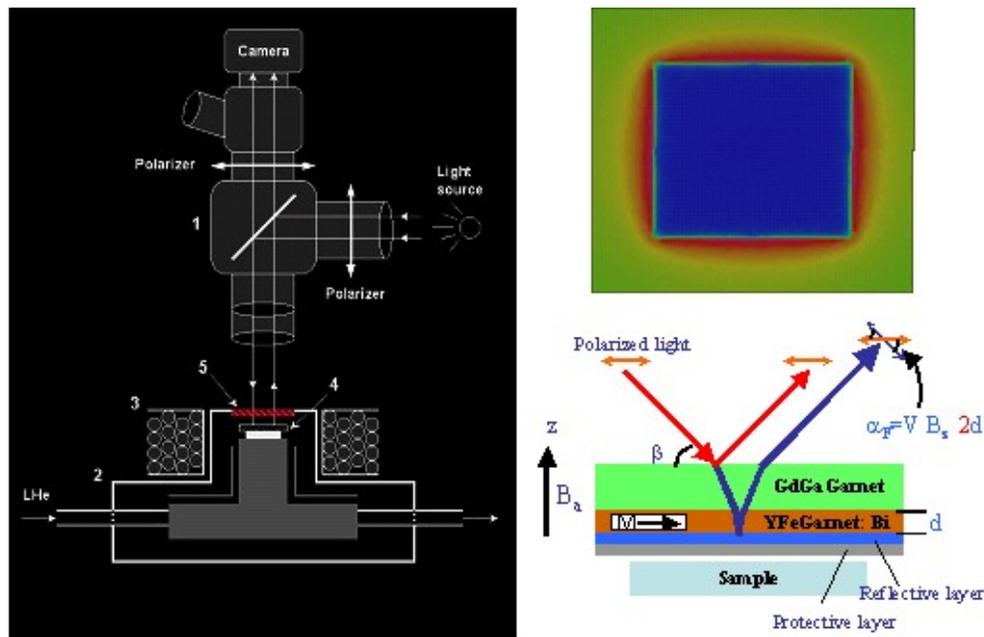
Figure 4: Left: MO setup at the UW ASC. Right top: finite element model calculation of the vertical field on top of a superconducting sample in the Meissner state. Due to geometry related field enhancement, the field is strongest at the mid-points of the four edges. Bottom right: principle of MO.
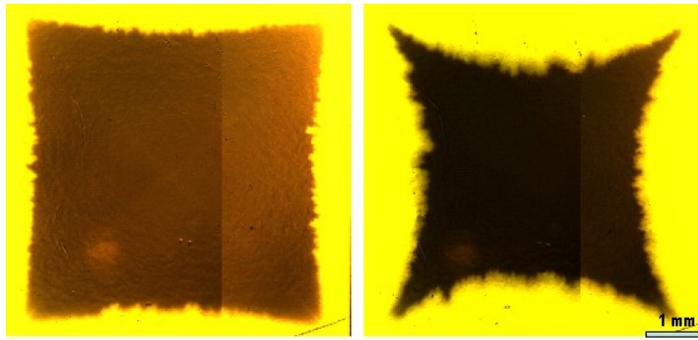
Figure 5: MO measurement of polycrystalline Wah-Chang sheet material in increasing external field at 6 K; left: 60 mT, right: 80 mT.

Figure 5 shows the results of magneto-optical measurements on a sample of polycristalline sheet material after a full sequence of processing including a strong etch, a high temperature heat treatment and a light etch. Considering the magnetization measurement on similar material in Fig. 3, one can conclude that the applied fields (taking into account geometrical field enhancement) in the MO plot in Fig. 3 are slightly (left case in Fig. 5) or significantly (right case in Fig. 5) above H_{c1}[4]. Above Hc1 magnetic flux lines (vortices) are thermodynamically stable inside the sample. In the absence of a surface barrier the vortices then penetrate the material, a process that is accompanied by a reduction of the Meissner surface current in the edges and penetration of currents further into the bulk. The boundary between the dark, field- and current-free and the light area is pushed further inward as the external magnetic pressure increases. The depth of penetration is related to the density and strength of vortex pinning centers (and thus the pinning critical current density). The shape of the field penetrated (light) region in Fig. 5 clearly reflects the increased field enhancement in the edge mid-points. An interesting feature of the result is the irregular pattern on the fringes of the flux free regions. The characteristic spatial dimension of those features is consistent with the surface roughness on the sample thin edges, which causes local increase of field enhancement as well as modulates the edge contour.

Although most magneto-optical measurements performed in the context of this study show more or less uniform flux penetration such as in Fig. 5, we also found some instances in which the field penetration was clearly non-uniform. Some of these cases were discussed in recent publications [1-3]. One of the samples cut from a large grain material (the large grain bi-crystal sample 1) is shown in Fig. 6. The sample was mechanically polished before the measurement. The MO image clearly shows irregular flux penetration, with the flux reaching deeper into the grain boundary than into the bulk. As also shown in Fig. 6 the grain boundary is almost vertical (Fig. 6c, 9°) in this case. The step at the grain-boundary is hardly noticeable (Fig. 6b, < 1 micron). The external magnetic fields at which the MO pictures were taken are also given in Fig. 6. These fields are small and could be below H_{c1}, even after taking into account geometrical field enhancement. The combination of magnetization and magneto-optical

---

4   Note that vortex penetration is not expected at fields below the thermodynamic critical field, $H_{c,therm}$, in a "perfect" superconductor. Field penetration at the lower critical field, H_{c1}, as observed here, indicates the presence of effects reducing the surface barrier, such as field enhancement on grain edges.

measurements eliminates uncertainties related to geometrical magnetic field enhancement, since in both measurements the magnetic field is applied in the same way. Figure 7 shows that in the large grain bi-crystal sample 3a (which features the same grain boundary as sample 1), the flux penetration occurs at fields close to or slightly exceeding H_{c1} [2]. The measurement was performed on the as received sample following a light mechanical polish. The irregular flux penetration above H_{c1} would point to differences in vortex pinning strength between grain boundary and bulk. It is not unexpected that magnetic vortices are particularly mobile when aligned with the grain boundaries, as the pinning forces are lowest in that configuration. Although the question of whether the field penetration is premature (= below H_{c1} of the bulk or surface) cannot be resolved unambiguously, both these measurement results show one thing clearly: the surface barrier is mostly suppressed, as evidenced by the flux penetration occurring close to H_{c1} and as evidenced by the smooth transition from the Meissner to the mixed state in the magnetization data. This transition occurs approximately at the point at which the virgin curve "turns over."
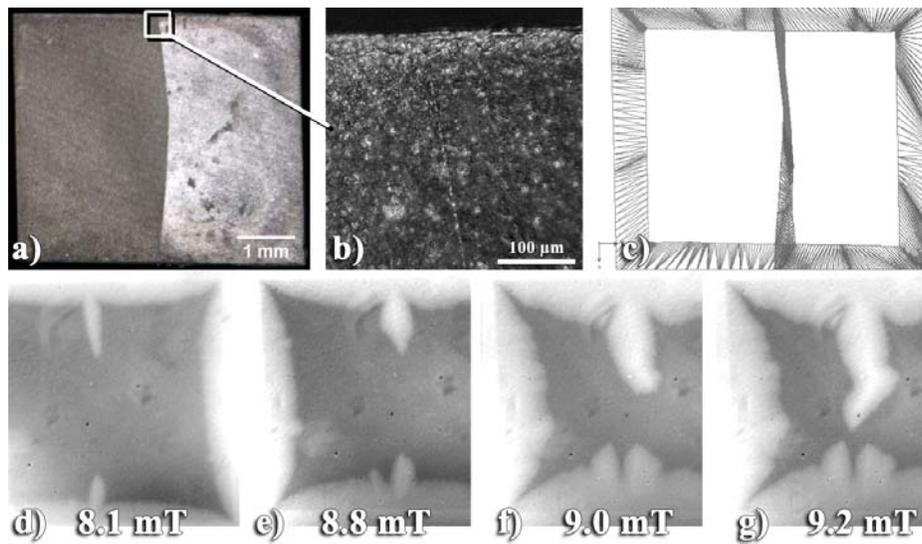
Figure 6: Bi-Crystal #1 a) with b) a height map detail from the area indicated, showing sub 5 µm topography at the grain boundary and c) a 3D model of the bi-crystal showing that the boundary is almost vertical. A series of MO images, d)-g), at increasing field (T=5.6 K ZFC), shows preferential flux penetration at the grain boundary.
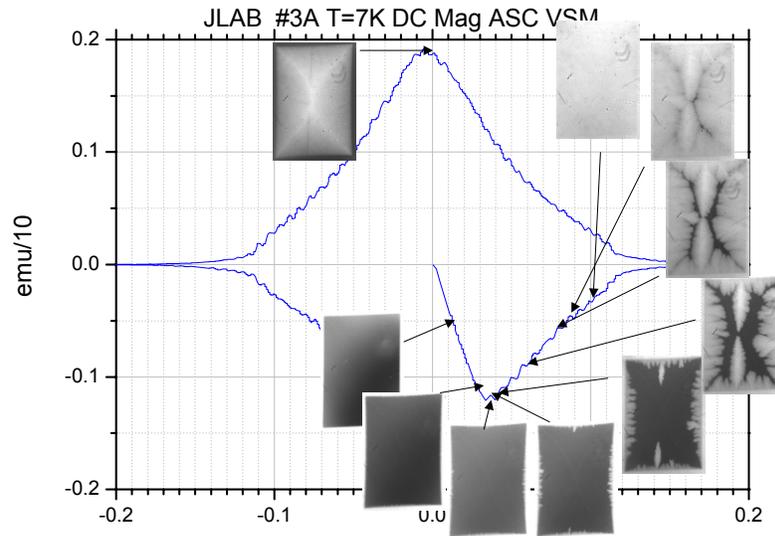
Figure 7: MO measurement of large grain bi-crystal sample 3a in different external fields at 7 K combined with a magnetization measurement obtained on the same sample. Sample dimensions: 4.67 mm width, 3.35 mm length, 0.34 mm thickness; External magnetic field in T, magnetization in emu.
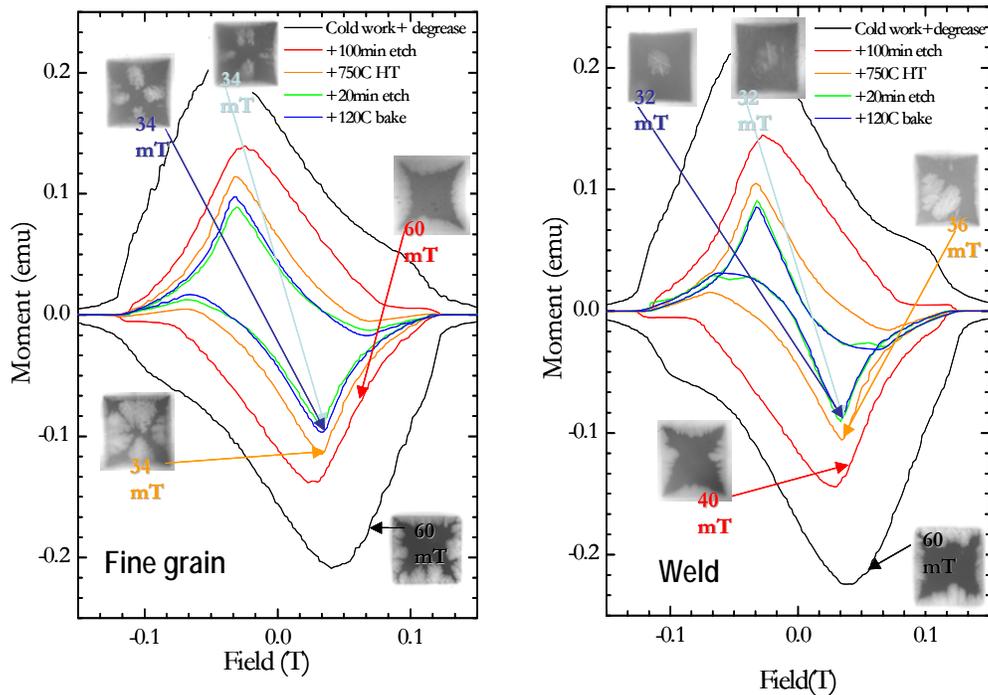
Figure 8: MO and magnetization measurements of polycrystalline regular and weld type samples along the cavity processing route. Left: regular material, Right: weld material; Sample dimensions: 2.75 × 2.75 × 1.5 mm.

Figure 8 shows that the non-uniform flux penetration above H_{c1} is exacerbated as the material is processed further along the cavity-processing route [3]. The figure also

shows that the irreversible component (i.e., the width of the hysteretic loop) in the magnetization is reduced at the same time. This was already seen in earlier studies [5]. Both these results indicate that vortex pinning is progressively reduced in the grain boundary, first as the mechanical damage layer is removed, then as the material is annealed (and hydrogen removed) and etched further. The final, low temperature heat treatment step does not seem to affect the bulk pinning properties further, since it is a treatment that can only affect a very thin (< 1 micron) surface layer. The measurements shown in Fig. 8 were obtained on samples made from polycrystalline sheet as well as welded polycrystalline sheet material.

As briefly mentioned before, the sample surface topology can also affect the outcome of the magneto-optical measurement. Variations of film to sample distance, for instance, as a result of >10 micron size topological features of the sample would modulate the MO-result accordingly. In this case the vertical field component would appear to be lower in deeper lying regions because of the larger distance to the detector film. For > 100 micron topology features (e.g., deep machining marks), when the surface topology significantly affects the sample thickness, one also expects a deeper flux penetration because of the reduction of total cross-sectional, forcing the pinning current to flow over a wider area (and thus penetrate deeper into the sample). None of these effects, however, were found to be dominant in the results discussed above.

3.4.6   Discussion

Combined magnetization and magneto-optical analysis of high purity Nb for SRF has provided the following results:

1. MO imaging shows non-uniform flux penetration in high purity Nb for SRF including large and small grain as well as weld type material. In large grain samples the role of grain boundaries in the preferential penetration of flux is shown. This behavior occurs at fields close to H_{c1}, indicating suppression of the surface barrier to flux penetration. Possibly first penetration also occurs below the bulk H_{c1}.
2. The "optimization" (strong BCP etch, heat treatment at 700-800°C, light BCP etch, 120°C bake) reduces global magnetization hysteresis (much of which comes from the surface) but enhances non-uniform flux penetration. Cavity performance is well known to improve after application of chemical etching processes similar to those used here. Our study does show that such treatments are capable of reducing vortex pinning, in particular in grain boundaries.

We also believe that we can exclude topological effects to be the cause of the MO flux penetration patterns found. Further studies are needed to understand the implications of the above findings for the high-field RF case. There are two related issues, which are believed to impact the cavity RF performance: Meissner current blocking effects, e.g. in grain boundaries or "premature" vortex penetration in areas of reduced superconductivity. Figure 9 is showing the "signature" of a current blocking effect in an MO result. We found no case being that clear cut. Also the screening of the data for evidence of premature flux penetration is still ongoing.
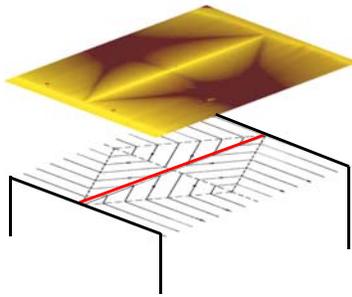
Figure 9: "Signature" of a current blocking effect in a vertical field MO measurement.

3.4.7 References

1. P. Lee and P. Bauer et al., "An Investigation of the Properties of BCP Niobium for Superconducting RF Cavities," Proc. of the Pushing the Limits of RF Superconductivity workshop, Argonne National Laboratory Report ANL-05/10, Kwang-Je Kim and Catherine Eyberger, Eds., pp. 84-93, March 2005.
2. P. J. Lee, A. A. Polyanskii, A. Gurevich, A. A. Squitieri, D. C. Larbalestier, P. C. Bauer, C. Boffo, H. T. Edwards, "Grain Boundary Flux Penetration and Resistivity in Large Grain Niobium Sheet," to be published in the 2005 RF Superconductivity workshop proceedings, Cornell University.
3. A. A. Polyanskii, A. A. Squitieri, M. C. Jewell, P. J. Lee, A. Gurevich, D. C. Larbalestier, P. Bauer, L. Bellantoni, C. Boffo, H. Edwards, Fermilab, Batavia, "Inhomogeneous Flux Penetration in Niobium Sheet Samples Across the Cavity Production Route," to be published in the 2005 RF Superconductivity workshop proceedings, Cornell University.
4. A. A. Polyanskii, D. M. Feldmann, and D. C. Larbalestier, "Magneto-Optical Characterization Techniques," *The Handbook on Superconducting Material*s, David Cardwell and David Ginley, Eds., Institute of Physics UK, p. 1551, 2003.
5. H. Bathe, F. Herrmann, P. Schmueser, "Magnetization and Susceptibility Measurements on Niobium Samples for Cavity Production," Proc. of the 8th Workshop on RF Super-conductivity, Abano Terme, Italy, V. Palmieri and A Lombardi, Eds., LNL-INFN-133-98, published in Part. Accel. 60 (1998) 121-134.

3.5 Field Emission Overview: Cleanliness and Processing

Detlef Reschke, DESY, D- 22603 Hamburg, Germany
mail to: detlef.reschke@desy.de

3.5.1 Abstract

Despite the substantial improvements of preparation and processing procedures during the last years, field emission still imposes the major limitation of high gradient superconducting (s.c.) accelerator structures. The key role for field emission free accelerator cavities plays the cleanliness of the inner surface. Contaminations like particles and chemical residues as well as surface irregularities have been identified as major sources of field emission. This paper shortly summarizes the present picture of field emission in s.c. cavities. The standard final cleaning and assembly procedures, alternative cleaning approaches as well as the effect of various processing techniques are discussed.

3.5.2   Introduction

Field emission is the major limitation of s.c. cavities for high gradient accelerator applications. Particles, surface irregularities and chemical contaminations like hydrocarbons have been identified to create field emission. This stresses the importance of the final cleaning and assembly procedures applied to the cavity and its auxiliaries. Moreover particular care has to be taken avoiding any recontamination during the subsequent cavity handling and the operation of the accelerator modules. Dedicated processing techniques during cavity test and/or operation often result in an improvement of the performance of a field emission loaded cavity.

When applying today's standard preparation procedures, typical field emission loading in well-prepared cavities at 1.3 GHz starts at gradients E_{acc} of (20–25) MV/m. No systematic degradation between vertical tests and horizontal results is found [1] in contrast to older results [2]. Single-cell cavities with their relaxed complexity of necessary components and assembly often achieve gradients far beyond 30 MV/m without field emission [3,4]. Recently at TTF an electropolished 1.3-GHz nine-cell cavity achieved 35 MV/m without field emission in beam operation [5] (Figure 1).
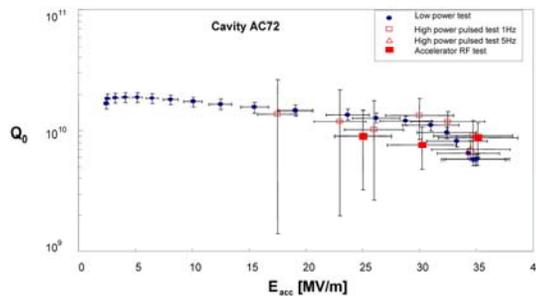
Figure 1: Q(E)-performance of the first 1.3-GHZ nine-cell cavity with E_{acc} = 35 MV/m in beam operation. No degradation between low power acceptance test and accelerator operation is observed.

3.5.3   Present Picture of Field Emission

A comprehensive overview of cavity related field emission is given in [6] and the references therein. The contributions to the RF Superconductivity Workshops show the historical development starting from 1980 up to now. Though a lot of well founded investigations were done in the last years, still our knowledge of the surface conditions is poor compared to semiconductor industry. Firstly the complex shape of cavities does not allow direct application of most of the powerful surface analysis techniques to the inner cavity surface. Secondly the SRF community is small in manpower and money compared to semiconductor industry.

The following chapter sketches the instruments used for field emission investigations, the nature of field emitters and their processing.
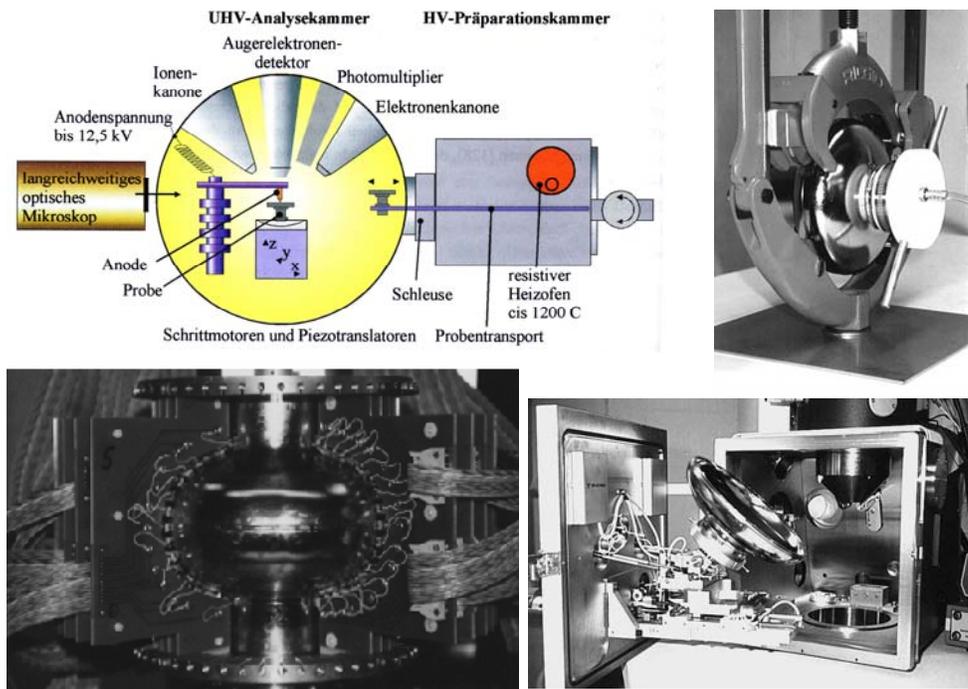
Figure 2: Sketch of the field emission scanning microscope at the University of Wuppertal (top left), temperature mapping system on 1.3-GHz single cell cavity (bottom left), apparatus for cutting and SEM investigation of 1.5-GHz cavities at Cornell (top + bottom right).

3.5.3.1 *Instruments*

During the last years a number of dedicated instruments have been developed for the investigation of field emission properties and its origin. The location of an individual field emission site and its characteristic properties (see below) in cavities can be analysed by temperature [7,8] (Figure 2) or x-ray [9] mapping techniques on the outer cavity surface. These methods use the heat and the Bremsstrahlung created by the emitted electrons hitting the cavity surface again. The complex shape of accelerator cavities prevents the application of most of the surface analysis techniques to the inner surface. For qualitative and quantitative FE investigations samples [10] or—as a destructive method—cut cavities have to be used [11] (Figure 2). Samples of a few-cm^2 size can be prepared and handled easily. Thus they are well suited for detailed qualitative analysis, e.g., in a field emission scanning microscope (Figure 2) equipped with SEM, Auger analysis, ion sputtering, spectral analysis of light, heating furnace, etc. Also samples are suitable for experiments with intentional contamination. Disadvantageous is their small surface area compared to a cavity resulting in a poor statistics for 'natural' emitters. The analysis of an RF tested and subsequently cut cavity gives highest correlation between the preparation procedure and the RF field emission characteristic. Though these experiments are very costly and work intensive, a continuation would be useful to deepen our understanding.

3.5.3.2 *Nature of Field Emitters*

Most field emitters are conducting (metallic) particles of irregular shape with a typical size of 0.5–20 µm. Investigations with DC field emission microscopes and samples in RF fields show that only 5–10% of the particles emit. Hydrocarbon contaminations of the surface caused by improper vacuum conditions also result in field emission. Both, DC and RF field emission are well described by the modified Fowler-Nordheim law:

$$I \propto S_{FN} \cdot \frac{(\beta_{FN}E)^2}{\Phi} \cdot \exp\left(-\frac{C\Phi^{3/2}}{\beta_{FN}E}\right) \tag{1}$$

with   I   emission current
        S_{FN} Fowler-Nordheim fit parameter
        β_{FN} Fowler-Nordheim field enhancement factor
        E   surface electric field
        Φ work function
        C   constant

The factor β_{FN} gives the local field enhancement at the emitter. Typical observed values vary between 50 and 500 [12]. Often emitters with a high β_{FN} can be modified by processing and the β_{FN} decreases resulting in a reduced field emission loading of the cavity. Practically the decrease of the Q-value is shifted to higher fields and the slope is reduced. Usually the Fowler-Nordheim fit parameter S_{FN} is not correlated to the physical size of the emitting particle or surface irregularity.

With some minor exceptions there is no substantial difference between the DC and RF field emission process.

After long and controversial discussions the present knowledge supports the tip-on-tip model as an appropriate explanation of the experimental observations. One major counter argument against the tip-on-tip model was the field enhancement factor, which does not exceed 10-20 for simple geometric structures. This is in contradiction to the measured values up to a few hundred, both in cavities and on samples. Experiments at Saclay [13,14] and Wuppertal [15] resulted in the idea and proof of a nm-scale microtip on top of a µm-sized particle (Figure 3), which explains the observed β_{FN} -values. Within this geometric model adsorbed gases and oxide layers play an important role modifying A_{FN} and β_{FN}. The observed activation of emitters between 200ºC and 800ºC is explained as a modification of the boundary layer between the substrate (Nb) and the particle together with a modification of the adsorbed gases on the particles. A major role plays the cracking of the isolating Nb_2O_5-layer and the formation of carbides, sulfides and graphite. Carbon is adsorbed out of the residual gas and sulfur is diffusing out of the Nb. These effects result in an enhancement of β_{FN} by a factor of 2-3 and of A compared to the pure geometrical field enhancement. Firing a Nb surface with emitting particles at > 1200ºC renders the surface emission free, which can be argued either by a smoothing of the jagged particle structure or by a strong influence of the interface between niobium and the emitter.

It should be noted that the 120ºC bake-out [16] is not expected to affect the field emission behavior, but the final confirmation is still missing.
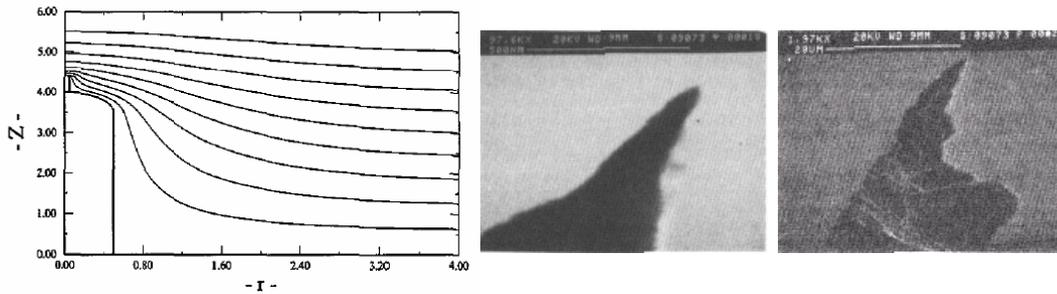
Figure 3: Calculated equipotentials for two superposed hemispherically capped cylindrical projections (left), SEM pictures of sharp emitting structures (middle, right) (courtesy of Saclay).

3.5.3.3 *Processing of Field Emitters*

During the operation of field emission loaded cavities or DC investigations of single emitters often processing takes place resulting in a deactivation or modification of the emitter. Mostly the emitter is destroyed or at least the onset field increased, but in some cases the emission becomes stronger or new emission sites are created. Processing in cavities can be distinguished between RF and helium processing using moderate RF power and cw-like operation and, on the other hand, high peak power processing, well known as HPP [17,18]. RF processing in its most simple way takes place during any operation of the cavity, especially during the first power run after preparation. To enhance the effectivity a partial pressure of pure and particle filtered helium gas can be used. HPP uses very high RF power, typically a few hundred kW up to MW, and short pulses of a few hundred μsec.

The various models [6] describing the processing effects partially vary significantly, thus I will concentrate on few main features. Fundamental for all explanations of processing is a high current density emitted by the emission spot. Following the simplest argumentation the high current density results in a strong heating of the emitter and its final melting and destruction. Many experimental observations can only be explained, if the adsorbed gases are taken into account. In case of helium processing often a slow modification of the emission behavior is observed, which can be interpreted as a modification of the adsorbed gases caused by the bombardment with helium ions. Partially this conditioning effect is reversible after a warm-up and cool-down cycle.

A conclusive model for HPP proposed by J. Knobloch [19] also starts with a high current density from a nm-scale emission spot, which leads to a local melting. New is the addition of a feedback loop resulting in the formation of a plasma above the emitter, which finally gives the energy to let explode the μm-sized particle. The plasma is also the origin of the characteristic post-processing signature ("star-burst") (Figure 4). Star bursts are only visible with a SEM and can be explained as modification of the surface oxide layer (fluorine depletion). The figures are known since the 18th century as Lichtenberg figures observed in discharging experiments.

Some processing results of cavities will be discussed in a later section.
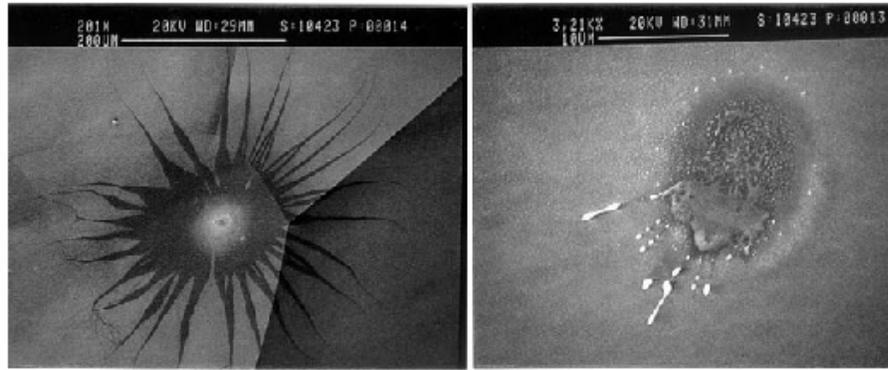
Figure 4: SEM pictures of a "star burst" (left) and an exploded emitter after HPP (courtesy of Cornell).

3.5.4 Standard Preparation Procedures

A particulate contamination can be chemically dissolved, thermally evaporated or physically removed. The latter is based on overcoming the sticking force of the particle at the surface and the subsequent transport out of the cavity. The basics of cleaning technology can be found in dedicated textbooks, e.g., [20,21]. An excellent discussion of cavity relevant aspects is given in ref. [22].

The following chapter will sketch the present cleaning and assembly technology. It follows closely the respective chapters of ref. [23]. A personal summary of open questions is listed at the end of this chapter.

3.5.4.1 *Final Chemical/Electrochemical Treatment*

Beginning with a number of excellent results on electropolished L-band single-cell cavities at KEK [3,24], the discussion of the superior surface treatment [25,26]— buffered chemical polishing (BCP) vs. electropolishing (EP)—came up again during the last years. At present the results of numerous single-cell cavities and nine-cell cavities support a higher reproducibility of gradients above 35 MV/m using electropolishing [3-5]. Explanations discussed for the superiority of EP are the differences in surface roughness, formation of oxide layers, etching at grain boundaries and residues of the used acids.

The commonly used EP mixture consists of HF and H_2SO_4 in a volume ratio of 1:9. For best removal of hydrogen, produced during the chemical reaction, a horizontal set-up is preferred. If a copper electrode is used, an additional oxipolishing with HNO3 and HF is necessary to remove copper traces from the niobium surface [4]. The standard BCP mixture contains $HF:HNO_3:H3PO_4$ in a volume ratio of 1:1:2. Typical for the final treatment is a removal of (10 - 40) μm of the niobium surface. After draining the acid, the cavity is rinsed immediately with water of at least DI-quality. For best removal of acid residues, typically the rinsing is performed in several steps ending with an ultra-pure water rinse ($\rho \geq 18$ MΩcm; particle filtered ≤ 0.2 μm). Both for BCP and EP closed, PLC controlled systems with integrated rinsing capability for DI or pure water are state-of-the-art (Figure 5). The used acid quality varies, but is often "pro analysi" or better. Additional particle filtration is often integrated in the chemical system.

Figure 5: Closed BCP facility at Jlab (courtesy of Jefferson Lab), EP facility at Nomura Plating (courtesy of Nomura Plating, Japan), EP facility at DESY.

3.5.4.2 *High Pressure Rinsing*

At present repeated rinsing with high-pressure ultra-pure water (HPR) is the most effective tool to avoid field emission loading [27,28]. Typically, HPR systems (Figure 6) work with a water flow between 7 l/min and 20 l/min and a pressure between (80-150 bar), which allows removal of particles larger than a few micrometer [22]. To avoid any recontamination, the cavity is rinsed in a clean room environment, in a glove box or is closed with protection flanges. Depending on the complexity of the assembly procedures, the number of rinses varies up to six times, e.g., the TTF nine-cell cavities are rinsed once after the BCP or EP treatment and additionally up to five times after the assembly of the flanges. The repeated rinses are advantageous in order to rinse out particles, which have been loosened off the cavity surface, but depending on the water flow conditions have been transported and redeposited inside the cavity. Experience at DESY showed that it is important to avoid drying before starting the first rinse. A possible explanation is that after drying particles stick stronger to the surface and removal becomes more difficult.

The technical installations like pump, piping, turntable and nozzle system differ widely and so are not described. It only should be stressed, that the final particle filter (pore size ≤ 0.2 μm) has to be placed as closely to the nozzle as possible with no moving parts (i.e., valves) between filter and nozzle.

Quality control aspects of HPR systems are twofold. Provided that the water system produces the desired pure water quality, the high pressure pump, valves and filter units can act as sources of contaminations (particles, hydrocarbons) of the high-pressure water in case of a component failure. An on-line measurement with respect to the above mentioned contaminations is highly desirable, but to my knowledge not realized in any lab. Secondly, it was tried to monitor the cleaning effect by measuring the particles rinsed out of the cavity using a particle counter [29] or a filter [30,31]. During the first HPR after BCP or EP a large amount of particles is rinsed out of the cavity. All materials used in the cavity preparation like rubber, copper, steel and even large particle up to >100 μm are found. In subsequent rinses the particle number decreases. At TTF it was tried to find a correlation between the number of particles rinsed out of the cavity during the final rinse to the onset of field emission in the first power run of the following vertical cavity test. Figure 6 shows data of 2003, which at least indicate a

trend. At JLab no correlation between particle numbers and cavity results was found [30].
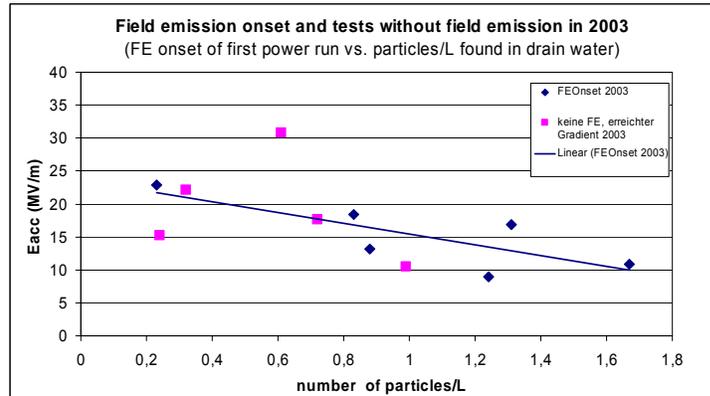
Figure 6: A rotational transformation.

3.5.4.3 *Assembly and Drying*

The importance of a contamination free assembly for a good cavity performance is beyond any doubt. Nevertheless it is often overlooked, that essential conditions for a contamination-free assembly are given by the design of all involved components long before the cleanroom actions start. An unsuited design results in difficult and inadequate cleaning as well as improper assembly conditions. Especially the flange connections and the gaskets attached to the cavity, which necessitate an easy handling as well as a reliable leak tightness, are of outstanding importance [32] (Figure 7).
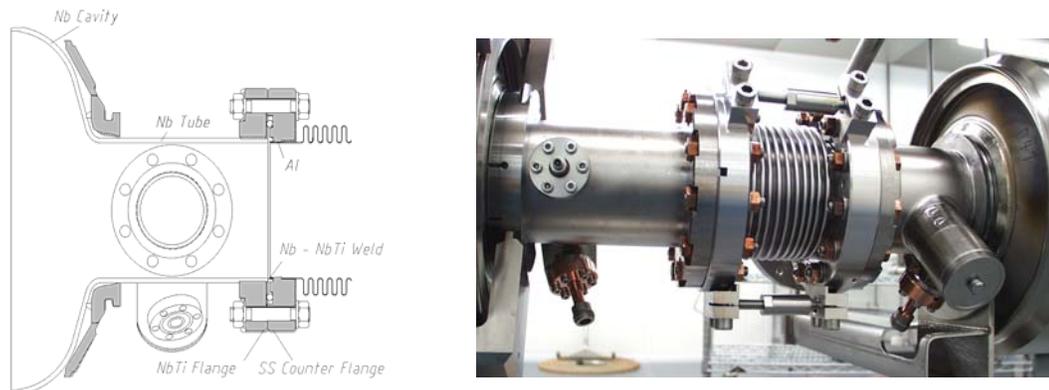
Figure 7: Flange design and bellow connection of the TTF cavities using NbTi-flanges and massive aluminum gaskets

After cleaning and drying, the cavity and its components are assembled in a cleanroom environment better than class 100 or a comparable glove box. Blowing off both, the components and tools, with pure ionized gas immediately before the assembly in front of a particle counter can be used as a good check for the particle contamination as well as a final removal of remaining particles. This is of particular importance during the final assembly of a cavity or the connection of cavities before beam operation, where no cleaning can be applied afterwards. It is evident, that the handling and

assembly time at an open cavity should be as short as possible. Finally, best design and cleaning will not help, if the cleanroom staff is not well trained and highly motivated.

Due to the enhanced sensitivity of a wet surface to particle trapping [33], the drying procedure requires highest cleanliness. Depending on the laboratory, the type of cavity, and the preparation status (cavity with open or closed flanges), different drying procedures are in use.

- Drying of an open cavity in a clean room environment better than class 100 or a comparable glove box requires minimum handling of the cavity.
- Drying by vacuum pumping is suited for a rinsed (and possibly pre-dried) cavity with assembled flanges and requires a water-resistant pumping station. An additional gas by-pass can improve the pumping conditions.
- Drying using a particle-filtered flow of pure gas needs additional handling and assembly, if a closed connection between cavity and supply line is required. The danger of recontamination has to be carefully considered to the gain in drying time compared to an open drying.

To accelerate the drying procedure, the cavity can be rinsed with alcohol, methanol, etc. or the temperature can be increased. Methanol rinsing was widely used with good results in the past, but at present it is to a great extent avoided due to handling and safety reasons. Moreover, the improved quality of the final water rinses made the additional cleaning effect of the alcohol dispensable. The realization of an increased temperature (T > 50-60ºC) in a high quality laminar flow gives substantial technical difficulties and is not applied up to now. In contrast, warming up a cavity during vacuum pumping under relaxed clean room requirements (> class 1000) is used in several laboratories with good success and lead to the discovery of the "baking effect."

After washing and rinsing, the components attached to the cavity are dried similarly to the above described procedures. Due to missing systematic investigations, no final comparative assessment of the drying procedures can be given. At TTF—depending on the state of preparation—open drying or open pre-drying in combination with vacuum pumping gives good results on single- and nine-cell cavities.

3.5.4.4   *Pumping and Venting*

To avoid any risk of a harmful hydrocarbon contamination, oil-free pump stations equipped with a helium leak detector and a residual gas analyzer are standard technique for the evacuation of s.c. cavities and accelerator modules [34]. Usually, after the installation of the modules to the accelerator, the beam vacuum is pumped by additional ion getter pumps.

The cleaning and assembly of vacuum connections inside the clean room are described above. Outside the clean room the situation becomes more difficult, but careful double-layer wrapping with anti-static foil, thorough manual cleaning (e.g. wiping with alcohol, blowing with pure gas) and the use of mobile local clean rooms allow clean vacuum connections. Though it is still common practice during the vertical cavity tests to connect the pump line partially without local clean rooms, this needs to be improved. In any case back streaming towards the cavity has to be prevented.

Venting is done using pure, dry and particle filtered nitrogen or argon gas to avoid contamination with particles and humidity [20]. Laminar venting prevents particle transport due to turbulences in the pump line and cavity (Figure 8). Closely related is the influence of various gases on the cavity performance. Unfortunately different investigations came to contradicting results [5,34], even for gases like nitrogen and

argon. Further tests are necessary. Without doubt is the harmful impact of hydrocarbons, i.e. caused by a defect of a conventional pump stand using an oil-sealed rotary pump.
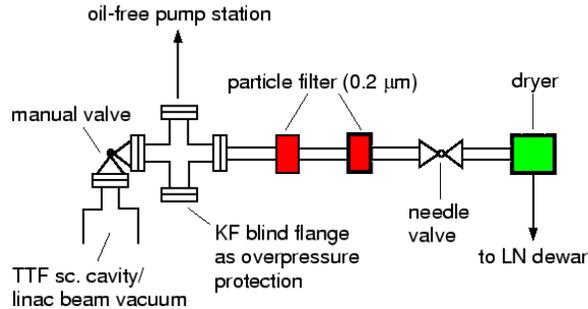
Figure 8: Schematic lay-out of the set-up used for venting of cleaned vacuum systems at TTF.

3.5.4.5   *Risks of Contamination*

The described cleaning steps and handling procedures have proven their suitability for good and reliable cavity performance during the last years. Nevertheless in some cases field emission at low gradients or a degradation of the cavity performance, e.g., between horizontal test and beam operation, occurs. Often the source of the contamination is hardly to determine after the event, but careful analysis of test results showed a significantly reduced onset of field emission gradient, if irregularities during preparation could be identified [31,35]. Typical irregularities are vacuum leaks, faulty assemblies and problems during chemical treatment or HPR. Furthermore the complexity of the preparation process hinders or prevents testing the influence of one individual step alone. A typical example is the high pressure rinsing, which is followed by at least drying and pumping.

Besides irregularities even the regular preparation process contains procedures, which hold a high risk of contamination. The TTF preparation procedure is taken as an example.

- During the TTF preparation the final HPR cleans a single cavity without its power coupler (HPR would destroy the gain of a former RF conditioning of the power coupler). Until beam operation it is necessary to disassemble and assemble three flange connections at each cavity without further possible cleaning. It is stressed that opening a bolt-nut connection is one of the strongest sources of particle contamination.
- There is a general risk of insufficient cleaning of the partially complex components, i.e., power coupler, gate valve, beam position monitors, etc., attached to cavity and accelerator module. A clean room compatible design is strictly required. During the horizontal assembly no further cleaning of the inner cavity surface is possible!
- After the final horizontal system test of a TTF cavity, the accelerator module has to be completed, equipped, transported and assembled to the accelerator. Depending on the exact procedures, up to five times evacuating and venting is necessary. Though extensive precautions are taken and there is no negative experience, the risk of particle contamination is present.

Some improvements, which partially require substantial new developments, are described in the next sections.

3.5.4.6 *Practical Consequences and Open Questions (Personal View)*

The first topics to be mentioned result from general rules of clean room work, practical experience of cavity preparation and common sense. In fact, they are less technical improvements than good laboratory practice, but nevertheless often ignored. As mentioned above, the design of all used components must be adapted to clean room requirements, i.e,. well-selected materials, good cleaning possibility, suited for easy handling and assembly. A good organization of the work flow as well as a suited design of the infrastructure simplify the preparation and avoid unnecessary actions. The treatments of each cavity inside and outside the clean room as well as the condition of infrastructure have to be documented. A complete documentation is essential for cavity data analysis and failure search. The cavity preparation has to be stopped in case of any preparation irregularity, which makes a successful RF test doubtful, and to be started again with an adequate cleaning.

The important question of the best choice of acid mixture for the EP or BCP surface treatment is still open and except of BCP 1:1:1, which shows some excellent results, only few investigations using alternative mixtures [29,36,37] are published. On the other hand pragmatically argued: Why looking for alternative acid mixtures instead of optimizing the proven ones? Rinsing with hot pure water ($T \geq 80$ºC) after etching or polishing can improve the removal of acid residues due to the high solubility. Experiences in high purity stainless steel tube production show a faster drying after hot instead of cold water rinse. Thus, the risk of recontaminating the sensitive wet surface of a cavity or component after the final (high pressure) rinse is reduced. Furthermore, the required purity and particle filtration of the acid mixture as well as the cleanliness of the preparation environment ("good" lab standard, clean room 10.000 or better?), especially for large-scale production, are still not finally settled.

The operation experience of various HPR systems during the last years suggests technical improvements as well as quality control requirements. Quality control aspects are already discussed in the above "High pressure rinsing" chapter. It is stressed again, that the check of the water quality i.e. the particle numbers as close to the nozzle as possible is of outstanding importance for a reliable preparation. The relevance of particle measurements of the drain water is still open. New clever ideas (e.g., particle concentration by deposition on Nb samples) are needed urgently. In HPR systems with moving spray cane, the cane is in contact with one or more bearings. Due to their signs of wear, this gives a high risk of contamination transport into the cavity. A design with fixed cane, enclosed bearings and all moving parts as far away as possible from the cavity is preferable. Though the outside of the cavity is cleaned while entering the clean room, an additional outside HPR maybe helpful to avoid contamination transport from the chemistry area to the cl.100 assembly area. This holds especially for multi-cell cavities with their complex shape. Obviously, a higher pressure than 100-150 bar, which is widely used at present, results in a reduced size of removable particles. Calculating the forces [22], the particle size decreases inversely to the square root of the pressure. Within the limits given by damaging the niobium surface [29] a gain of 30-40% reduction in particle size can be achieved theoretically.

The influence of storing a high performance cavity using typical gases like argon, nitrogen or clean room air is not fully explored yet (see "Pumping and Venting"), but good results were achieved for clean room air and nitrogen [5].

Finally the general avoidance of bolted flanges with their high risk of particle contamination should be mentioned. Though there are many unsolved questions, like for example how to realize an ultra pure welding procedure under clean room conditions, this option is it worth to be investigated further, especially for large scale applications. First tests with two 1.3 GHz seven-cell cavities connected by electron beam welding to a "superstructure" were successful [38].

3.5.5   Alternative Cleaning Approaches

Following the requirements of semiconductor industry a number of advanced cleaning techniques have been developed for smooth wafers [20-22]. Due to the complex shape of the inner surface most of them are not applicable to cavities. After first considerations and pilot tests only megasonic and dry-ice cleaning seem to have potential for cavity cleaning.

The principle of megasonic cleaning is similar to ultrasonic, but with frequencies around 1 MHz. The cleaning effect is based on high power pressure waves inside the cleaning solution less than on cavitation. Particles down to 0.1 μm can be removed from wafer surfaces. First cavity results showed promising results [39], but also the need to develop an oscillator applicable inside the cavity to realize a high transmission of megasonic power. The transportation of particles out of the cavity requires a high flow rate, which is no problem for an open cavity, but might need some technical effort for cavities with assembled flanges.

Dry-ice cleaning with CO_2-snow allows effective cleaning of sub-micron particles and film contamination by a combination of mechanical, thermal and chemical effects (Figure 9). The cleaning process acts local, mild, dry, without residues and requires no additional cleaning agent. Cleaning of niobium samples and first cavity tests show promising results [40]. As the particle transport is based on a gas flow out of the cavity, horizontal cleaning of cavities seems to be possible in contrast to HPR. Furthermore, the dry cleaning would preserve the effect of preconditioning of a RF power coupler attached to a cavity.

Figure 9: Test of the CO_2-snow nozzle system in a cut NbCu cavity.
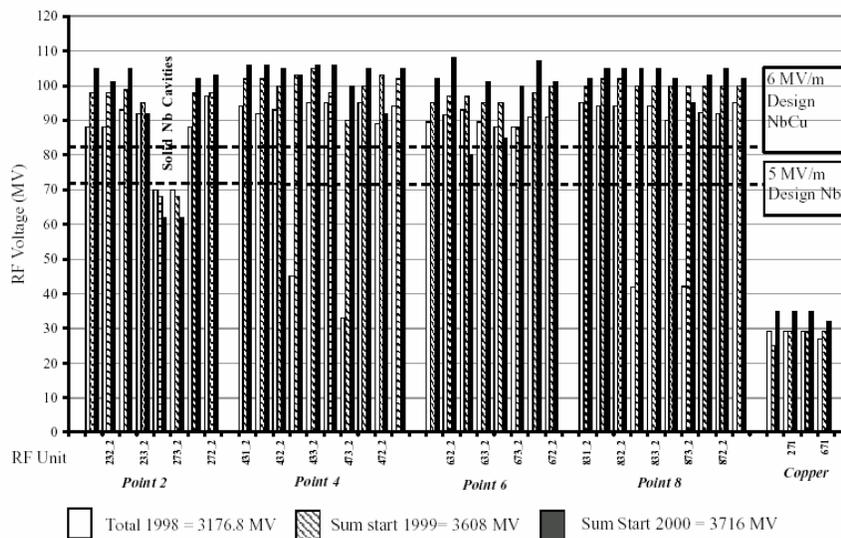
Figure 10: RF unit voltages after conditioning in 1998, 1999, and 2000 (courtesy of CERN).

3.5.6   Processing in Accelerator Structures

Nearly every cavity shows some processing in the first power run after the preparation procedure either in a vertical test or the horizontal accelerator operation. Usually after this initial processing or—in rare cases—activation the field emission properties are more or less stable as long as the cavity stays under clean vacuum conditions. After a clean and successful preparation no field emission is observable up to the individual quench limit of the cavity.

3.5.6.1   *RF Processing in LEP2*

Large-scale examples of the benefit of RF processing are the 272 NbCu-cavities of LEP2. After approaching the design gradient of 6 MV/m, additional successful processing periods increased the average gradient up to 7.47 MV/m in 2000 [41] (Figure 10). Both, pulse and cw processing have been applied. The benefit of in-situ helium processing on some severely degraded cavities was limited.

3.5.6.2   *High Peak Power Processing on TESLA Cavities*

HPP was applied successfully to several five- and nine-cell cavities both at Cornell and DESY. Starting from comparatively low gradients of (10-15) MV/m with heavy field emission loading an improvement to (20-28) MV/m took place (Figure 11) [42]. After HPP usually field emission was still present at enhanced field levels.
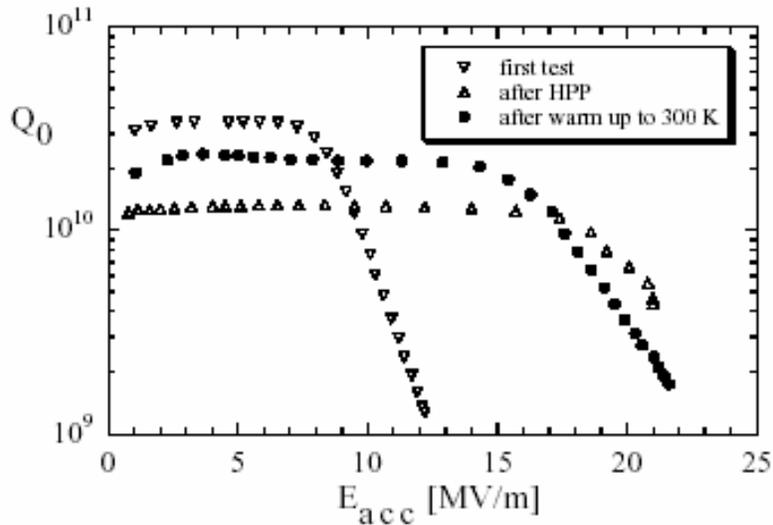
Figure 11: Cavity C19 before and after HPP. The Q_0 recovered partially after warm up to room temperature [42].

In few cases in-situ HPP on modules in the TTF linac was carried out. After the installation of module 2 only an integral check of all eight cavities operating at the same gradient was possible due to limited time. Applying the full TTF pulse (10Hz, 500/800 µs rise/flat-top time) 20 MV/m could be reached. The gradient was limited by coupler breakdowns. One cavity showed heavy field emission. This cavity was dominating the cryogenic losses of the whole module. Applying in-situ HPP to this cavity performance improved significantly. The heat load of module 2 with all cavities operating at 20 MV/m was reduced from 21 W to 6.5 W, corresponding to an average quality factor of $Q_0 = 6 \cdot 10^9$ [43] (Figure 12). The processed cavity still showed some field emission. By detuning of the cavity the heat load of the remaining seven cavities reduced to 2.9 W at 20 MV/m giving a Q_0 of $1.3 \cdot 10^{10}$.
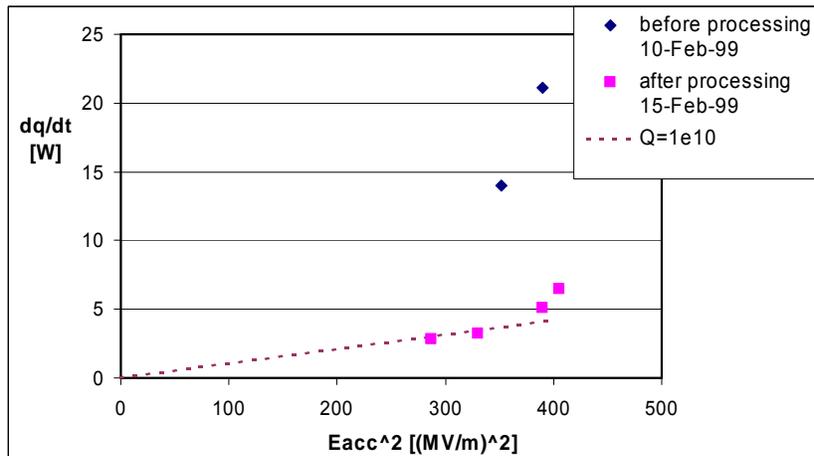
Figure 12: Heat load of module 2 before and after in-situ HPP.

3.5.6.3 *High Peak Power Processing at Gradients above 30 MV/m on TESLA Cavities?*

Detailed studies of HPP clearly indicate that for successful HPP the field during HPP needs to be 1.5 to 2 times higher than the desired operating field [16]. Hence a gradient of 30 MV/m requires (45–60) MV/m during HPP, which for the geometry of the TESLA cavities corresponds to a magnetic surface field of (188–251) mT. These field levels are in the order or above the critical magnetic surface field of the niobium, resulting in the hard limit of a thermal breakdown of the cavity. As the propagation of a thermal breakdown takes in the order of a millisecond, an effective HPP at high gradients requires comparatively short RF pulses. As calculated in Table 1 for a given gradient the required RF power for in-situ HPP increases substantially with decreasing pulse length. Assumed is a loaded Q-value of $3 \cdot 10^6$, which is dominated by the Qext of the current TTF coupler with its limited tuning range. Though no exact limitation for the application of HPP can be given, it seems to be difficult to exceed gradients of around 30 MV/m for the present design and technical boundary conditions of the TESLA cavities. This stresses again the need of excellent preparation and handling procedures for high gradient cavities.

Table 1: Necessary RF power for HPP depending on gradient and pulse length for $Q_L = 3 \cdot 10^6$.

Eacc [MV/m]	Pulse length [µs]		
	200	400	500
40	2.45 MW	0.79 MW	0.57 MW
60	5.5 MW	1.77 MW	1.28 MW
80	9.77 MW	3.15 MW	2.28 MW

3.5.7 Summary

The present picture of field emission in srf cavities is not complete, but well substantiated. Today's standard cleaning, handling and assembly procedures often allow an excellent cavity performance meeting the requirements of the next accelerator projects. Nevertheless field emission, resulting in undesirable dark currents, is still the main limitation, if usable gradients above 20 MV/m are required. Therefore further improvements of the standard preparation procedures as well as the development of alternative approaches are necessary. A decisive role plays the further development of efficient quality control procedures.

3.5.8 Acknowledgments

The author would like to thank all colleagues for their support with information, especially C. Antoine, P. Kneisel, D. Kostin, L. Lilje, R. Losito, W.-D. Moeller, H. Padamsee, K. Saito, and B. Visentin.

3.5.9 References

1. Editors: R. Brinkmann, K. Flöttmann, J. Rossbach, P. Schmüser, N. Walker, H. Weise; TESLA Technical Design Report, DESY 2001-011, ECFA 2001-209, TESLA Report

2001-23, TESLA-FEL 2001-05, 2001.

2. T. Furuya, "Preparation and Handling of Superconducting RF Cavities," Proc. of the 4th Workshop on RF Superconductivity, Tsukuba, Japan, 1989, p. 305.

3. M. Ono et al., "Achievement of 40 MV/m Accelerating Field in L-Band SCC at KEK" and K. Saito et al., "Superiority of Electropolishing over Chemical Polishing on High Gradients," Proc. of the 8th Workshop on RF Superconductivity, Abano Terme, Italy, 1997, p. 472.

4. L. Lilje et al., "Improved surface treatment of the superconducting TESLA cavities," Nucl. Instrum. Methods 516(2-3), 213 (2004).

5. L. Lilje et al., "Achievement of 35 MV/m in the superconducting nine-cell cavities for TESLA," Nucl. Instrum. Methods 524(1-3), 1 (2004).

6. H. Padamsee et al., RF Superconductivity for Accelerators, John Wiley & Sons Inc., Hoboken, NJ, 1998.

7. H. Piel, Proc. of the 1st Workshop on RF Superconductivity, Karlsruhe, Germany, 1980, p. 85.

8. J. Knobloch et al., Rev. Sci. Instrum. 65(11), 3521 (1994).

9. R. W. Röth, Thesis WUB-DIS 92-12, University of Wuppertal, 1993.

10. Several contributions to the Workshops on RF Superconductivity by Cornell University, Jefferson Lab, CEA Saclay and University of Wuppertal.

11. J. Knobloch, H. Padamsee, Proc. of the 7th Workshop on RF Superconductivity, Gif sur Yvette, France, 1995, p. 95.

12. T. Habermann et al., Part.Acc. 53, 77 (1996).

13. M. Jimenez et al., J. Phys. D 27, 1038 (1994).

14. R. Noer, Proc. of the 6th Workshop on RF Superconductivity, CEBAF, Newport News, Virginia, USA, 1994, p. 236.

15. N. Pupeter et al., Part.Acc. 61, 137 (1998).

16. B. Visentin, Proc. of 11th Workshop on RF Superconductivity, DESY, Lübeck/Travemünde, Germany, 2003, paper TuO01 (http://srf2003.desy.de/).

17. I.E. Campisi, IEEE Trans. Magn. 25, 134 (1985).

18. J. Graber, Nucl. Instrum. Methods in Phys. Res. A 350, 572 (1994).

19. J. Knobloch, H. Padamsee, Part. Accel. 61, 1998, [433-468]/169-204 (1998).

20. D. L. Tolliver ed., Handbook of Contamination Control in Microelectronics, Noyes Publications, 1988.

21. W. Kern ed., Handbook of Semiconductor Cleaning Technology, Noyes Publications, 1993.

22. P. Kneisel, B. Lewis, Proc. of the 7th Workshop on RF Superconductivity, Gif-sur-Yvette, France, 1995, p. 311.

23. D. Reschke, Proc. of the 10th Workshop on RF Superconductivity, Tsukuba, Japan, KEK Proc. 2003-2, 2003, p. 144.

24. K. Saito, "Recent Developments in SRF Cavity Cleaning Techniques at KEK," Proc. of the 9th Workshop on RF Superconductivity, Santa Fe, New Mexico, USA, 1999, p. 118.

25. P. Kneisel, "Surface Preparation of Niobium," Proc. of the 1st Workshop on RF Superconductivity, Karlsruhe, Germany, 1980, p. 27, and references therein.

26. D. Bloess, "Chemistry and Surface Treatment," Proc. of the 2nd Workshop on RF Superconductivity, Geneva, Switzerland, 1984, p. 409.

27. Ph. Bernard et al., Proc. of the 3rd European Particle Accelerator Conference, Berlin, Germany, 1992, p. 1283.

28. P. Kneisel et al., Proc. of the 6th Workshop on RF Superconductivity, Newport News, Virginia, USA, 1993, p. 628.

29. D. Bloess, CERN, private communication.

30. J. Delayen et al., Proc of the 2004 Linear Accelerator Conference, Lübeck, Germany, 2004, p. 226.

31. D. Reschke, "New Aspects of Quality Control during Preparation of TTF 1.3GHz

Cavities," Proc. of the 9th Workshop on RF Superconductivity, Santa Fe, New Mexico, USA, 1999, p.159.

32. K. Zapfe-Düren et al., "A New Flange Design for the Superconducting Cavities for TESLA," Proc. of the 8th Workshop on RF Superconductivity, Abano Terme, Italy, 1997, p.457.
33. K. Saito et al., "Study of Ultra-Clean Surface for Niobium SC Cavities," Proc. of the 6th Workshop on RF Superconductivity, Newport News, Virginia, USA, 1993, p. 1151.
34. K. Saito, Proc. of the 10th Workshop on RF Superconductivity, Tsukuba, Japan, KEK Proc. 2003-2, 2003, p.423.
35. C. Z. Antoine, "A Statistical Analysis of the Risk of Dust Contamination during Assembly of RF Superconducting Cavities," Proc. of the 6th Workshop on RF Superconductivity, Newport News, Virginia, USA, 1993, p. 1047.
36. C.Z. Antoine et al., "Alternative Approaches for Surface Treatment of Nb Superconducting Cavities," Proc. of the 9th Workshop on RF Superconductivity, Santa Fe, New Mexico, USA, 1999, p.109, and references therein.
37. L. Ponto, M. Hein, "Verfahren zur Elektrochemischen Politur von Niob," external report, WUB 86-17, BUGH Wuppertal, Germany, 1986.
38. J. Sekutowicz et al., "Status of the Superstructure," Proc. of the 10th Workshop on RF Superconductivity, Tsukuba, Japan, KEK Proc. 2003-2, 2003, p. 177.
39. K. Saito et al., Proc. of the 7th Workshop on RF Superconductivity, Gif sur Yvette, France, 1995, p. 379.
40. D. Reschke et al., Proc of the LINAC 2004, Lübeck, Germany, 2004, p. 830.
41. E. Ciapala et al., Proc. of the 10th Workshop on RF Superconductivity, Tsukuba, Japan, KEK Proc. 2003-2, 2003, p. 185.
42. W.-D. Moeller, M. Pekeler, "Measurements of TESLA Cavities for TTF," Proc. of the 5th European Particle Accelerator Conference, Sitges, Spain, 1996, p. 2103.
43. M. Pekeler, "Experience with Superconducting Cavity Operation in the Tesla Test Facility," Proc. of the 1999 Particle Accelerator Conference, New York City, New York, USA, 1999, p. 245.

3.6   Overview on High Field Q-Slope

Lutz Lilje, DESY, Notkestrasse 85, D-22607 Hamburg, Germany
mail to: lutz.lilje@desy.de

3.6.1   Abstract

The paper will review the effects related to an anomalous surface resistance increase observed in niobium radiofrequency cavities at surface fields corresponding to about 100 mT, the so-called 'Q-slope without X-rays.' Cavity measurements as well as sample studies are presented. Although the physics of the effect is yet to be understood, there exists an effective remedy: The low-temperature bakeout.

3.6.2   Introduction

The high field Q-slope was also dubbed the 'European headache' for a long time. While niobium quality was steadily increasing to the typical RRR values of about 300-600 used today, accelerating fields were limited to 20-30 MV/m (80-120 mT) in etched cavities in Europe and in the US. In Japan, KEK developed electropolishing as a niobium surface treatment with excellent results. Accelerating gradients of 40 MV/m

(160 mT) have been achieved in several single-cell cavities [1]. As EP looked much more attractive, an R&D program in collaboration of CERN, CEA Saclay and DESY was set up [2,3].

In their first tests, the cavities which were electropolished at CERN showed an unexpected performance limitation: the excitation curves exhibited a strong degradation in quality factor at high field as can be seen in Fig. 1. Field emission of electrons could be excluded as an explanation for the performance degradation since neither X-rays nor secondary electrons were observed. Temperature mapping revealed a global heating in the areas of high magnetic fields around the equator indicating a rapid increase of the microwave surface resistance towards high microwave fields.

In contrast to this observation, the excitation curves of the EP-treated cavities at KEK showed only a moderate drop of the quality factor and reached much higher accelerating fields.
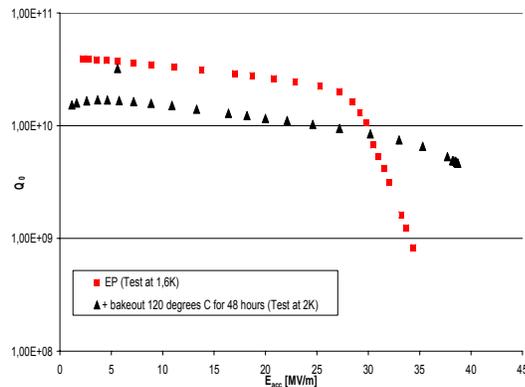
Figure 1: First observation of the bake-out effect on electropolished cavity at DESY.

3.6.3   The Description of the Q-slope

3.6.3.1   *RF Properties and Temperature Mappings*

Earlier at Saclay, a similar strong Q degradation was observed for chemically etched cavities, see Fig. 2 [4]. The temperature mapping for another etched cavity at DESY revealed a global heating of the surface similar to that in Fig. 3. It was discovered that the unsatisfactory performance could be considerably improved by applying a moderate thermal treatment to the finished cavity [4,5]. This will be called bakeout (or in-situ bakeout) hereafter. The procedure at Saclay was as follows. After the last high-pressure water rinsing, the cavities were evacuated and then heated up to 170°C for 70 h: The remarkable observation was that this low-temperature baking improved the quality factor at the highest field by nearly a factor of 3. This result was confirmed in other tests on BCP-treated cavities. However, tests revealed also that the baking procedure did not increase the maximum field level in chemically etched cavities.
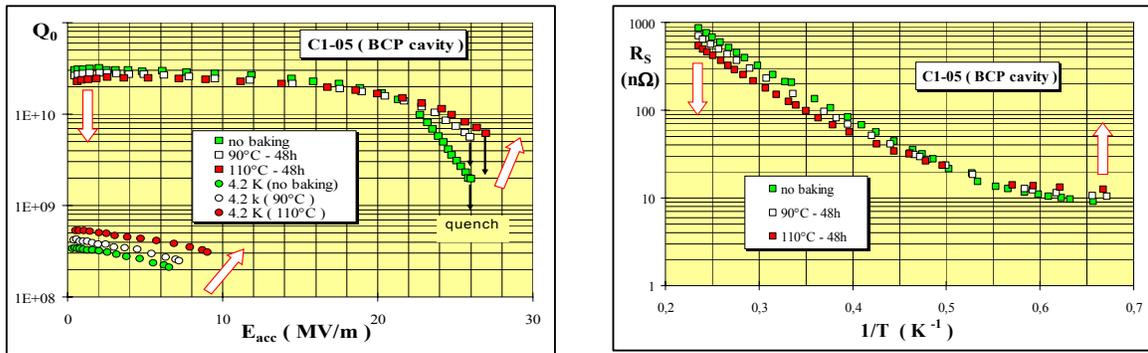
Figure 2: First observation of the bake-out effect on etched cavities in Saclay.
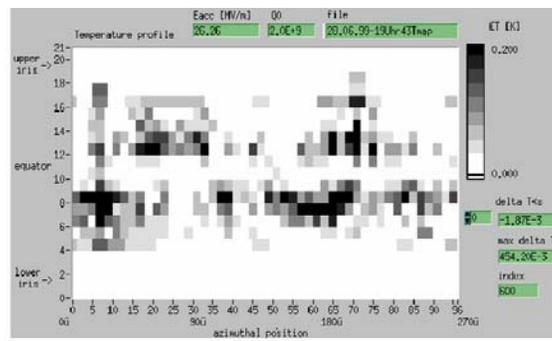
Figure 3: Temperature mapping of en etched cavity. Note the similarity of the zone affected by increased losses in the niobium surface.

Building on the experience with BCP cavities at Saclay and with EP cavities at KEK (where a bakeout at 85–100°C had been part of the standard preparation) it was decided to apply the bakeout to the EP cavities of the CERN–DESY–Saclay collaboration [2,3].
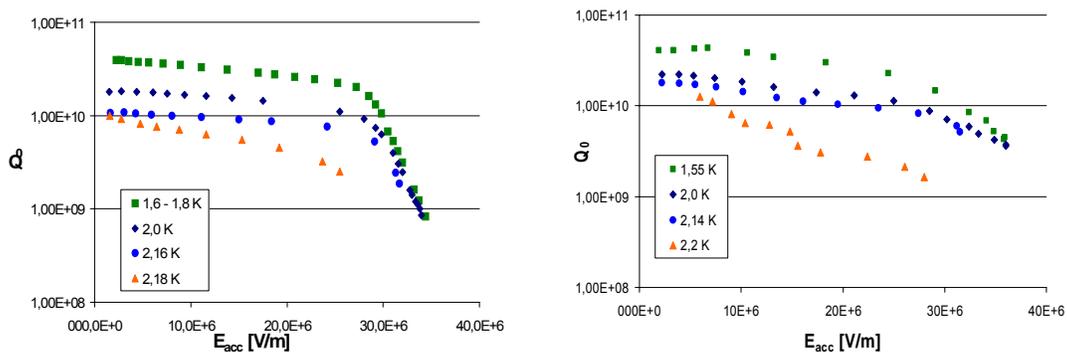
Figure 4: First observation of the Q-slope in electropolished cavities.
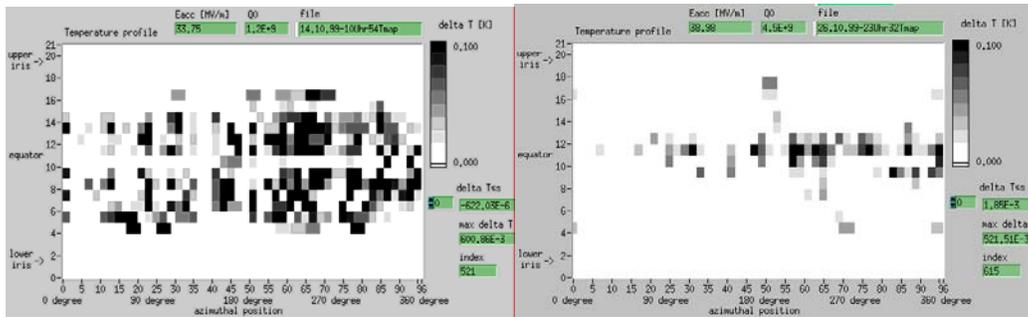
Figure 5: Temperature mappings of an electropolished cavity before and after 'in-situ' bake-out.

Figure 4 shows the excitation curves of an electropolished cavity before and after the bakeout at helium bath temperatures between 1.5 ºK and 2.2 ºK. At low field the quality factor exhibits the well-known temperature dependence which is caused by the exponential temperature dependence of the BCS surface resistance. However, the maximum achieved gradient and the corresponding Q_0 value are almost independent of the bath temperature as long as the helium coolant is in the superfluid state. These results are consistent with thermal model calculations. Only when the temperature is in the vicinity of the Lambda-point (2.17ºK) of liquid helium, where the transition from the superfluid to the normal-fluid phase takes place, a degradation of the quality factor due to insufficient cooling can already be seen at low field. This behaviour is very similar to the observations made at KEK. The temperature mapping shows a large area of heating before bake, whereas after bake-out only the equator region heats up (Fig. 5) [2].

The heat treatment of niobium cavities is a well known method to improve the performance. The temperature is in general quite high though: the TTF cavities are heat treated in an UHV furnace at 800°C for hydrogen degassing and stress annealing and afterwards at 1400°C for increasing the thermal conductivity of the bulk niobium. The surprising observation made with the bakeout effect is that a thermal treatment at such a low temperature, where the diffusion of any gases dissolved in the niobium lattice is extremely slow, has a major influence on the high-gradient performance. It is obvious that only the thin surface layer which is essential for the microwave superconductivity can be modified by the bakeout.

3.6.3.2   *Longtime Air Exposure*

The remarkable improvement of niobium cavities gained by electropolishing and bakeout will of course only be useful for the accelerator if the EP surface preserves its good properties over a long time period. In a first endurance test at Saclay an EP treated 1-cell cavity was exposed to clean air for two months without a significant change in performance. Another cavity has even been tested two years after its initial bakeout keeping high Q at high field. This was verified also in experiments at DESY (see Fig. 6) for a period of six months.
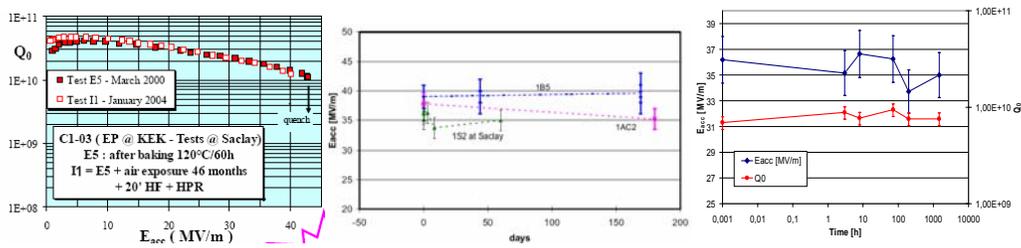
Figure 6: Exposure of a baked cavity to clean air. There is no change in cavity performance even for long exposure times.

3.6.3.3 *Bake-out Temperature*

The baking temperature is a critical parameter for the cavity performance. A summary of several cavity tests at DESY can be seen in Figure 7 for bakeout temperatures up to 140°C [6]. There is a clear trend towards temperature around 130°C giving higher Q_0. Similar results have been obtained at JLab. As can be seen in Figure 8 a temperature of up to 130°C can improve the BCS surface resistance further [7]. In other experiments the baking temperature was 145°C [8] or even 170°C [4,5]. However, it was found out that a bake at 170°C can even reduce the quench field of by 5 MV/m. Bakeout experiments at very high temperatures (200–600°C) confirm that the quench field degrades [9]. Therefore 140°C seems to be a reasonable upper limit to prevent that the benefit of the bakeout is counterbalanced by an increase in residual resistance. This conclusion is supported by the measurements made on 8.6 GHz niobium cavities [10].

	bake T(°C)	before bake	after bake	Gain	Ratio
	all	31.9	35.6	3.7	
Eacc,max	100-110	31.9	35.9	4.0	
(MV/m)	120-129	32.6	35.8	3.2	
	130-139	30.8	34.4	3.6	
	All	27.0	30.7	3.7	
Eacc	100-110	25.9	30.5	4.7	
@Q0=1× 10^10	120-129	27.9	29.4	1.5	
(MV/m)	130-139	28.2	29.6	1.5	
	All	1.9(2.3)	6.7(6.5)		3.5(2.9)
Q0(Eacc,max)	100-110	2.0(2.2)	5.3(5.1)		2.6(2.3)
EP(all cavities)	120-129	1.8(2.0)	9.2(7.7)		5.0(3.8)
(*10^9)	130-139	1.5(2.7)	8.0(8.9)		5.4(3.3)
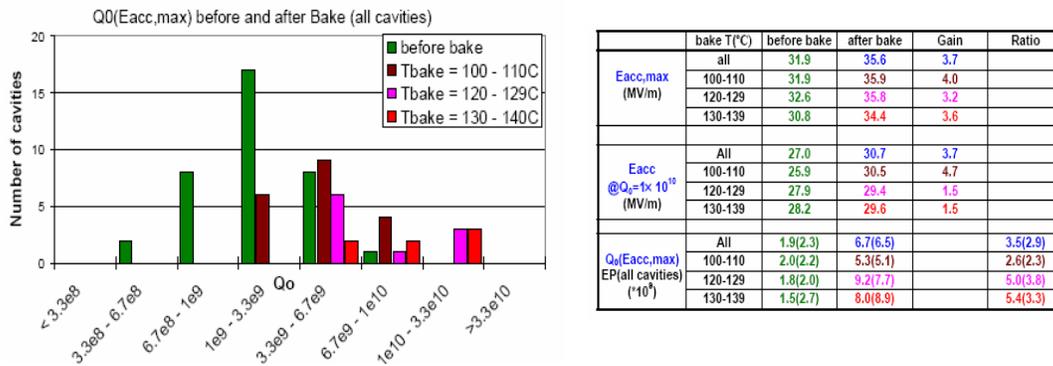
Figure 7: Dependence of the quality factor with bake-out temperature.

The change of the surface resistance (or the quality factor) can be interpreted as a contamination of the surface layer. This is supported by the fact that the mean free path decreases substantially with increased baking temperature. As a consequence a surface RRR value reduces when the baking temperature is above 130°C.
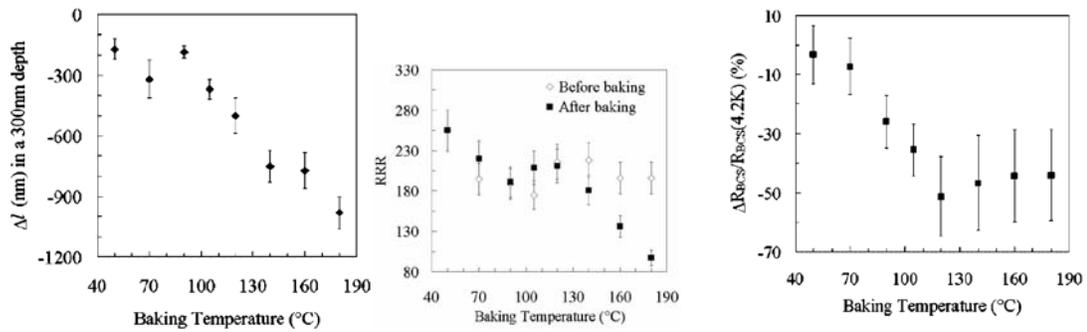
Figure 8: Dependence of surface properties with bake-out temperature.

3.6.3.4   *Depth of the Bake-Affected Zone in the Niobium*

P. Kneisel has made an experiment where he removed a thin layer from the niobium surface by oxipolishing and measured the surface resistance of the cavity [8]. He found that the reduction in R_{BCS} is lost after a removal of about 300 nm (Figure 9). The high field behaviour of another cavity was studied at DESY (Figure 10). After a removal of 120 nm the Q-slope re-appears. The slope is not fully back to the state before bake. The measurement is being continued. The surface sheath with reduced BCS surface resistance is hence eight times thicker than the London penetration depth ($= 32$ nm). The baking effect is due to changes within this surface layer.
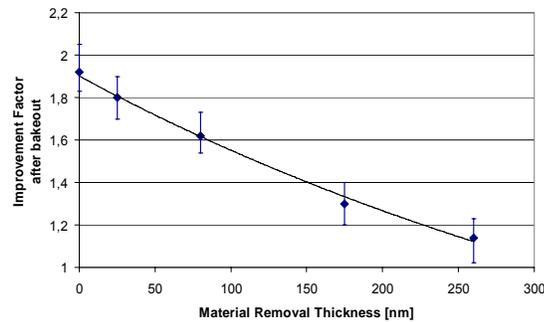
Figure 9: Change of the improvement factor of a baked cavity after removing material from the surface in small steps with oxipolishing. The benefit of the baking is lost after approximately 300 nm have been removed from the surface.
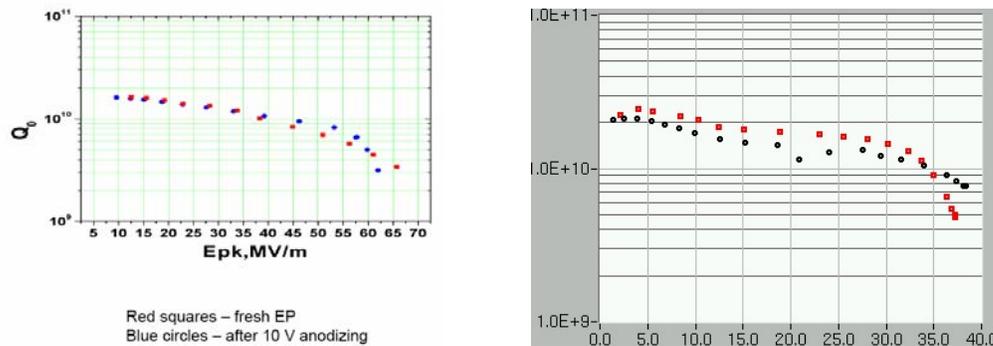
Figure 10: Oxipolishing of baked cavities after removal of 20 nm at Cornell (left) and 120 nm at DESY (right) lead to a re-appearance of the degradation of the quality factor.

3.6.3.5 *Surface Studies*

The results on the bakeout effect described show that the superconducting properties of niobium in a thin surface layer are changed. A simplified picture of the surface assumes that the niobium bulk is covered by several different oxides and adsorbates. These consist of

- a layer of adsorbates which consists of water, hydrocarbons and other gases
- a dielectric oxide layer of Nb_2O_5
- a layer of metallic NbO, which is weak superconductor ($T_c = 1.4K$)
- a layer of niobium metal with interstitially dissolved oxygen atoms ("oxygen lattice gas")
- the niobium bulk material with impurity atoms

In reality the niobium sheet material is polycrystalline and has features like grain boundaries. In the grain boundaries the diffusion of impurities is enhanced. An example is the diffusion of titanium during the high temperature treatment into the grain boundaries [11]. Lattice effects on the individual crystallites can serve as channels for oxygen atoms and therefore the oxidation might not be homogeneous. Oxidation can lead to stress between the surface oxide layer and the bulk metal [12].

This surface composition depends delicately on the surface treatments like etching, electropolishing, high temperature heating and 'in-situ' bakeout. The wet (electro-) chemical processes will inevitably contaminate the surface layer.

Several studies have been made to relate the surface layer composition to the superconducting properties of niobium. The depth probed by the magnetic field and the surface shielding currents is of the order of the magnetic penetration depth (30−40 nm). The result by Kneisel [8] has shown that about 300 nm are changed by the heating. This is nearly on order of magnitude larger than the London penetration depth.

In the 1970s low niobium cavity performance was frequently attributed to oxide layers. With the progress to higher gradients other effects like field emission [13], foreign material inclusions or hydrogen contamination [14] were considered the main limitations. The Q-drop has opened up the discussion again whether oxygen diffusion can be the reason for this effect.

A tool for investigations of the chemical composition is X-ray photoelectron spectroscopy (XPS), where energetic photons impinge on the surface and liberate

electrons whose energy is measured. The energy depends on the chemical bonds of the elements in the surface. The advantage of this method is that the chemical state of the surface is investigated.

In an Angular Resolved XPS (ARXPS) study [15] the dissolution of the Nb_2O_5 layer can be seen, as the photoelectron energy spectrum attributed to the fully oxidized state of niobium corresponding to Nb_2O_5 is reduced in intensity. The formation of intermediate oxidation states of the niobium between the fully oxidized Nb_2O_5 state and the metallic state can be seen (Figure 11).
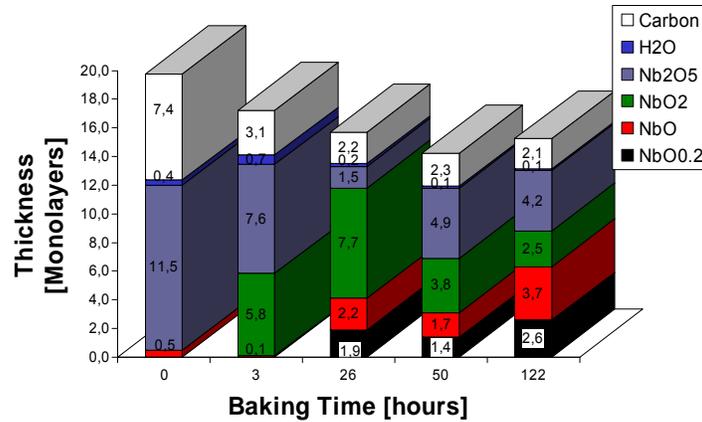
Figure 11: Change of the oxide structure with bake-out.

3.6.3.6 *Susceptibility Measurements on Samples*

Magnetic measurements on niobium samples are a useful tool to explore the surface treatments which improve cavity performance [16]. This idea is based on the fact that for pure niobium the ratio $\kappa = \lambda_L/\xi$ is in the order of unity, so that surface superconductivity and electromagnetic losses of microwave fields reside in thin surface sheaths of nearly the same thickness, given by the correlation length ξ and the penetration depth λ_L, respectively.

As expected, the bulk properties of the niobium samples, T_c, B_c, RRR and B_{c2}, remain invariant when different surface treatments such as chemical etching and electropolishing or a low-temperature bakeout are applied (Figure 12). In contrast to this, the superconducting properties of the surface itself are found to be strongly modified by these treatments. Evidence for surface superconductivity at fields exceeding the upper critical field B_{c2} of the bulk is found in all samples. The critical surface field B_{c3} is always larger than the value $B_{c3} = 1.695\ B_{c2}$ derived from the Ginzburg-Landau theory, the ratio $r32 = B_{c3}/B_{c2}$ amounts to 1.86 for BCP samples and 2.1 for EP samples. It increases further by baking the sample at 120−140°C for 24 to 96 hours. This enhanced surface field could be due to increased impurity contents of the niobium in a layer close to the surface and, related to this, a reduced electron mean free path.

	BCP	EP
T_c [K]	9.263 ± 0.003	
RRR	≈ 300	
surf. roughness on grain [nm]	≈ 1	
steps at grain bound.	1-5 μm	$\lesssim 0.1\mu$m
$B_c(0)$ [mT]	180 ± 5	
$B_{c2}(0)$ [mT]	410 ± 5	
$J_c(0,0)$ [A/mm^2]	240 ± 10	180 ± 10

Figure 12: Susceptibility measurements on niobium samples. The niobium bulk properties are not affected by 'in-situ' bake-out.

These results are consistent with the surface analysis studies performed on Nb indicating that baking causes a partial disintegration of the external Nb_2O_5 layer, the formation of suboxides (NbO, NbO_2) and most likely oxygen dissolution, causing a reduction in the mean free path. As observed in Fig. 13, the ratio of B_{c3}/B_{c2} grows faster by raising the baking temperature than by increasing the baking time, which is expected for a diffusion process.
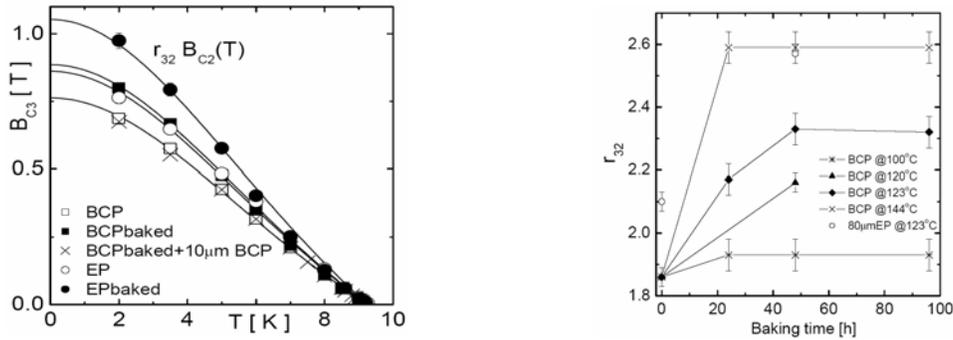
Figure 13: The susceptibility measurements show that the surface critical field B_{c3} changes with bake-out (left). The duration and temperature of the bakeout have been varied (right).

A most remarkable observation is that two different phases of surface superconductivity exist which are separated by a "coherent" critical surface field $B_{coh,c3}$: a coherent phase C for applied fields between B_{c2} and $B_{coh,c3}$ with bipolar shielding currents going around the whole cylindrical sample, and an incoherent phase I between $B_{coh,c3}$ and B_{c3} which is characterized by disconnected superconducting regions with normal zones in between. Both $B_{coh,c3}$ and B_{c3} depend on the surface preparation but the ratio $B_{coh,c3}/B_{c3}$ has the value 0.81 for all samples: BCP, EP, unbaked and baked (Figure 14). A power-law analysis of the complex conductivity and resistivity reveals that at $B_{coh,c3}$ a phase transition takes place between coherent and incoherent surface superconductivity. For the EP samples the exponents are in agreement with the expectation for percolation through a two-dimensional network of superconducting and resistive sections. A different behaviour is seen in the BCP samples, here the dimensionality of the network would have to be slightly larger that two. It might be

suspected that this may be related to weak links at the grain boundaries and to more complicated, nonplanar current paths in the surface layer.
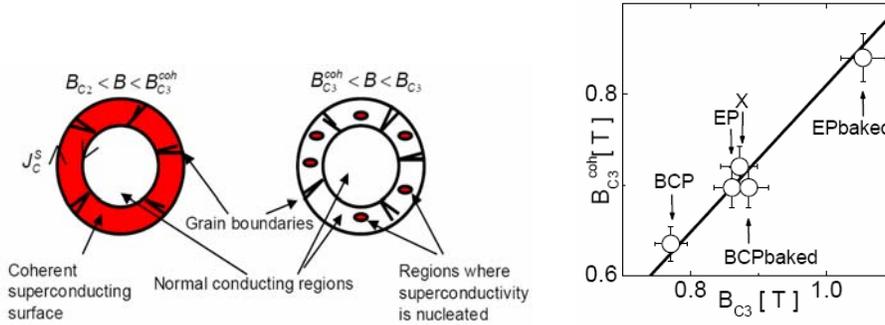
Figure 14: The susceptibility measurements show that the surface critical field B_{c3} changes with bake-out.

The surface current must be interpreted as the difference between two large counterrotating currents. Again, a clear difference between electropolished and chemically etched samples is observed: the BCP cylinders have a factor of six smaller critical surface currents (Figure 15). The lower currents for the BCP samples indicate that the surface currents have to follow more complicated orbits than in EP samples.
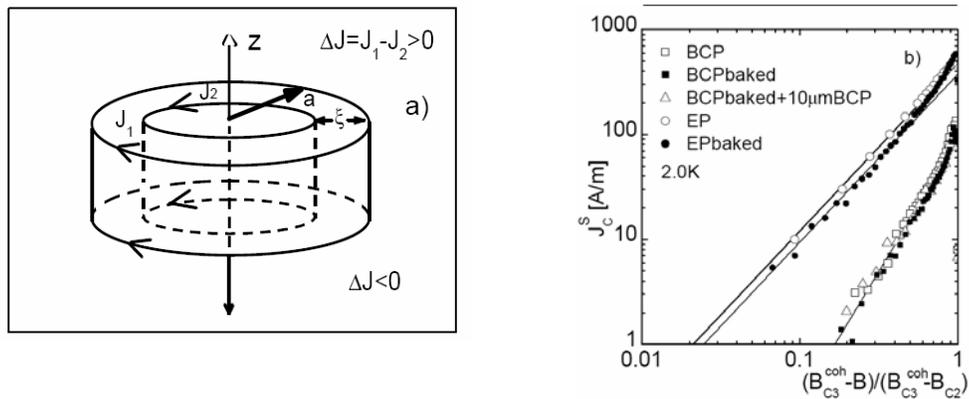
Figure 15: The susceptibility measurements show that the surface critical field B_{c3} changes with bake-out.

3.6.4 Summary

This paper tried to give an overview on the current status of experiments on the high field Q-slope. A lot of data has been presented but still a final model to explain the effect quantitatively is missing. A good overview on models for the high field slope is already available [17]. Even without the full theoretical understanding the Q-slope is a reproducible effect as its cure: the 'in-situ' bakeout. This combined with electropolishing has led to 'real' accelerating cavities achieving more than 35 MV/m [18].

3.6.5   Acknowledgments

The author would like to express his gratitude towards the colleagues of the TESLA collaboration and the colleagues from the SRF community for the many useful tips and discussions.

3.6.6   References

1. K. Saito et al., "Superiority of Electropolishing over Chemical Polishing on High Gradients," Proc. of the 8th Workshop on RF Superconductivity, Abano Terme, Italy, (LNL-INFN, Padova), 1998, pp. 759-813.
2. L. Lilje et al., "Electropolishing and in-situ Baking of 1.3 GHz Niobium Cavities," Proc. of the 9th Workshop on RF Superconductivity, Santa Fe, New Mexico, USA, LA-13782-C, 2000, pp. 74-76.
3. L. Lilje et al., Nucl. Instrum. Methods in Phy. Res. A 516, 213-227 (2004).
4. B. Visentin, J. Charrier, and B. Coadou, "Improvements of Superconducting Cavity Performances at High Gradients," Proc. of the 6th European Particle Accelerator Conference, 1998, p. 1885.
5. B. Visentin, J. Charrier, B. Coadou, and D. Roudier, "Cavity Baking: A Cure for the High Accelerator Field Q0 Drop," Proc. of the 9th Workshop on RF Superconductivity, Santa Fe, New Mexico, USA, LA-13782-C, 2000, pp. 198-202.
6. J. Hao, D. Reschke, A. Brinkmann, L. Lilje, "Low Temperature Heat Treatment Effect on High-field EP Cavities," Proc. of the 11th Workshop on RF Superconductivity, Lübeck/Travemünde, Germany, 2003, paper MoP16 (http://srf2003.desy.de/).
7. G. Ciovati, "Effect of low-temperature baking on the radio-frequency properties of Niobium superconducting cavities for particle accelerators," J. Appl. Phys. 96(3), 1 (August 2004).
8. P. Kneisel, "Preliminary experience with "in-situ" baking of niobium cavities," Proceedings of the 9th Workshop on RF Superconductivity, Santa Fe, New Mexico, USA, LA-13782-C, 2000, pp. 328-335.
9. B. Visentin, J. Charrier, and G. Congretel, "Change of RF Superconducting Parameters Induced by Heat Treatment on Niobium Cavities," Proc. of the 2001 Particle Accelerator Conference, New York, New York, USA, 2001, p. 1056.
10. F. Palmer, "Influence of oxide layers on the microwave surface resistance of superconducting niobium," PhD thesis, Cornell University, 1988.
11. C. Z. Antoine et al., "Evidence for the preferential diffusion and segragation of impurities at grain boundaries in very pure niobium used for radiofrequency cavities," Proc. of the 7th Workshop on RF Superconductivity, Gif sur Yvette, France, 1996, p. 647.
12. J. Halbritter, "On the Oxidation and on the Superconductivity of Niobium," Appl. Phys. A 43(1), (1987).
13. D. Reschke, "Untersuchungen an 3 GHz Niobresonatoren," PhD thesis, Universität Wuppertal, 1995, WUP-DIS 95-5.
14. R. Röth, "Untersuchungen zu anomalen Verlusten in Niobresonatoren," PhD thesis, Universität Wuppertal, 1993, WUP-DIS 92-12.
15. A. Dacca, G. Gemme, L. Mattera, and R. Parodi, "XPS analysis of the surface composition of niobium for superconducting RF cavities," Appl. Surf. Sci. 126, 219 (1998).
16. S. Casalbuoni, A.E. Knabbe, J. Kötzler, L. Lilje, L. von Sawilski, P. Schmüser, B. Steffen, "Surface Superconductivity in Niobium for Superconducting Cavities," 2004; accepted for publication in NIM A, DOI:10.1016/j.nima.2004.09.003; TESLA Report: TESLA 2004-06.
17. B. Visentin, "Q-slope at High Gradients: Review about Experiments and Explanations," Proc. of the 11th Workshop on RF Superconductivity, Lübeck, Germany, 2003, paper TuO01 (http://srf2003.desy.de/).

18. L. Lilje, P. Schmüser et al., "Achievement of 35 MV/m in the Superconducting Nine-Cell Cavities for TESLA," Nucl. Instrum. Methods A 524(1-3), 1-12 (2004).

3.7 High Q at Low and Medium Field

Gianluigi Ciovati

Thomas Jefferson National Accelerator Facility, Newport News, VA 23606, USA
Department of Physics, Old Dominion University, Norfolk, VA 23529
mail to: gciovati@jlab.org

3.7.1 Abstract

The surface resistance of a bulk niobium superconducting RF cavity as function of the surface magnetic field is often characterized by three peculiar dependencies at low, medium and high field. Understanding the causes and the physics behind these anomalous behaviors is important to improve the performance of superconducting cavities used in particle accelerators. In this paper attention will be focused on low and medium field regions by presenting experimental results of several cavity test series and reviewing the models that try to explain these nonlinearities of the surface resistance.

3.7.2 Introduction

The technology involved in the production of superconducting RF cavities made of bulk niobium has greatly evolved over the last ten years. In the last few years many single-cell and multi-cell cavities achieved peak surface magnetic fields close to the theoretical limit of niobium [1]. High-power testing of a superconducting cavity allows the exploration of nonlinearities in the surface resistance R_s as a function of the peak surface magnetic field B_{peak} by measuring the quality factor Q_0 ($R_s=G/Q_0$, where G is the geometrical factor) as a function of B_{peak}. A typical plot of Q_0 vs. B_{peak} is characterized by an increase of the quality factor up to about 20 mT, followed by a slow decrease ("slope") of Q_0 up to about 90 mT when a strong degradation of Q_0 appears even in the absence of field emission ("Q-drop").

For accelerators operating in continuous wave (cw) mode, dynamic losses dominate the operating costs and to reduce them it is necessary to use cavities with a high quality factor at medium to high fields. Therefore, it is important to understand the physics behind the Q-variations with field to develop procedures that will minimize the RF losses at the operating accelerating gradient.

3.7.3 Low Field Q-increase

3.7.3.1 *Experimental Results*

The low field Q-increase is an increase (about 40%) of the quality factor Q_0 between 2 and 15-20 mT peak surface magnetic field. It has been observed in many tests in several laboratories but mainly on cavities with resonant frequency of the fundamental mode (TM_{010}) above 1 GHz. For cavities with frequency below 1 GHz, there exists few data at very low field and even in those cases the low field Q-increase was rarely found. Fig. 1 shows this effect measured on a TESLA [2] 9-cell cavity at DESY, a CEBAF

Low Loss [3] single-cell measured at Jefferson Lab and a TESLA single-cell measured at Saclay.
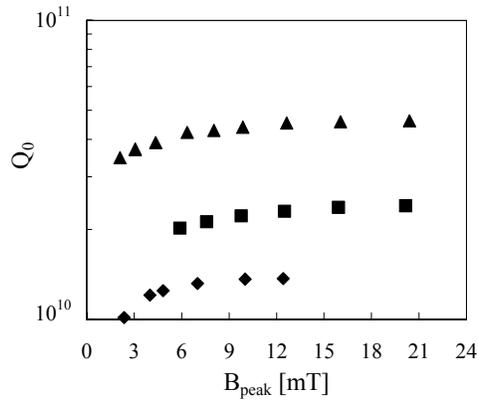
Figure 1: Low field Q-increase measured on a TESLA 1.3 GHz single-cell cavity at 1.7 K (triangles), a TESLA 1.3-GHz 9-cell cavity at 2 K (squares), and a CEBAF 1.48-GHz single-cell cavity at 2 K (diamonds).

It has been observed that the low-field Q-increase becomes more pronounced at lower temperatures: this effect, measured on a CEBAF Low Loss single-cell, is shown in Fig. 2. The error in Q_0 and B_{peak} is about 5%.
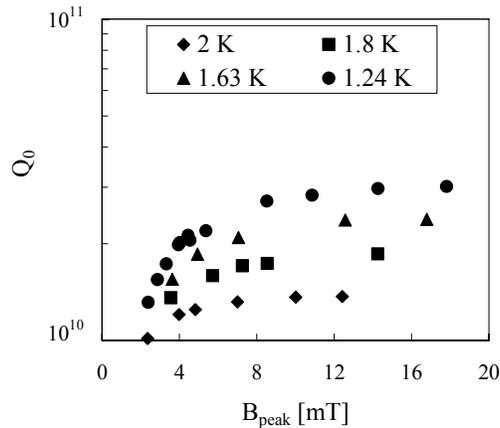
Figure 2: Low field Q-increase measured on a CEBAF Low Loss single-cell at different temperatures.

The B_{peak} at which the low field Q-increase saturates is also increasing at lower temperatures, as can be seen in Fig. 2. It is still possible to define a temperature independent residual resistance by subtracting the BCS surface resistance from the surface resistance at the saturation field at each temperature. The saturation peak magnetic field is inversely proportional to the temperature as shown in Fig. 3 along with the residual resistance.
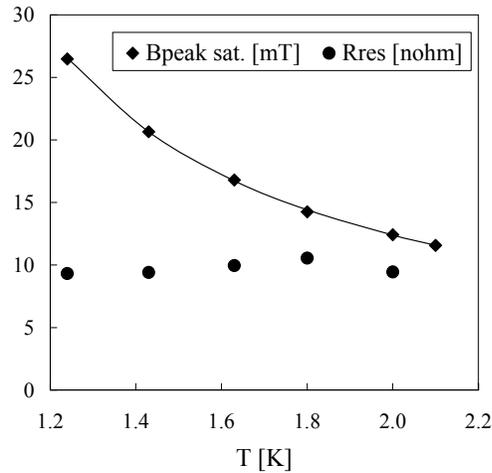
Figure 3: Peak magnetic field at which the low field *Q*-increase saturates (diamonds) and residual resistance (circles) as a function of temperature. The solid line corresponds to the fit $B_{peak}=1/(a+bT)$ with parameters *a* and *b* equal to -0.0325 1/mT and 0.0566 1/(mT K), respectively.

An additional result regarding the low field Q-increase is the fact that it is reduced by a high residual resistance. For example, this was observed on a CEBAF single-cell cavity where the residual resistance was increased by reducing the shielding of the Earth's magnetic field (Fig. 4).
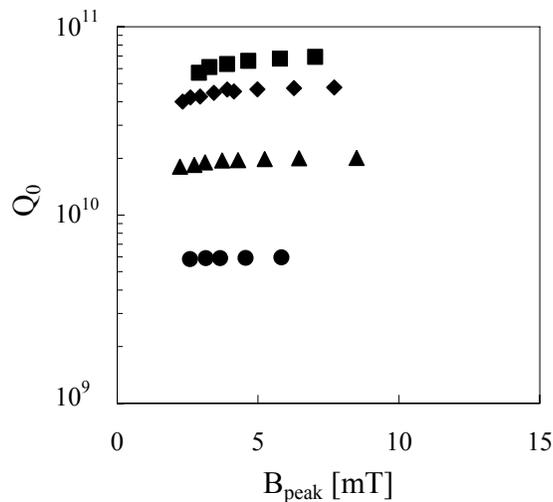
Figure 4: The low field *Q*-increase is reduced with increasing residual resistance: 4 nΩ (squares), 6 nΩ (diamonds), 13 nΩ (triangles), and 45 nΩ (circles).

A low temperature (100–150°C) "in situ" bake enhances the low field *Q*-increase. Figure 5 shows for example the low field Q-increase after the effect of baking a CEBAF single-cell cavity in UHV at 140°C for 48 h.
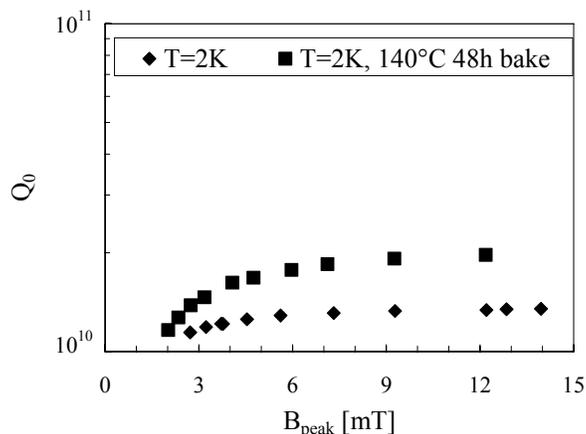
Figure 5: Low field *Q*-increase before (diamonds) and after (squares) baking a CEBAF single-cell cavity at 140°C for 48 h.

3.7.3.2   *Model Comparison*

Halbritter's [4] model for this effect involves non-equilibrium superconductivity. In particular, at low temperature and low RF fields thermal equilibrium between quasiparticles and phonon bath is not achieved. To allow this phenomenon to take place two conditions are necessary: a mismatch between the quasiparticle absorption and relaxation rate and the presence of localized states inside the superconducting niobium energy gap.

At a temperature of 2 K, a resonant frequency of 1.5 GHz and RF magnetic field of 2 mT, quasiparticles absorb photons from the RF field at a rate $1/\tau_{ab} \approx 2$ GHz. Under the same conditions, the quasiparticles relaxation rate $1/\tau_r$, which is the sum of the quasiparticle-phonon scattering rate plus the recombination rate, is only about 0.03 GHz.

Surface analysis studies show that the niobium surface is covered by few monolayers of hydrocarbon and water followed by about 5 nm of niobium pentoxide Nb_2O_5. Underneath that, there are few monolayers of niobium suboxides NbO, NbO_2 as well as NbO_x ($x<1$) channels and clusters injected deeper into the niobium during the oxidation process [4]. These NbO_x clusters introduce localized states in the niobium energy gap, as shown in Fig. 6.

At low RF field, quasiparticles are confined in these localized states yielding an average gap Δ^* smaller than the energy gap of pure niobium. This results in a higher surface resistance. At higher RF field, quasiparticles are driven out of the localized states and occupy states above the niobium energy gap, causing a decrease of the surface resistance to the proper BCS value. Once quasiparticles have energies greater than the niobium gap they are in thermal equilibrium with the phonons because those can easily transfer their energy to the helium bath (at 2 K the phonon mean free path is greater than the cavity wall thickness).
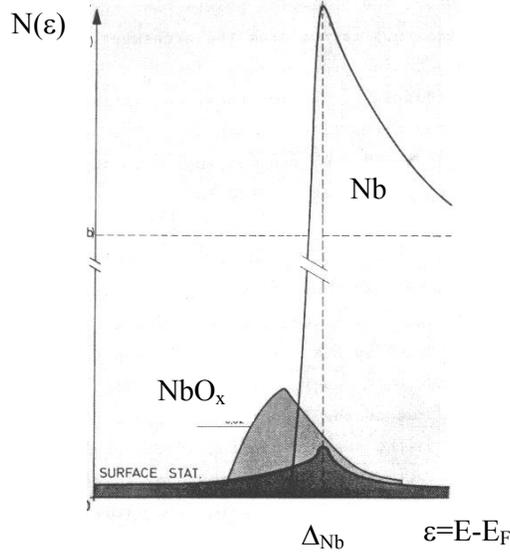
Figure 6: Density of states as a function of the energy of Nb (white area), NbO_x (grey area) and surface states (black area) from [5].

Halbritter gives the following formula for the absorbed RF power per unit area P:

$$P = \frac{R_s}{2}H^2 = \int n_c \lambda I_r(\varepsilon)\hbar\omega d\varepsilon, \tag{1}$$

where n_c is the density of states, λ is the RF penetration depth and I_r is the quasiparticle relaxation rate. Quasiparticles out of thermal equilibrium yield constant absorption, making the integral in (1) independent of the RF field amplitude. As a result the surface resistance is inversely proportional to the square of the RF field.

Figure 7 shows the data of Fig. 1 fitted with the formula

$$R_s = \frac{a}{B_{peak}^2} + b, \tag{2}$$

which shows very good agreement with the experimental data. The validity of this formula has been proved in many more experiments as reported in [5].

The values of the fit parameters a and b at different temperatures for the CEBAF Low Loss single-cell data of Fig. 2 are indicated in Table 1. There is no clear temperature dependence of a, while parameter b decreases at lower temperatures, reflecting the decrease of the BCS surface resistance.
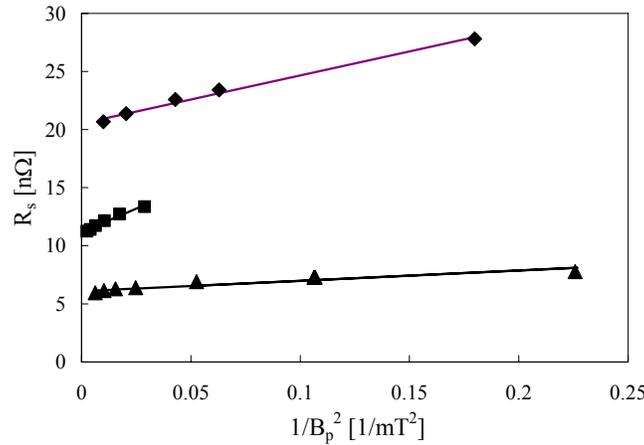
Figure 7: Surface resistance as function of $1/B^2_{peak}$ for the CEBAF Low Loss single-cell (diamonds), TESLA 9-cell (squares), and TESLA single-cell (triangles). The solid lines are the result of the fit with equation (2).

Table 1: Fit parameters a and b of Eq. (2) as function of temperature.

Temperature [K]	a [nΩ mT^2]	b [nΩ]
1.24	71.00	9.57
1.43	74.14	9.91
1.63	88.68	11.52
1.80	72.92	15.13
2.0	41.36	20.52
2.1	66.18	24.27

The model for the low field Q-increase can explain the temperature, baking and residual resistance dependences in the following way:

- the quasiparticle relaxation rate is proportional to $T^{3.5}$ so that at lower temperature there is a greater mismatch between absorption and relaxation rates, resulting in an enhancement of the low field Q-increase
- after low-temperature baking oxygen diffusion forms more niobium oxide clusters, increasing the density of localized states. This effect increases the term a/B^2_{peak} in (2)
- high residual resistance means a strong coupling between quasiparticles and phonons which prevents any mismatch and therefore reduces the low field Q-increase effect.

The model gives a fairly complete qualitative description of the experimental results but quantitative predictions are difficult, since it is strongly dependent on the surface morphology and the oxidation process.

3.7.4 Medium Field Q-slope

Beyond the field at which the low field Q-increase saturates, the cavity quality factor begins a gradual decrease. This continues up to a field where the degradation becomes stronger due to either field emission or Q-drop (typically 90 mT peak surface

magnetic field). This region of gradual reduction is called "medium field Q-slope" and is a more or less pronounced common feature of all niobium superconducting cavities. Figure 8 shows an example of this Q-slope on three different cavities: an SNS 6-cell, $\beta=0.61$, 805-MHz tested at 2.1 K; a TESLA 9-cell, 1.3-GHz tested at 2 K; and a CEBAF single-cell 1.48-GHz tested at 2 K.
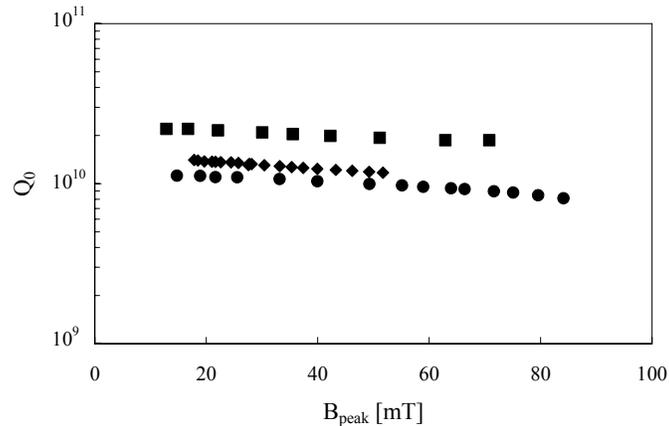
Figure 8: Medium field Q-slope for SNS 6-cell, $\beta=0.61$, 805-MHz at 2.1 K (diamonds); TESLA 9-cell, 1.3-GHz at 2 K (squares); and CEBAF single-cell 1.48-GHz at 2 K (circles).

3.7.4.1   *Experimental Results*

The medium field Q-slope is temperature dependent: it increases significantly when the helium bath temperature is above the lambda point (T = 2.17 K), it has a minimum at about 2 K and it increases at lower temperatures [6,7]. This dependence is shown in Fig. 9.

Low-temperature baking also seems to affect the medium field Q-slope and, in particular, seems to depend on the baking conditions: at Jefferson Lab and DESY, baking is done by flowing hot nitrogen and air on the outer surface of the cavity while at Saclay hot helium gas is used. The medium field Q-slope degradation after baking is less pronounced in cavities measured at Saclay [8]. Figure 10 shows an example of this effect measured on a CEBAF single-cell cavity at 2 K [5].
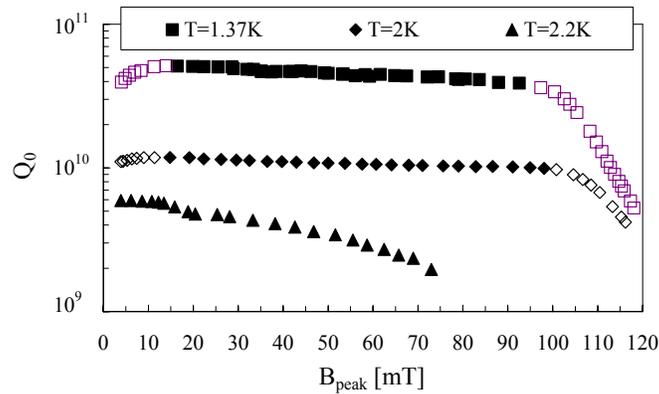
Figure 9: Temperature dependence of the medium field Q-slope (solid symbols) measured on a CEBAF single-cell cavity.
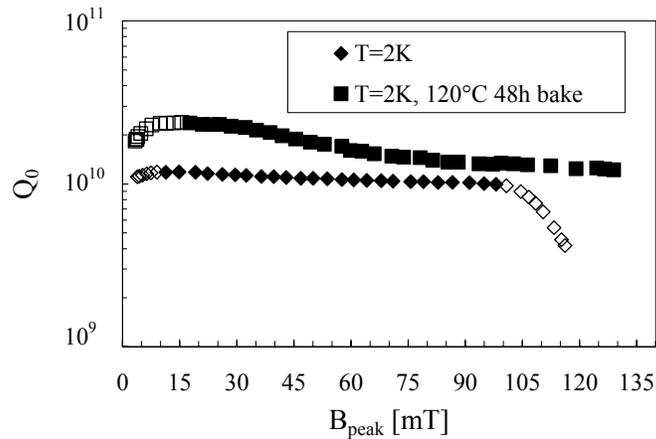
Figure 10: Medium field Q-slope (solid symbols) measured before and after baking on a CEBAF single-cell cavity.

Another treatment that influences the medium field *Q*-slope is post-purification of the cavity obtained by heating the cavity in a vacuum furnace at about 1200−1400 °C in the presence of titanium as a solid state getter. In many cases the *Q*-slope is reduced after such treatment [9].

3.7.4.2   *Models Comparison*

A model of the medium field *Q*-slope by Halbritter [10] involves heating of the RF surface to a temperature above the helium bath temperature due to the niobium-helium thermal resistance. The surface resistance is expressed as a Taylor series with even exponents of the peak surface magnetic field:

$$R_s\left(T, B_{peak}\right) = R_{s0}\left[1 + \gamma\left(T\right)\left(\frac{B_{peak}}{B_c}\right)^2 + O\left(B_{peak}^4\right)\right], \tag{3}$$

where R_{s0} is the surface resistance at about 15 mT, $B_c = 200$ mT is the niobium critical field and T is the He bath temperature. The medium field Q-slope is represented by the variable $\gamma(T)$. $\gamma = 1$ implies a 25% increase in surface resistance between 15 and 100 mT peak surface magnetic field. From Ginzburg-Landau theory, the value of gamma should be lower than 0.2 but it is enhanced by the niobium thermal resistance. Halbritter gives the following approximated formula for $\gamma(T)$:

$$\gamma(T) \approx R_{BCS}(T)\frac{B_c^2\Delta}{2kT^2}\left(\frac{d}{\kappa} + R_K\right),$$ (4)

where κ and R_K are the niobium thermal conductivity and Kapitza resistance respectively, d is the wall thickness.

Another possible cause for the medium field Q-slope is the presence of oxide channels, especially along grain boundaries, creating weak links in the RF penetration field region. The critical field of $Nb\text{-}NbO_x\text{-}Nb$ weak links is about 15 mT which is comparable to the peak surface field where the Q-slope starts. Above this field Josephson fluxons start to penetrate and generate nucleation and pinning (hysteresis) losses.

According to Halbritter [11] these hysteresis losses are expressed by a linear relationship between surface resistance and RF field $R_s \propto \omega B_{rf}$. Data have been analyzed using the following simple equation:

$$R_s = a + bB_{peak},$$ (5)

where the parameter b represent the medium field Q-slope.

3.7.4.2.1 Cavity Production Results

In this section the values of the medium field Q-slope for three cavity production series will be compared with the predictions of equations (3) and (5). Over the last two years, Jefferson Lab has been involved with the production and testing of about 80 6-cell 805 MHz cavities of two different β values ($\beta = 2L/\lambda$ where L is the cell length and λ is the wavelength of the fundamental mode) for the SNS proton linac [12]. In addition, three cryomodules, two for the CEBAF upgrade (SL21 and NL11) and one for the FEL upgrade (FEL3), each made of eight 7-cell 1.5 GHz cavities have been built [13]. DESY has been working on the production of 9-cell 1.3 GHz cavities for TTF [14] and their most recent data will be presented.

Figure 11 shows the values of γ and b for the SNS $\beta = 0.61$ cavity production. The average values are $\gamma = 3.4 \pm 1.2$ and $b = 0.087 \pm 0.031$ nΩ/mT. After cavity MB26, a new preparation procedure was adopted consisting of more buffered chemical polishing (200 μm instead of 50 μm material removal) after hydrogen degassing in a vacuum furnace at 600 °C for 10 h, longer water rinsing after chemical treatment and longer high-pressure water rinsing (2×4 h instead of 2×1 h). This had no significant effect on the medium field Q-slope while it helped in reducing the residual resistance from an average of 9.3 ± 3.5 nΩ to 4.8 ± 1.1 nΩ and increasing the field emission onset by about 6 MV/m peak surface electric field.

Figure 12 shows the values of γ and b for the $\beta = 0.81$ cavities tested to date. The average values are $\gamma = 4.86 \pm 2.53$ and $b = 0.114 \pm 0.076$ nΩ/mT. The average residual

resistance is 7.8 ± 2.7 nΩ. It is interesting to note the larger value of γ for HB32 and HB38 which were baked at 120 °C for 48 h.
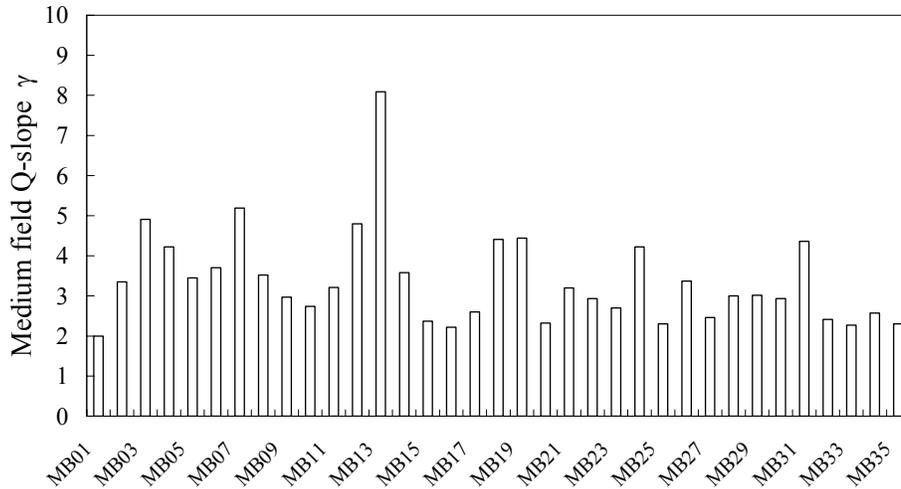
Figure 11: Medium field Q-slope γ for the 35 SNS β=0.61 cavities tested at 2.1 K.
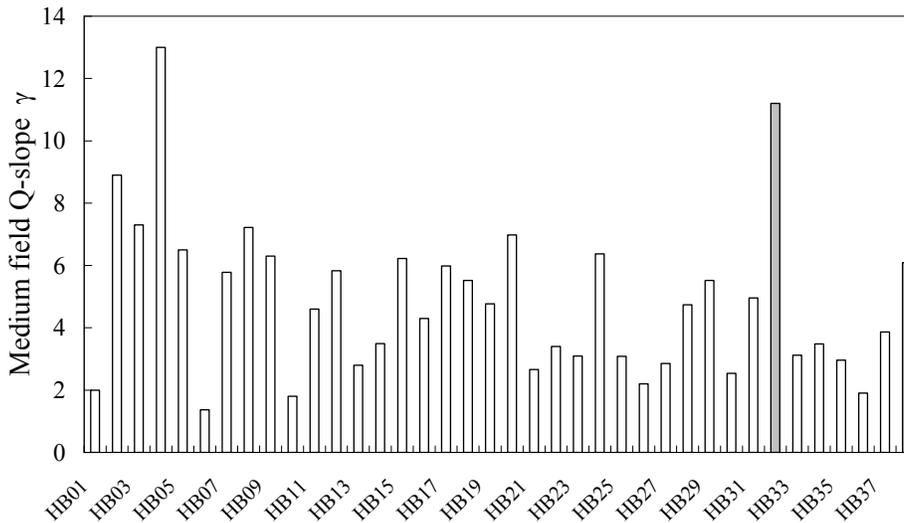
Figure 12: Medium field Q-slope γ for 38 SNS β=0.81 cavities tested at 2.1 K. The grey bars refer to cavities which were baked "in situ" at 120°C for 48 h.

Figure 13 shows the medium field Q-slope γ for the CEBAF cavities: the ones installed in the SL21 cryomodule were characterized by strong contamination and early field emission onset but the performances kept improving over time reaching very low values of γ for the NL11 (named also "Renascence") production. For the latter, the improved procedures from the SNS cavity production were adopted. Again, for cavities LL02 and LL04 the slope increased by about a factor of three after "in situ" baking at 120°C for 48 h. The average values of γ and b are indicated in Table 2 along with the

average values for the other cavity production runs discussed in this article. The average value of residual resistance is 6.8 ± 4.6 nΩ.
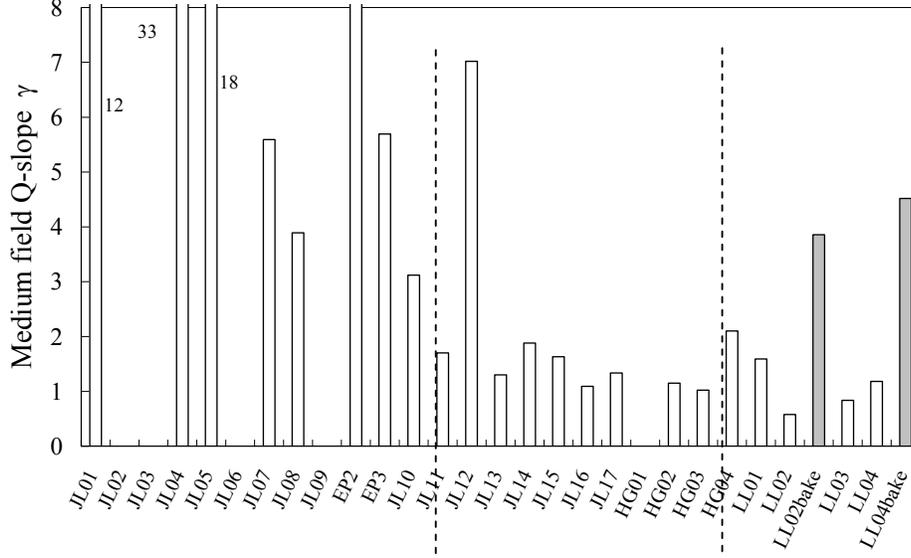
Figure 13: Medium field Q-slope γ for CEBAF cavities. The dashed line separates the cavities produced for cryomodules SL21, FEL3 and NL11. The cavities for NL11 were tested at 2.07 K while the rest were tested at 2 K. The grey bars refer to cavities that were baked at 120°C for 48 hours.

Figure 14 shows the medium field Q-slope γ for TESLA cavities [15] measured at 2 K. There is no significant difference between cavities that had only the hydrogen degassing at 800°C for 2 h and the ones that were post-purified at 1350°C for 3 h with Ti. In both cases, however, the medium field Q-slope increased after baking at 120°C for 48 h except for cavity AC80.

The average value of the medium field Q-slope is: $\gamma = 1.73 \pm 1.67$ and $b = 0.090 \pm 0.176$ nΩ/mT.

Table 2: Average medium field Q-slope γ and b and fit correlation factors r^2 for different cavity productions.

Cavity Type	γ	r^2	b [nΩ/mT]	r^2
SNS β=0.61	3.38 ± 1.20	0.926	0.087 ± 0.310	0.907
SNS β=0.81	4.86 ± 2.53	0.865	0.114 ± 0.076	0.848
CEBAF/SL21	12.3 ± 10.2	0.917	0.360 ± 0.295	0.898
CEBAF/FEL3	2.38 ± 1.97	0.893	0.092 ± 0.079	0.849
CEBAF/NL11	1.91 ± 1.04	0.901	0.068 ± 0.045	0.930
TESLA	1.73 ± 1.67	0.964	0.090 ± 0.176	0.966
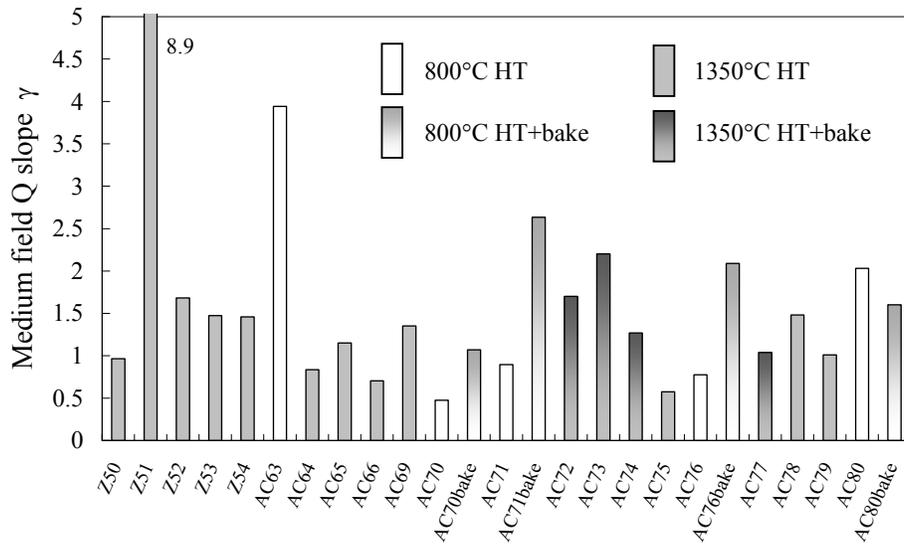
Figure 14: Medium field Q-slope γ for TESLA cavities tested at 2 K.

It appears from the data analysis of the medium field Q-slope that for strong slopes (γ values greater than about 2) the quadratic dependence of equation (3) gives the best fit, suggesting heating as the main cause for the slope. For low values of slope and after baking, the linear dependence (5) becomes a good data fit and, in particular, after baking is consistently better than the quadratic fit. This might suggest that when the heating is low, hysteresis losses become measurable and dominate the slope due to an increased number of weak-links after baking. This effect is shown (Fig. 15) by plotting in the surface resistance as function of the peak surface magnetic field before and after baking for the data shown in Fig. 10.
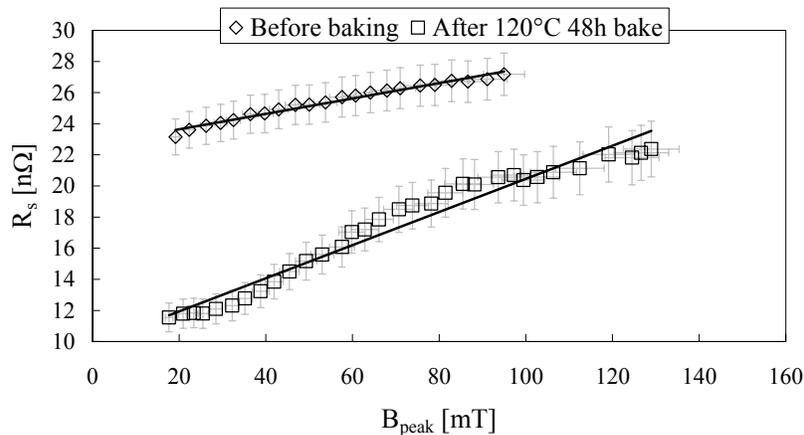
Figure 15: Surface resistance as function of the peak surface magnetic field for the data of Fig. 10. Solid lines represent fits with linear equation (5), showing the slope increase after baking.

3.7.4.2.2 Medium Field Q-slope Analysis

The experimental data suggest that the main contribution to the medium field Q-slope comes from heating of the RF surface due to the poor niobium-helium thermal interface. This is supported by the fact that the slope is temperature dependent, being high above 2.17 K when niobium is cooled by He I, and below 2 K when the Kapitza resistance dominates. Furthermore, cavities built with thicker niobium show stronger slope than thinner ones (SNS cavities are 3.8 mm thick while CEBAF and TESLA cavities are 2.5-2.8 mm thick) and cavities with higher thermal conductivity generally show a reduced slope. On the other hand, thermal models predict significant smaller slopes than experimentally measured [16,17] and low-frequency quarter-wave and half-wave resonators show less marked temperature dependence of the medium field Q-slope [18].

The importance of the Kapitza resistance on the Q-slope at 2 K is not clear: the stronger slope for cavities baked with hot nitrogen/air than for cavities baked with hot helium could be related to a higher Kapitza resistance, although there are no direct measurements after baking; but cavities whose outer surface was chemically etched (TESLA) show comparable Q-slope to cavities that did not receive such treatment (CEBAF). Measurements of Kapitza resistance [19] show lower values for chemically etched surfaces.

Another possible source of additional heating of the RF surface could be contamination of the inner surface from particulate or chemical residues as was probably the case for CEBAF/SL21 cavities. On the other hand the cavity production data shows that there is no correlation between Q-slope and residual resistance.

Finally, the experimental data seems to sustain the hypothesis of hysteresis losses due to oxides weak-links which grow after low-temperature baking.

3.7.5 Conclusions

Understanding non-linear behavior of the Q-value as a function of RF field level is very important to reduce the cryogenic losses of high-gradient superconducting cavities operating in cw mode.

Measurements of low field Q-increase are well described by a model involving quasiparticle-phonon non-equilibrium enforced by localized states within the niobium energy gap. Low-temperature baking seems to be effective in enhancing this effect.

There exist no models that can quantitatively account for the value of the medium field Q-slope. Experimental data indicate that material properties influencing the niobium-helium thermal interface such as thermal conductivity, wall thickness, and Kapitza resistance play an important role. Surface contamination and hysteresis losses appear also to be possible causes. A general remark is that the results obtained from cavity productions show large scatter in Q-slope data and this is an additional indication that the sources of the slope and the parameters that influence it are not yet clear and under control. To maintain the improvement of the quality factor by low-temperature baking at high gradient it is important to develop a baking procedure that will minimize its impact on the medium field Q-slope. From the theoretical point of view, recent studies [20] show that there might be an intrinsic dependence of the BCS surface resistance on the RF field, which could account for part of the Q-slope.

3.7.6 Acknowledgments

3.7.7 References

1. L. Lilje, Proc. of the 2004 European Particle Accelerator Conference, Lucerne, Switzerland, 2004, pp. 129-131.
2. R. Brinkmann et al., TESLA – Technical Design Report, DESY, Hamburg, Germany, 2001.
3. P. Kneisel et al., Proc. of the 2004 Linear Accelerator Conference, Lübeck, Germany, 2004, to be published.
4. J. Halbritter, Proc. of the 10th Workshop on RF Superconductivity, Tsukuba, Japan, 2001, pp. 292-301.
5. J. Halbritter, Proc. of the 1st Workshop on RF Superconductivity, Karlsruhe, Germany, 1980, pp. 190-214.
6. G. Ciovati, *J. of Appl. Phys.* **96**(3), 1591-1600 (2004).
7. P. Kneisel, Proc. of the 8th Workshop on RF Superconductivity, Abano Terme, Italy, 1997, p. 463.
8. B. Visentin, Proc. of the 11th Workshop on RF Superconductivity, Lübeck/Travemünde, Germany, 2003, paper MoP19 (http://srf2003.desy.de/).
9. H. Safa, Proc. of the 10th Workshop on RF Superconductivity, Tsukuba, Japan, 2001, pp. 279-286.
10. J. Halbritter, Proc. of the 38th Eloisitron Workshop, Erice, Italy, 1999, p. 59.
11. J. Halbritter, *J. Supercond.* **8**, 691-703 (1995).
12. www.sns.gov
13. A.-M. Valente, Proc. of the 2004 European Particle Accelerator Conference, Lucerne, Switzerland, 2004, pp. 1105-1107.
14. W.-D. Moeller, Proc. of the 10th Workshop on RF Superconductivity, Tsukuba, Japan, 2001, pp. 212-215.
15. http://tesla.desy.de/~oracle/ttf_gui_home.htm
16. D. Reschke, Proc. of the 8th Workshop on RF Superconductivity, Abano Terme, Italy, 1997, pp. 385-394.
17. K. Saito, Proc. of the 11th Workshop on RF Superconductivity, Lübeck/Travemünde, Germany, 2003, paper ThP17 (http://srf2003.desy.de/).
18. M. Kelly, Proceedings of the Workshop on Pushing the Limits of RF Superconductivity, Argonne report ANL-05/10, March 2005, p. 278.
19. A. Boucheffa, M. X. Francois, Proc. of the 7th Workshop on RF Superconductivity, Gif sur Yvette, France, 1995, pp. 659-663.
20. A. Gurevich, Proceedings of the Workshop on Pushing the Limits of RF Superconductivity, Argonne report ANL-05/10, March 2005, p. 17.

3.8 Low, Medium, High Field Q-Slopes Change with Surface Treatments

Bernard Visentin

CEA-Saclay, DSM / DAPNIA / SACM, 91191 Gif / Yvette Cedex – France

mail to: bvisentin@cea.fr

3.8.1 Abstract

Several surface treatments such as hydrofluoridric chemistry, hot chemistries, plasma discharge, different kinds of baking, etc. modify the $Q_0(E_{acc})$ profile of bulk niobium cavities. The analysis of these modifications allows a critical comparison with theoretical predictions. Furthermore, the high field Q-slope improvement by baking and its insensitivity to additional hydrofluoridric chemistry, points out the impact of diffusion phenomenon inherent to any thermal treatment. Additional experiments are undertaken at Saclay to benefit from this statement in order to simplify the baking process.

3.8.2 Introduction

To improve the cavity performances and reach higher intrinsic quality factor Q_0, higher accelerating field E_{acc} or higher quench field, it is necessary to understand the Q_0 vs. E_{acc} curve (Fig. 1). For that purpose, several paths have to be explored:
- Macroscopic experiments developed on niobium cavity which give a direct access to the $Q_0(E_{acc})$ profile. Advances on this way can be made independently of theory and surface analysis through more or less empirical observations and arguments.
- Microscopic surface analyses on niobium samples are useful for punctual verification, to sustain a theoretical argument or to suggest new macroscopic experiments. Unfortunately by this way, it is difficult to have a direct link with macroscopic observations (Q-slope, for example). For that reason, surface analyses remain strongly connected to theories and to experiments on cavity.
- Theory that can ensure physical explanation if it is in agreement with observations from macroscopic experiments.

The subject of this paper is to describe macroscopic experiments carried out at Saclay and based on surface treatments that modify the $Q_0(E_{acc})$ profile. These results will be confronted to theories developed to explain the different parts of $Q_0(E_{acc})$ characteristics.

3.8.3 Q-Slopes

In Fig.1, the curve $Q_0(E_{acc})$ shows clearly three parts with different slopes at low, medium and high fields (LF,MF and HF Q-Slopes). These three parts are visible on bulk niobium cavities regardless of their resonant frequency (Fig. 2). Theories that can be proposed to explain the Q-slopes origin are:
- at low field , the NbO_x clusters theory [1]
- at medium field, several theories based on thermal dissipation [2]

- at high field, among a lot of theories [3], the Interface Tunnel Exchange [1] or the Magnetic Field Enhancement [4] can be mentioned, although that last one cannot explain the high field Q-slope similarity observed on chemically (BCP) and electropolished (EP) cavities (see Fig. 1).
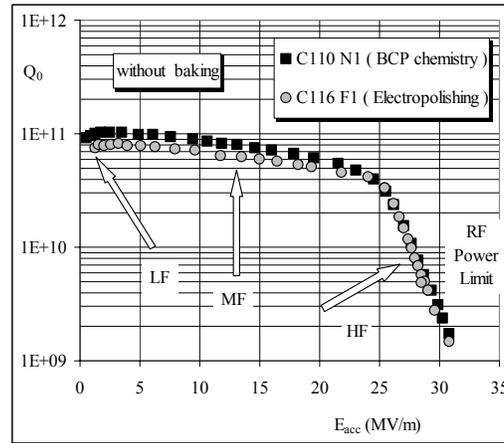
Figure 1: Q_0 vs. E_{acc} curve showing the different Q-slopes for cavities (1.3 GHz) treated with standard chemistry (BCP) and electropolishing (EP). We can note Q-slope similarity (especially at high field) for cavities with BCP or EP chemistry.
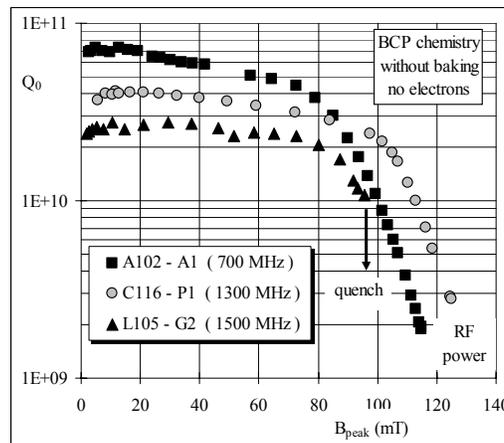
Figure 2: Q-slopes of monocell niobium cavities, with BCP chemistry, designed at different resonant frequencies (700, 1300 and 1500 MHz).

3.8.4 Baking at Low Temperature

3.8.4.1 *Description*

Baking is the first known treatment able to modify the three Q-slopes. It was first discovered on a BCP cavity after it underwent a soft heat treatment (110°C for

48 hours), the inner volume being pumped in ultra high vacuum (UHV) [5]. The consequences for its performances were (Fig. 3):

- the R_{BCS} decrease about 50% at 4.2K,
- the residual resistance R_{res} increase,
- the Q-slope enhancement at low field,
- the slight flattening of the medium field Q-slope,
- the strong Q-slope improvement at high field.

These observations are the mark of the "baking effect" and it can be demonstrated that it also takes place in baking under air at the atmospheric pressure [6] (Fig. 4). Furthermore, without such treatment, cavities (even electropolished) do not reach 40 MV/m (Fig. 5).

The high field Q-slope improvement after baking is quasi-definitive: almost four years after baking, storage in open-air on shelves, the cavity shows an unchanged profile (Fig. 10).
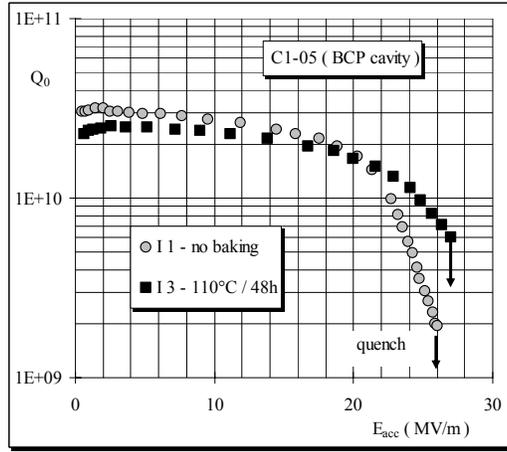
Figure 3: Q-slopes change after UHV baking on a BCP cavity.

3.8.4.2   *Baking Consequence for the Medium Field Q- Slope*

The baking effect on the medium field Q-slope reported in [7] from RF tests on CEBAF and TESLA multi-cell cavities show an increase by a factor of 3 or 4 and a change from a quadratic to a linear dependence.

According to the experimental results obtained at Saclay the analysis is different. Saclay data are fitted in using the formula from the Halbritter's model [1]:

$$(R_S - R_0)/R_0 = 1 + \gamma B_P^2 / B_C^2 , \qquad (1)$$

where $R_0 = R_S(B_P = 13mT)$, $B_C = 200\ mT$, and $B_P/E_{acc} = 4.221 lmT/(MV/m)$ or $4.156\, mT/(MV/m)$ for D122 cavity.

Data are analysed between 3 and 18 MV/m to prevent the influence of the low and high field Q-slopes. Results are compiled from twelve RF tests made on eight one-cell

cavities, two of them being electropolished. A quadratic variation is found before and after baking, with a slight flattening ($\Delta\gamma/\gamma \sim 5\%$) after baking (Figs. 6-7).

The very different results between these experiments and those reported in [7] are probably to be found in the difference of the conditions in which the baking was performed in each laboratory.
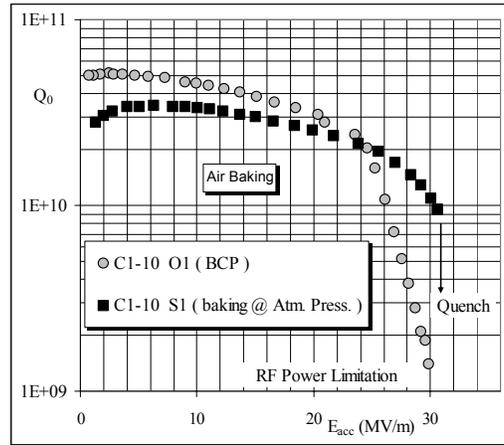
Figure 4: Air baking at the atmospheric pressure of a BCP cavity.
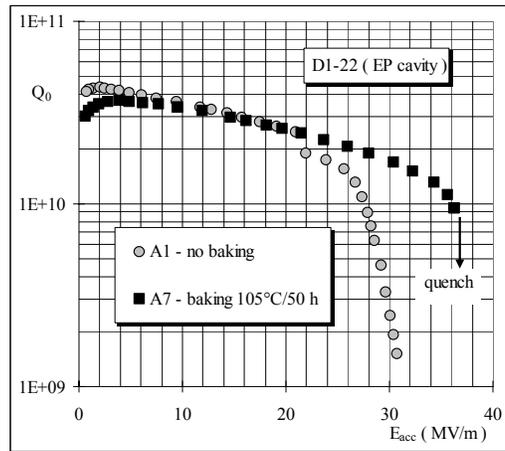
Figure 5: UHV baking on an electropolished cavity.
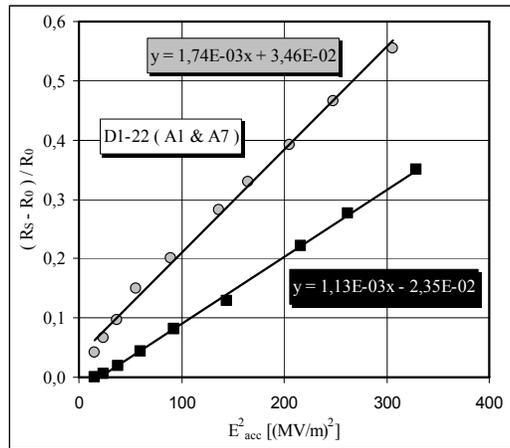
Figure 6: Quadratic behaviour of the medium field Q-slope before and after baking (B_P/E_{acc} = 4.156 mT/MV/m).
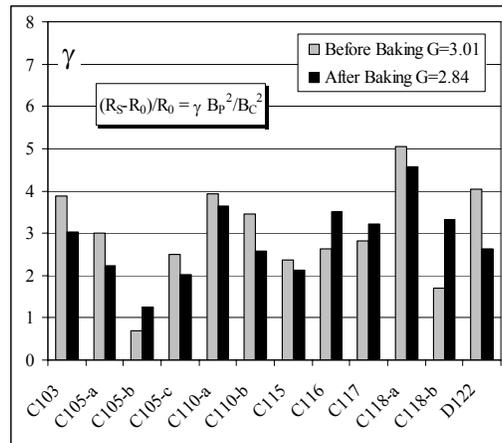
Figure 7: Gamma factor of the medium field Q-slope before and after UHV baking on BCP cavities, except for C103 and D122 (electropolishing) and for C110-b (air baking).

3.8.5 Surface Treatment by Hydrofluoridric Acid

Surface treatment by hydrofluoridric acid is commonly and successfully used at Saclay to suppress field emission from the cavity surface (Fig. 9-C1, Fig. 10-I1), especially when emitters can not be removed by an additional high pressure rinsing (HPR). This result can be explained by the Nb surface renovation. During hydrofluoridric chemistry (HF), Nb pentoxide surface layer is dissolved according to the chemical reaction (Equation 2):

$$Nb_2O_5 + 10HF \rightarrow 2H_2NbOF_5 + 3H_2O \,. \tag{2}$$
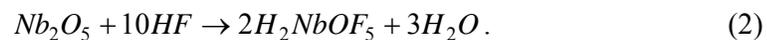
Nb$_2$O$_5$-Nb interface is also affected by this chemistry on a sizeable depth. Although this statement should be verified by surface analysis on samples, a change in the surface resistance R$_S$ (Equation 3) is clearly shown on baked cavities after hydrofluoridric chemistry (Fig. 8 and Table 1). The consequence of such a treatment is a trend to restore the R$_{res}$ value before baking and in a smaller extent the R$_{BCS}$ one. The energy gap Δ seems unchanged before and after HF chemistry. Of course, the R$_S$ change after HF chemistry has consequences on the Q-slope profile:

$$R_S = R_{BCS} + R_{res} = \frac{A\omega^2}{T} e^{-\Delta/kT} + R_{res}.$$ (3)
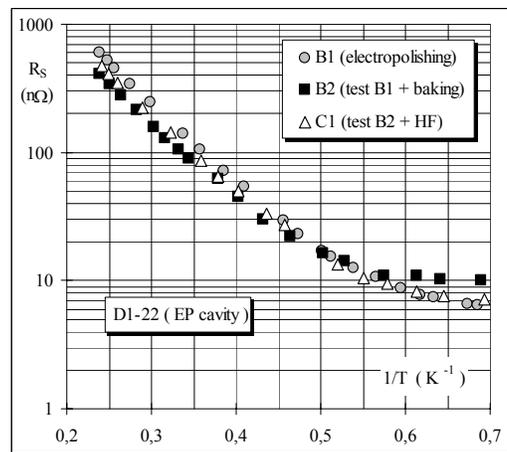
Figure 8: Surface resistance change after baking and HF chemistry.

Table 1: Change of surface resistances after baking treatment,
followed by HF chemistry

| Cavity | Test | | R$_S$@1.5 K | Aω^2 | R$_{res}$ |
	N^o	Chemistry	nΩ	10^5nΩK	nΩ
C103	E1	EP	6,0	2,3	4,6
	E4	Baking	9,1	1,3	8,3
	G1	HF	6,3	1,5	5,5
C105	J1	BCP	1,8	2,4	1,2
	K1	Baking	3,2	1,5	2,7
	L1	HF	2,2	2,0	1,7
C116	P1	BCP	7,1	2,1	6,2
	P2	Baking	8,3	1,3	7,4
	Q1	HF	6,1	1,3	5,5
D122	B1	EP	6,5	2,1	6,0
	B2	Baking	10,0	1,4	9,7
	C1	HF	7,1	1,7	6,7

3.8.5.1 *Low Field Q-Slope Analysis*

Due to R_S modifications, we can see on Fig1,5ures 9 and 10 that the low field Q-slope, enhanced by baking (Fig. 9-B2, Fig. 10-E5 a2,0nd F1), is removed by HF treatment (Fig. 9-C1, Fig. 10-I1) and that the slope before 2,1baking (Fig. 9-B1) is roughly recovered. Moreover, an additional baking restores the1,3 Q-slope enhancement (Fig. 9-C2). Surface treatments by baking and HF chemistry have an opposite effect on Q-slope at low field.

Consequently, the origin of the Q-slope at low field (H < 10 mT) is probably localised at the interface niobium-oxide or very close to the niobium surface, in the small layer removed by HF chemistry. These observations anyway, are not incompatible with the NbO_x clusters theory [1] that gives an explanation for the low field Q-slope.

3.8.5.2 *High Field Q-Slope Analysis*

Modifications by HF chemistry are only visible at low field. Medium and high field Q-slopes are unaffected. Especially, the high field Q-slope before baking is not restored and the baking benefit is maintained (Fig. 10-I1). This means that the changes induced by baking to remove the high field Q-slope, are deep enough to be unaffected by HF chemistry (renovation of Nb_2O_5 layer and Nb-oxide interface). This observation refutes particularly the "Interface Tunnel Exchange" (ITE) theory [1] which argues that the decrease of Nb_2O_5 thickness during baking explains the Q-slope removal.

After HF chemistry the metal-oxide interface is rebuilt with interstitial oxygen forming a bad superconducting layer (Nb_4O, Nb_6O), true origin of the high field Q-slope according to the theory [8]. In this theory, Q-slope removal after baking is explained by the oxygen dilution in the bulk. However, HF treatment applied on baked cavity does not restore the initial Q-slope (before baking), refuting consequently this theory.

As we have already noted, the baking treatment was made four years before: the baking effect and the cavity change can considered as definitive.
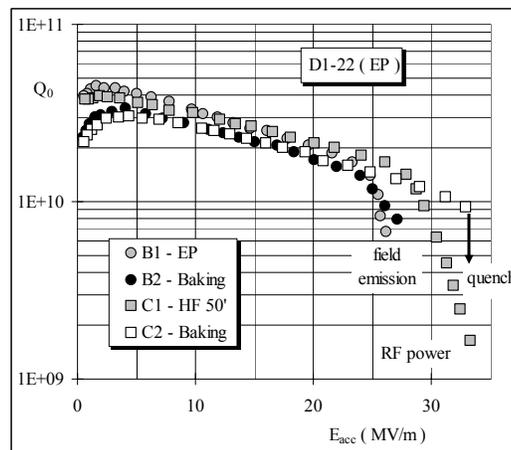
Figure 9: HF chemistry suppresses field emission and modifies Q-slope at low field.
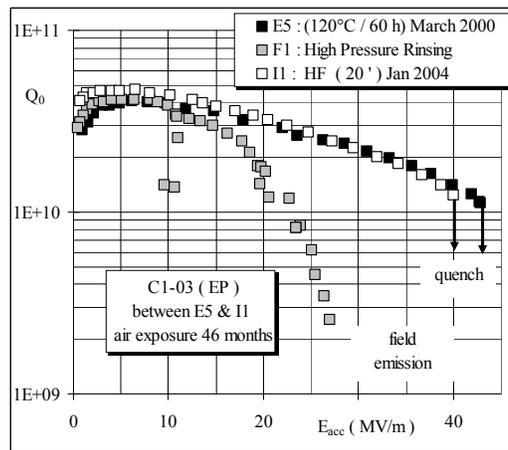
Figure 10: HF treatment and its consequences on a baked EP cavity (field emission and low field Q-slope).

3.8.6 Diffusion Process

Before the baking effect discovery, the oxygen diffusion, concomitant to any heat treatment, has been widely considered. This is because a lot of oxygen is found at the niobium surface as niobium oxide, sub-oxides or as interstitials and because it easily diffuses in the bulk material, even at low temperature [9].

To evaluate this process, we can use a simple model based on the second Fick's law giving an analytic solution (Equation 4) for the concentration of a diffusing element in a semi-infinite medium:

$$C(x,t)/C_S = erfc\frac{x}{2\sqrt{D(T)t}}, \tag{4}$$

where $D(T)$ is the diffusion coefficient of the considered element [10], with initial condition in the bulk $C(x,0) \equiv 0$ and the boundary condition on the surface $C(0,t) = C_S$. According to this model, we can see in Fig. 11 for the usual baking parameters ($T = 120°C / t = 60$ hours) that oxygen penetration by diffusion is similar to the RF penetration depth at 2 K (~ 50 nm) and that other elements likely to be present at the surface (nitrogen or carbon) diffuse 100 times less than oxygen.
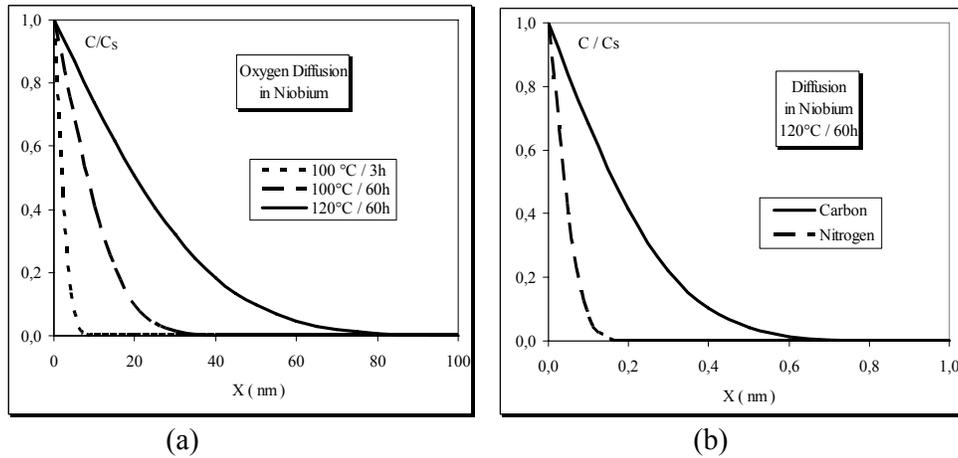
Figure 11: a) Oxygen diffusion profiles in Niobium for different temperatures and baking times. b) Nitrogen and Carbon diffusion profiles at 120°C for 60 hours.

Some observations of the baking effect can be directly attributed to the oxygen diffusion like the decrease of the R_{BCS} resistance through its dependence on the electron mean free path [11]. The high field Q-slope can also be linked to the diffusion process because a strong correlation has been observed at Saclay between the E_{acc} value of the high field Q-slope onset and the baking time (Fig. 12).

The right parameters to improve the performances of the cavity by baking seem to be 100°C for 60 hours (Fig. 13) with a "moderate" oxygen concentration in the RF superconducting layer to dope niobium. At higher temperatures (up to 250°C), decreases of Q_0, quench field and critical temperature T_C have been observed [12]: this corresponds to niobium pollution with probably too much oxygen under the surface. Above 250°C, Nb_2O_5 is totally dissolved and the trend is reversed with the increase of these parameters, corresponding to oxygen depletion on the cavity surface.

All these observations lead to think that the oxygen diffusion process plays a crucial role in the cavity performances at high field.

We studied the effects of temperature and time changes to corroborate the diffusion hypothesis: "fast baking" (145°C / 3 hours) should be roughly equivalent in terms of diffusion to the usual baking (110°C / 60 hours) and lead to a similar behavior for the high field Q-slope. This prediction was experimentally observed on Nb cavity after "fast baking" treatment [13], under UHV conditions, using infrared heaters and remote thermal sensor (Fig. 14) to regulate the temperature for three hours.

Moreover, "fast baking" process can be implemented with cavity open ended in an oven to avoid restrictive UHV requirements and risks of helium leaks after thermal treatment. This technique includes a baking under Argon atmosphere [14] to prevent the uncontrolled oxygen diffusion coming from the Niobium surface. This treatment can be realized, in practice, after chemistry and before cavity preparation in clean room.
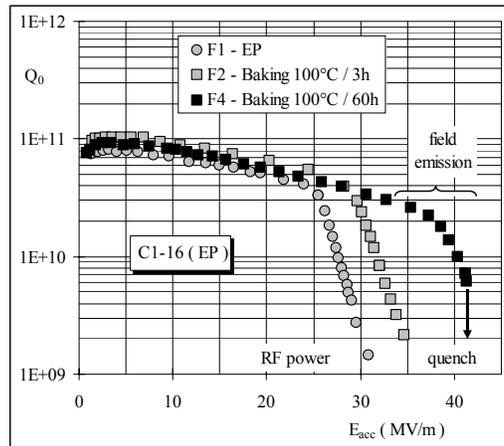
Figure 12: The E_{acc} value of the Q-slope onset is increasing with the baking time.
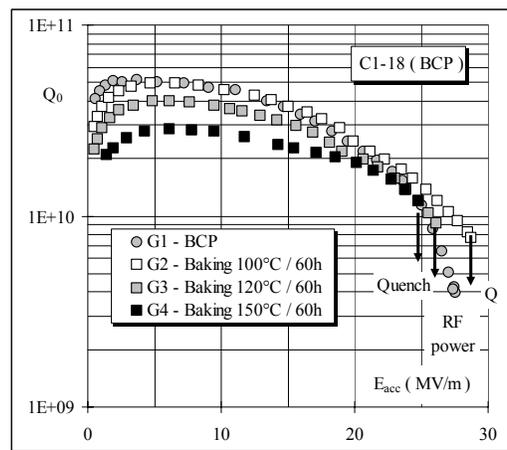
Figure 13: Deterioration of Q_0 and quench position with the increase of UHV baking temperature.

Figure 14: 1.3 GHz cavity, IR heaters and thermal sensor used in "fast baking" experiment

3.8.7 Surface Treatments by Hot Chemistry

These surface treatments are characterized by an acid attack of the niobium pentoxide by baths of nitric-phosphoric or nitric-sulphuric acids at 110°C during one hour.

$$6\,Nb + 10\,HNO_3 \rightarrow 3\,Nb_2O_5 + 10\,HNO + 5\,H_2O$$

$$Nb_2O_5 + 2\,H_3PO_4 \rightarrow Nb_2O_2(PO_4)_2 + 3\,H_2O$$

$$Nb_2O_5 + n\,H_2SO_4 \rightarrow Nb_2O_{5-n}(SO_4)_2 + n\,H_2O$$
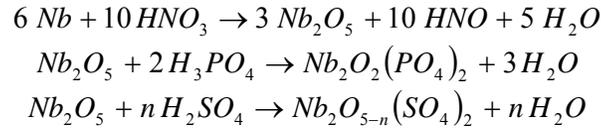
As we can see on Fig. 15, such treatments cause a general deterioration of Q-slopes at medium field with a less marked transition between medium and high field Q-slopes. These results are only incidentally reported here, because of the general and disappointing deterioration of the $Q_0(E_{acc})$ curve. Causes of this deterioration are not well understood at this moment but they are certainly due to a surface pollution correlated with a thermal diffusion of some elements.
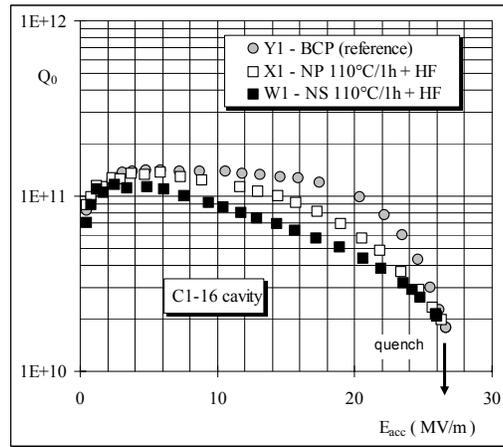
Figure 15: Treatments by hot chemistries lead to the medium field Q-slope worsening.

3.8.8 Conclusion

Modifications of Q-slopes, induced by some specific treatments of the cavity surface, can help us to understand the $Q_0(E_{acc})$ curve:
- Hydrofluoridric chemistry improves the low field Q-slope, suggesting its origin in the Nb_2O_5 -Nb interface. This is compatible with the cluster theory,
- HF treatment is very useful to suppress the field emission. Applied on a baked cavity, this treatment does not affect the high field section of the curve. High field Q-slope and its cure by baking find their origin in the niobium metal and not at the interface. This result refutes the "Interface Tunnel Exchange" and the "Bad Superconducting Layer" models as theoretical explanations,
- Baking modifies low, medium and high field parts of the curve with an increase of the slope at low field, its suppression at high field and a trend toward flattening at medium field.

- Strong correlation between high field Q-slope and oxygen diffusion leads not only to consider this diffusion as a consequence of the cavity baking but as the probable real cause of the high field Q-slope improvement.

Experiments on "fast baking" are in accordance with this hypothesis. Moreover, performed in an oven under argon atmosphere, this method simplifies the baking process, saving time and avoiding the UHV requirements.

3.8.9   Acknowledgments

I wish to especially thank my Saclay colleagues A. Aspart, Y. Gasser, J.P. Poupeau, B. Coadou and J.P. Charrier for their enthusiasm and efficiency in performing cavity preparation and RF tests, without forget M. Jablonka for the careful proofreading of this paper.

3.8.10   References

1. J. Halbritter, "Material Science of Nb RF Accelerator Cavities: where do we stand 2001?" Proc. of the 10th Workshop on RF Superconductivity, Tsukuba, Japan, 2001, paper MA006 (http://conference.kek.jp/SRF2001)
2. G. Ciovati et al., "Effect of Low Temperature Baking on Nb Cavities" Proc. of the 11th Workshop on RF Superconductivity, Lübeck/Travemünde, Germany, 2003, paper WeO14 (http://srf2003.desy.de/)
3. B. Visentin, "Q-Slope at High Gradients: Review of Experiments and Theories" Proc. of the 11th Workshop on RF Superconductivity, Lübeck/Travemünde, Germany, 2003, paper TuO01 (http://srf2003.desy.de/)
4. J. Knobloch et al., "High Field Q Slope in SC Cavities due to Magnetic Field Enhancement at Grain Boundaries" Proc. of the 9th Workshop on RF Superconductivity, Santa Fe, New Mexico, USA, LA-13782-C, 1999, p. 77.
5. B. Visentin et al., "Improvement of Superconducting Cavity Performances" Proc. of the 6th European Particle Accelerator Conference, Stockholm, Sweden, 1998, p. 1885.
6. B. Visentin et al., "A High Gradient Q-Slope: Non "in-situ" Baking, Surface Treatment by Plasma and Similarities between BCP & EP Cavities" Proc. of the 11th Workshop on RF Superconductivity, Lübeck/Travemünde, Germany, 2003, paper MoP19 (http://srf2003.desy.de/)
7. G. Ciovati, "High Q at Low and Medium Field," Proceedings of the Workshop on Pushing the Limits of RF Superconductivity, Argonne report ANL-05/10, March 2005, p. 52.
8. H. Safa, "High Field Behaviour of SCRF Cavities" Proc. of the 10th Workshop on RF Superconductivity, Tsukuba, Japan, 2001, paper MA008 (http://conference.kek.jp/SRF2001)
9. F. L. Palmer, "Influence of Oxide Layers on the Microwave Surface Resistance of Nb" *IEEE Trans. Magn.* **23**(2), 1617 (1987).
10. G. Horz et al., eds., *Physics Data: Gases and Carbon in Metals, Part VIII: Nb*, Fachinformationszentrum Energie-Physik-Mathematik GmbH., Karlsruhe, 1981.
11. P. Kneisel, "Preliminary Experience with "in-situ" Baking of Nb Cavities" Proc. of the 9th Workshop on RF Superconductivity, Santa Fe, New Mexico, USA, LA-13782-C, 1999, p. 328.
12. B. Visentin et al., "A Non Electropolished Nb Cavity Reached 40 MV/m at Saclay" Proc. of the 8th European Particle Accelerator Conference, Paris, France, 2002, p. 2292.
13. B. Visentin et al., "First results on Fast Baking" Proc. of the 12th Workshop on RF Superconductivity, Ithaca, USA, 2005, paper TuP05 (http://www.lns.cornell.edu/public/SRF2005/).

106

14. B. Visentin et al., "Alternative Baking Process for Mass Production of Nb SCRF Cavities" Proc. of the 10th European Particle Accelerator Conference, Edinburgh, Scotland, 2006 – to be published.

3.9 Thin Film Coatings for RF Superconductivity

G. Wu[†], H. L. Phillips
Jefferson Lab, Newport News, VA 23606, USA
mail to: genfa@jlab.org

3.9.1 Abstract

Niobium on copper technology has been a viable and attractive alternative to solid niobium for some applications of RF superconductivity. It becomes a "must have" technology for some applications. Interests are growing to dramatically improve the performance of niobium thin film cavities. Different coating processes are considered and in development around the world. The latest status and results for these different coating processes will be presented. Alternative coating technology will also be discussed.

3.9.2 Introduction

Recent development in RF superconductivity (SRF) is both exciting and limiting. The single-cell elliptical RF cavities based on solid niobium are reaching accelerating gradients of 40 MV/m [1]. Multicell cavities are not far behind, with 35 MV/m frequently obtained from TESLA-style 9-cell cavities [1]. While the solid-niobium-based SRF is approaching its theoretical limit, the cost of the solid niobium remains much too high. The future development of SRF technology becomes reducing cost or finding alternative materials to exceed the 40-50 MV/m accelerating gradient limitation due to the theoretical magnetic field limitation. The answer could well be the SRF based on thin film technology: the copper based niobium thin film cavity for near term cost reduction and, for long-term, the new material cavity, employing for example Nb_3Sn, for the accelerating gradient to reach well beyond the 40-50 MV/m limitation.

The successful LEP-II [2] proved the viability of thin film technology in particle accelerators. Since copper material can be one tenth of the cost of niobium, plus the potential for much lower manufacturing cost, the thin film technology has potential to reduce the particle accelerator cost dramatically. The technology would be a real benefit for a muon storage ring, which calls for large 200-MHz cavities [3]. The existing magnetron sputtered niobium thin film cavity achieved 20 MV/m for single cell elliptical RF cavity at 1500 MHz [4]. From the perspective of thin film deposition process, the magnetron sputtering technique has some limitations to achieve the most desirable film structure. The process has relatively low impacting energy and has difficulty to form a high quality thin film on some areas inside an elliptical cavity due to the low deposition angle [5].

Most discussions associated with niobium thin film on copper are covered in these proceeding by Calatroni [6], and a comprehensive survey of superconducting materials are covered by Palmeri and Tajima [7,8], also in these proceedings. This paper will

focus on the various processes used in creating the film coatings, especially on those processes that feature the higher kinetic energy.

3.9.3 Technical Challenges

While thin film technology is promising, many challenges remain. The current niobium thin films coated in magnetron sputtering systems show columnar structure, which was totally different from the large crystals in solid niobium. The large grain density and the intra-grain defects may be the causes for the high field Q-drop [4]. Some high temperature annealing can reduce the grain density, but is not practical for the copper substrate. One way to achieve the film structure close to that of solid niobium is to increase the surface adatom mobility while the film grows [9]. Several processes were explored to achieve this in niobium thin film coatings, which will be described later. Epitaxial growth was observed in niobium thin films both in magnetron sputtering process with heated sapphire substrate [10] and in plasma vacuum deposition with unheated sapphire substrate [11]. The film thickness was around one micron-meter and not a comfortable case to show the real benefit of solid niobium like film structure. The niobium films on copper substrate have not achieved the same quality as the films based on sapphire substrate.

The current technologies to coat niobium thin film apply to the basic RF accelerating structures with relatively simple geometries. The film quality could suffer dramatically or sometimes actually not be feasible to deposit in some RF structures like split-loop resonator or power couplers.

Any new material coatings need to overcome the geometry difficulty and demonstrate better surface quality than niobium with respect to the critical magnetic field and surface resistance.

3.9.4 Current Status of Thin Film Coatings

The current thin film coating activities within the SRF community can be categorized into three main efforts. These are the coatings of non-niobium materials, the coating of niobium using traditional sputtering technique, and the coatings of niobium using alternative vacuum processes. Traditional sputtering coated niobium film and non-niobium material can be found in several papers in the proceedings of the Workshop on Pushing the Limits of RF Superconductivity held at Argonne in September 2004. [6-8].

Australian National University (ANU) continues to explore the electroplating process for lead-tin alloy coating on copper substrate [12]. This cost effective process bodes well for ANU's heavy ion linac. The electroplating uses the commercial Schloetter MSA plating solution to deposit Pb(96)Sn(4) alloy film onto the copper substrate. After process optimization, the cavities achieved 26 MV/m peak electric fields and 65 mT peak magnetic fields. The best accelerating gradient reached 3.9 MV/m.

Many new materials have been investigated at INFN-Legnaro and Padua University [7]. A majority of the depositions were based on the magnetron sputtering process. Deposition angle studies showed the shadow effect for the magnetron sputtering process. Effort has been taken to improve geometric configuration to address the shadow effect and improve the coating rate [13]. A biasing grid was introduced in the

standard magnetron sputtering system to both promote the surface atom rearrangement and re-sputter the impurities [13]. Molecular chemical vapor deposition (MOCVD) for Nb_3Sn [7] and liquid solution diffusion method [14] were developed at Padua University. If successful, these processes should work well for RF structures with complex geometries.

The RF surface resistance of MgB_2 film was investigated at Los Alamos National Lab. The result shows the recently discovered superconductor remains hopeful for possible SRF applications [8].

While CERN and ACCEL/Cornell continued to study the niobium coatings by traditional magnetron sputtering, a biased mechanism was planned to improve the coating qualities. Initial result from CERN showed an improved surface smoothness when certain bias voltage was applied [6].

A separate effort from Cornell University in collaboration with the York University focused on optimization of the traditional magnetron sputtering process [10]. The goal is to reduce the impurities, defects, improve the grain boundary morphology, and preserve the high quality of the thin film surface after coating. One such film showed a remarkably higher H_{c1} compared to benchmarking solid niobium sample, which suggested an even higher maximum accelerating gradient for a possible thin film cavity than solid niobium cavity. To aid such a process optimization, different metals were investigated to replace the copper substrate. In principle, such metals should have a good thermal conductivity at liquid helium temperature and a higher melting point temperature than copper.

Peking University has been working on biased magnetron sputtering for several years [15]. Currently, the copper quarter wave resonator reached 4-5 MV/m at 4.2 K with Q_0 close to 10^9. Judged from the superconducting transition curve, biasing of the substrate did improve the film quality, but has yet to reach the full potential of biased magnetron sputtering. An intermediate layer of NbN was introduced through reactive sputtering to study the effect of mismatch between niobium and copper interface. The study remains an ongoing effort.

The materials modification lab at SANDIA started to use their Pulsed Ion Beam Ablation Deposition system to explore the high-energy niobium thin film coatings. The MgB_2 film was also made, which showed a T_c at 11K. Some contamination was evident [16].

The INFN/Roma2 and Soltan institute started a joint venture to investigate niobium coatings using the vacuum arc process [17]. The improvement of the thin film quality was dramatic in terms of RRR as high as 80 and solid niobium like transition temperature. Recent RF measurement showed the low field RF surface resistance was of the same magnitude as the solid niobium. The high vacuum condition was generally considered the main reason for the good film quality. The higher deposition energy not only improved the film adhesion to the substrate, but also created a densely packed film structure. The ionized nature of the niobium reduces the film growth shadow effect caused by the non-90° deposition angle commonly seen in low energy deposition processes. The macro-particle remains a concern for this vacuum process. A cylindrical arc system is currently under development. The goal is to develop a successful filter which can screen out the macro-droplets while maintaining sufficient deposition rate.

Alameda Applied Science Corporation started to develop a similar cylindrical vacuum arc deposition system (CED) capable to coat 1.5 GHz CEBAF 7-cell Low Loss

cavities [18]. A Venetian-blind filter prototype was built to investigate the effectiveness of macro-particle filter. The CED system was also being used to coat MgB_2 films.

Jefferson Lab has developed an ECR plasma coating system [11] to investigate how the deposition energy can influence the film growth to achieve a thin film with solid niobium like material properties. The process has all the advantages from vacuum arc process, plus the relatively narrow energy span for fully ionized depositing niobium atoms. The resulting film achieved high RRR of 50 and transition temperature close to that of solid niobium. The high deposition energy helped to produce an epitaxially grown niobium thin film on a sapphire substrate. The niobium films on copper substrates showed an improved crystal orientation following the increased deposition energy. Due to some atom backscattering, the current sample system was limited by the niobium source capacity to have a film thicker than 500 nm. A coating prototype system for 500 MHz single cell cavities is currently under development [19] in collaboration with Cornell University. The plasma efficiency and niobium source capacity are expected to improve dramatically. The uniformity of the thin film quality is the goal of the prototype.

A recent work by Gurevich suggests that vortex penetration field threshold in niobium material can be increased by applying a multilayer coating consists of alternating superconducting and insulating layers with thickness less than the London penetration depth [20]. Such surface engineering suggests a possible accelerating gradient inside a SRF cavity far higher than that of solid niobium.

Table 1 summarizes the recent results from different niobium coating processes.

3.9.5   Future Studies

Based on the complex geometry of RF structures, we propose to the SRF community to start a new research front to focus the coating technology on the need to be robust in obtaining coating uniformity. Such activities should include investigating substrate materials other than copper. Plasma coating needs to be expanded to study the coating of RF structures with complex geometry. Chemical vapor deposition (CVD) needs to be explored, as well as its derived processes such as MOCVD, plasma enhanced CVD, and photo, even laser assisted CVD. Table 2 lists several simple niobium compounds and their boiling point temperature, which can be the starting material to explore the CVD processes for niobium. One such process involving NbI_5 has been proposed by Hand [21]. It is worth noting that NbI_5 also may be used for liquid processes, since it melts around 200°C when decomposing also starts.

Table 1: Comparison of niobium films on sapphire by several coating processes

Coating processes	T_c(K)	ΔT_c(K)	RRR[***]	Crystallization (measured by X-ray diffraction)	Film structure by XTEM analysis
Magnetron Sputtering	9.5	0.3	5-10	Range from oriented to less oriented, depends on deposition angle.	Columnar growth Some voids present at high deposition angle
Biased Magnetron Sputtering	9.6	>1K	7-15	N/A	Columnar growth
Vacuum Arc Deposition[*]	9.25	<0.02	20-100	Preferred orientation, other orientations exist	Columnar growth, densely packed
Energetic vacuum deposition[**]	9.1	0.07	50	Perfectly oriented	Epitaxial in some films.

* T_c measured by different method.
** Sample made at deposition energy around 123 eV on sapphire substrates.
*** RRR measured on sapphire substrates.

Table 2: Simple niobium compounds and their boiling point temperature

Nb compounds	Boiling point (°C)
NbF_5	234
$NbCl_5$	250
$NbBr_5$	360
$NbBr_3$	400

The early electroplating work at SIEMENS showed the possibility to do niobium coating onto complex RF structures. This is worth revisiting, since post processing may be able to overcome the disadvantages associated with the electroplating process.

The most important work for the alternative materials research should be the investigation of the critical magnetic field, followed by the surface resistance. The real viability of A15 superconductors and MgB_2 for SRF applications has not yet been demonstrated. But several coating processes such as Nb_3Sn by liquid solution diffusion method [7,14] and MgB_2 by HPCVD [22] bode well for complex RF structures.

3.9.6 Conclusion

We expect elliptical RF cavities coated with niobium thin films will soon be available from enhanced magnetron sputtering and vacuum deposition processes; realistic surface resistance will be measured and correlated to thin film physics. Those deposition processes are aimed to improve the niobium thin film coating at the material structure level. It is reasonable to speculate that the path to the coating free of high field Q-drop should be clearer, which should help us to take advantage of the full potential of the niobium thin film technology.

Niobium cavities have shown accelerating gradients close to the ultimate performance limitation. The search for alternative materials that can exceed that limitation of niobium bears significant importance to the future of the RF superconductivity, and thus deserves increased attention.

3.9.7   Acknowledgments

The authors are grateful to the following colleagues who provided their recent research status and some valuable discussions: S. Calatroni (CERN), H. Padamsee (Cornell Univ.), T. Tajima (Los Alamos), L. Hand (Cornell Univ.), W. Frisken (York Univ.), K. Zhao, J. Hao, F. Zhu (Peking Univ.), N. Lobanov (Australia National Univ.), R. Russo, S.Tazzari (INFN/Roma2), M. McFarland, A. Gehran (Alameda Applied Science Co.), and T. Renk (Sandia).

3.9.8   References

1. K. Saito, Proc. of 2003 Particle Accelerator Conference, Portland, p. 462 (2003).
2. P. Brown, et. al., 9th Workshop on RF Super-conductivity, Santa Fe, (1999), edited by B. Rusnak, Los Alamos National Laboratory, Los Alamos, 1, (1999).
3. H. Padamsee, 2001 Particle Accelerator Conference, Chicago, Illinois U.S.A., p. 468 (2001).
4. V. Arbet-Engels et al., Nucl. Instrum. Methods A 463 (2001), 1-8.
5. D. Tonini et al., "Morphology of niobium films sputtered at different sputtering target-substrate angle" in Proc. of 11th workshop on RF superconductivity (2003), edited by D. Proch, 2003, paper ThP11 (http://srf2003.desy.de).
6. S. Calatroni, Proceedings of the Workshop on Pushing the Limits of RF Superconductivity, Argonne report ANL-05/10, March 2005, p. 149.
7. V. Palmieri, Proceedings of the Workshop on Pushing the Limits of RF Superconductivity, Argonne report ANL-05/10, March 2005, p. 158.
8. T. Tajima, Proceedings of the Workshop on Pushing the Limits of RF Superconductivity, Argonne report ANL-05/10, March 2005, p. 219.
9. J.A. Thornton, J. Vac. Sci. Technol. 11 (1974), 666.
10. L.N. Hand et al., "Characterization of Niobium Thin Films and a Bulk Niobium Sample with RRR, SIMS and a SQUID Magnetometer" in Proc. of 11th workshop on RF superconductivity (2003), edited by D. Proch, 2003, paper ThP071 (http://srf2003.desy.de).
11. G. Wu et al., J. Vac. Sci. Technol. A 21(4), (2003).
12. N.R. Lobanov and D.C. Weisser, "Lead-Tin Plating Split Loop Resonators," Proc. of 11th Workshop on RF superconductivity (2003), edited by D. Proch, 2003, paper TuP20 (http://srf2003.desy.de).
13. G. Lanza et al., "New magnetron configurations for sputtered Nb onto Cu," Proc. of 12th workshop on RF Superconductivity (2005), edited by H. Padamsee (to be published).
14. S.M. Deambrosis et al., "A15 Superconductors: Alternative to Nb for RF Cavities," Proc. of 12th workshop on RF Superconductivity (2005), edited by H. Padamsee (to be published).
15. K. Zhao, J. Hao, F. Zhu, private communications.
16. T.J. Renk, private communications.
17. A. Cianchi et al., "Superconducting Niobium Film for RF Applications," Proc. of EPAC'04, Lucerne, Switzerland, Published by the European Physical Society Accelerators Group (EPS-AG) and CERN (2004), pp. 1108-1110, http://accelconf.web.cern.ch/accelconf/e04/default.htm
18. M. McFarland, A. Gerhan, private communications.
19. A-M.Valente et al. "Niobium Thin Film Cavity Deposition by ECR Plasma," Proc. of EPAC'04, Lucerne, Switzerland, Published by the European Physical Society Accelerators Group (EPS-AG) and CERN (2004), pp. 1108-1110, http://accelconf.web.cern.ch/accelconf/e04/default.htm

112

20. A. Gurevich, "Enhancement of rf breakdown field of superconductors by multilayer coating," Appl. Phys. Lett. 88, 012511 (2006).
21. L. Hand, Proc. of Thin Film for SRF 2005, Jefferson Lab, Newport News, VA, USA.
22. X. Zeng et al., "In situ epitaxial MgB_2 thin films for superconducting electronics," Nature Mater. 1, pp. 35-38, (2002).

3.10 New Geometries: Elliptical Cavities

J. Sekutowicz

DESY, Notkestraße 85, 22603 Hamburg, Germany

mail to: jacek.sekutowicz@desy.de

3.10.1 Introduction

Achieving high accelerating gradients beyond 35 MV/m was and is of great relevance for linear accelerators based on the superconducting technology. This goal has been the motivation for R&D programs at many laboratories of the TESLA Collaboration [1] for more than the last decade. The gradients were reached worldwide in single-cell cavities and recently they have been demonstrated in four electro-polished 9-cell structures at DESY [2]. After the International Technology Recommendation Panel decision, announced in August 2004, one shall ask the question again: by what means can we push further the routinely achieved accelerating gradients for the future International Linear Collider (ILC) [3]. It seems obvious that the higher purity of niobium and the improvement of surface cleaning procedures play here the main part. Additionally, further optimization of the cell geometry resulting in lower B_{peak}/E_{acc} and E_{acc}/E_{peak} ratios is desired because cavities will be less sensitive to the normal conducting impurities in the material and to the field emission from residual particulates on the cavity wall.

The second optimization of the cell geometry is with respect to the cryogenic load. For the cryogenic load minimization one chooses geometries with low magnetic field at the cavity wall (high geometric factor G) and with high efficiency of converting the cavity stored energy to an accelerated particles (high (R/Q)) [4].

The third direction in the optimization, we will discuss in this paper, is minimization of the interaction between a high accelerated current and parasitic resonances of a superconducting cavity. Here, preferable shapes shall have possible small longitudinal $k_∥$ and transverse $k⊥$ loss factors of HOMs and sufficient amplitude of their e-m fields at locations of the HOM dampers and couplers.

In general, optimization of the cell geometry is always a kind of trade-off between one of the chosen criteria mentioned above and the two others. There is no "golden cavity" suitable for a whole variety of accelerators based on the superconducting technology and the optimization has to take the application into account.

In the next sections we will mainly discuss the geometry of inner cells because, with very few exceptions, these dominate RF properties of a multi-cell structure.

3.10.2 RF Parameters of Inner Cell

Figure 1 shows a superconducting inner cell with the geometric parameters we use to optimize the RF-parameters, which are listed in Table 1. It is the simplest geometry

based on two ellipses with assumption that the contour is a smooth curve of the C1 class. The cell length and the equator diameter are not free parameters. The first one is matched to β of an accelerated beam. The second is utilized to match required frequency of the accelerating mode. The first column of the table shows criteria for the optimization. The second and the third columns list RF-parameters relevant for the optimization and direction of the optimization (arrows). The fourth column displays the most efficient geometric parameters (bold fonts) in varying the RF parameter(s) shown in the same row. Other listed geometric parameters serve for a final adjustment.
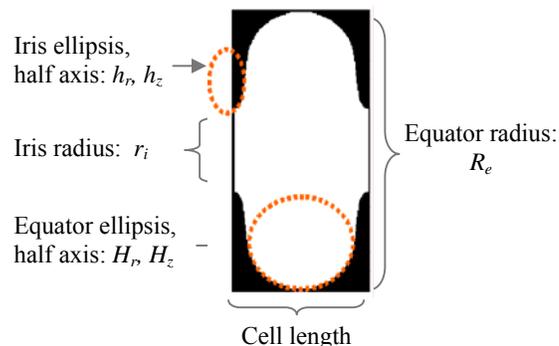
Figure 1: Geometric parameters of an inner cell.

Table 1: Criteria and RF-Parameters

Criterion	RF-Parameter	Opt.	Geometric Parameters
High gradient	E_{peak}/E_{acc} B_{peak}/E_{acc}	↓	r_i ↓ h_r, h_z, H_r, H_z
Low cryogenic load	$(R/Q) \cdot G$	↑	r_i ↓ (H_r, H_z)
Low HOM impedance	$k_\parallel, k\perp$	↓	r_i ↑

The aperture radius r_i has dominant influence on the cell optimization. This was studied in 1990 by E. Haebel and A. Mosnier [5]. By closing the iris one enhances electric field on axis, and increases the energy gain, even at the same stored energy in the cell. An example is shown in Fig. 2. Two 1.5-GHz inner cells differ only in r_i. The normalized electric field on axis is much higher for the cell with the smaller iris. Figure 3 summarizes the studies presented in [5]. All three showed RF parameter changes in a desirable direction when the iris radius becomes smaller. Unlike this, the cell-to-cell coupling k_{cc} and both loss factors $k_\parallel$ and $k\perp$ changed in a "wrong" way. An example for a 1.5-GHz cell is shown in Figs. 4 and 5. The coupling factor k_{cc} decreases dramatically by almost one order of magnitude when the iris radius decreases by a factor of two. A weak k_{cc} limits the number of cells in a multi-cell structure for the field flatness reason, as discussed later. The loss factors increase rather fast with decreasing iris radius. This

makes the interaction between beam and HOMs stronger and limits threshold current in an accelerator.

As shown in Table 1, we may correct the B_{peak}/E_{acc} factor modifying the cell shape in the equator region. A general rule is that increased volume for the magnetic flux lowers B_{peak} on the wall. Again, two 1.5 GHz cells with different equator region
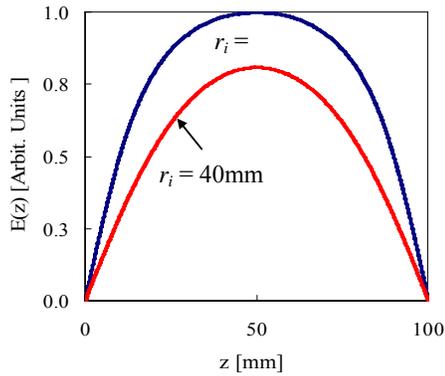
Figure 2: Electric field on axis for two inner cells with the different aperture radiuses of 20 and 40 mm.
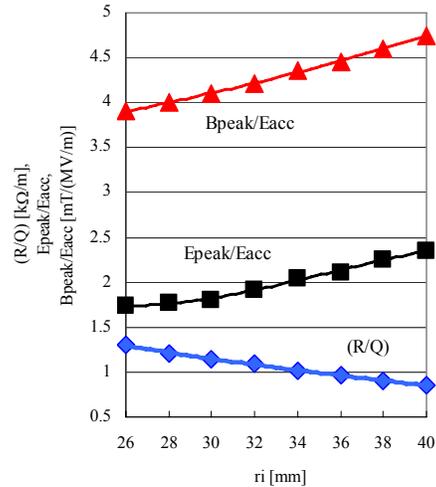
Figure 3: 1.5-GHz inner cell; accelerating mode parameters vs. iris radius.

geometry are shown in Fig. 6a. Their normalized magnetic flux on the wall is displayed in Fig. 6b. The cell with the bigger equator volume has 10% lower B and for the same surface resistance of the Nb wall it will have approximately 20% less cryogenic loss than the other cell Similarly, E_{peak}/E_{acc} can be improved by a proper shaping of the iris ellipsis. An example is shown in Fig. 7a. The cell with larger h_z has a 20% lower E_{peak}-
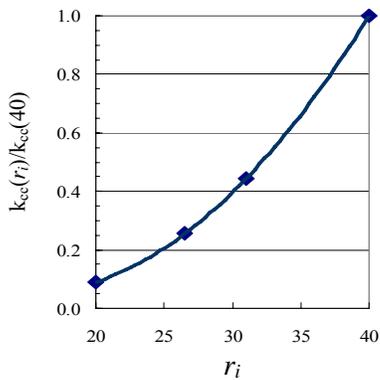
Figure 4: Normalized k_{cc} vs. r_i.
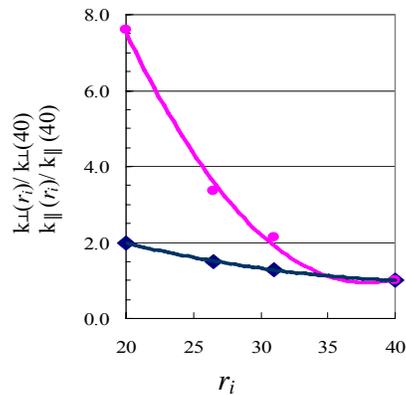
Figure 5: Normalized loss factors vs. r_i; monopole $k_\parallel$ (circles) and transversal $k_\perp$ (diamonds).

value (Fig. 7b). In general "enlarged surface" and bigger radiuses at the iris region lower the peak electric field. Table 2 contains RF data of various inner cells of multi-cell cavities, which have been prototyped or are under production. The two first cells
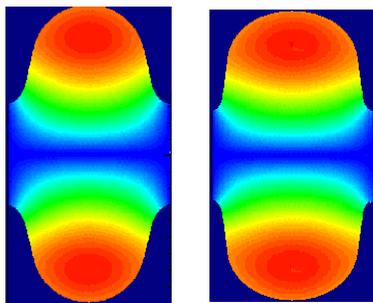
Figure 6a: Two 1.5-GHz cells with small volume in the equator region (left) and big volume (right). Colors illustrate B flux.
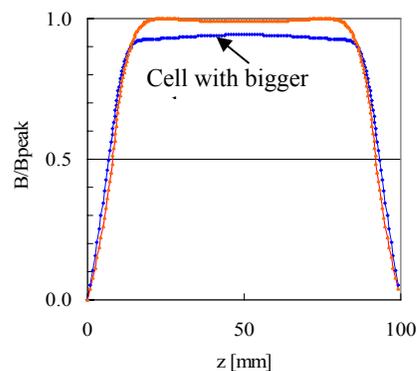
Figure 6b: Normalized magnetic flux for two 1.5-GHz cells with different geometry of the equator region.

(bold fonts) are listed here as a reference. The cavities based on these cells were designed in 1985 and 1992, respectively. The cells with $\beta = 1$ (except OC shape) match well the criteria we mentioned in Table 1. The TESLA cavities and the CEBAF upgrade high gradient (HG) cavities were designed with respect to the high gradient operation (low E_{peak}/E_{acc}). The low loss (LL) CEBAF upgrade cavity was designed to minimize the cryogenic loss. Finally, the shape of RHIC cooler cavity was chosen to keep interaction of HOMs with accelerated beam as low as possible. The computer simulation showed that its geometry allows for acceleration up to 2 A beams with the 5-cell cavity based on this cell.

The medium β cells are designed for moderate operating conditions. The only demanding RF-parameter for the fabrication is the cell-to-cell-coupling. This we will comment in the next section.
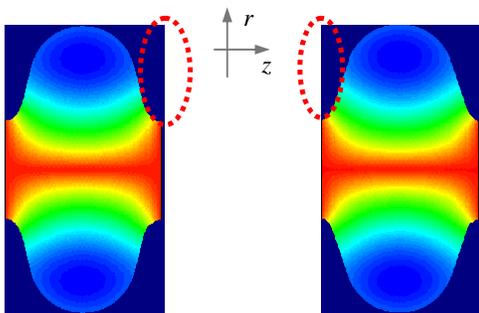
Figure 7a: Two 1.5-GHz cells with different ellipses in the iris region. Left: $2h_z$=25mm,. $2h_r$=42mm. Right: $2h_z$=20mm, $2h_r$=42mm. Colors illustrate E field.
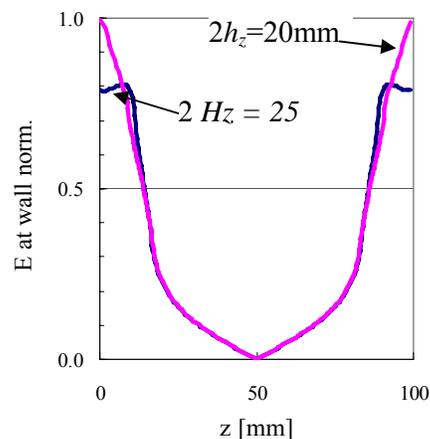
Figure 7b: Normalized E on metal wall for two 1.5-GHz cells shown in Fig. 7a.

Recently, two new shapes have been proposed for ILC. The first, re-entrant (RE) shape was studied and proposed at Cornell University [12], the second low loss shape at

1.3 GHz is proposed by DESY/KEK collaboration [13]. Both shapes are shown in Fig. 8. The RF-parameters are listed in Table 3. Both shapes could be used for standard 9-cell structures or for weakly coupled cavity pairs of $2\times$ 8-cells, so-called superstructures [14] (Fig. 9). Both shapes are difficult to clean and new cleaning methods must be developed to remove all particulates from the surface.

Table 2: RF-Parameters of Various Inner Cells

		CEBAF OC $\beta=1$	TESLA $\beta=1$	CEBAF -12 HG $\beta=1$	CEBAF -12 LL $\beta=1$	SNS $\beta=0.61$	SNS $\beta=0.81$	RIA $\beta=0.47$	RHIC Cooler $\beta=1$
f_o	[MHz]	**1448.3**	**1278.0**	1468.9	1475.1	792.8	792.8	793.0	683.0
f_π	[MHz]	**1497.0**	**1300.0**	1497.0	1497.0	805.0	805.0	805.0	703.7
k_{cc}	[%]	**3.29**	**1.9**	1.89	1.49	1.52	1.52	1.52	2.94
E_{peak}/E_{acc}	-	**2.56**	**1.98**	1.96	2.17	2.66	2.14	3.28	1.98
B_{peak}/E_{acc}	[mT/(MV/m)]	**4.56**	**4.15**	4.15	3.74	5.44	4.58	6.51	5.78
R/Q	[Ω]	**96.5**	**113.8**	112	128.8	49.2	83.8	28.5	80.2
G	[Ω]	**273.8**	**271**	266	280	176	226	136	225
R/Q·G	[Ω·Ω]	**26421**	**30840**	29792	36064	8659	18939	3876	18045
$k_\perp$ (σ_z=1mm)	[V/pC/cm^2]	**0.22**	**0.23**	0.32	0.53	0.13	0.11	0.15	0.02
$k_\parallel$ (σ_z=1mm)	[V/pC]	**1.36**	**1.46**	1.53	1.71	1.25	1.27	1.19	0.85
Reference		**[6]**	**[7]**	[8]	[4]	[9]	[9]	[10]	[11]

OC= Original Cornell shape, HG= High Gradient shape, LL= Low Loss shape

Table 3: New Shapes Proposed for ILC

		RE $\beta=1$	LL-1.3GHz $\beta=1$
k_{cc}	[%]	1.8	1.52
E_{peak}/E_{acc}	-	2.23	2.31
B_{peak}/E_{acc}	[mT/(MV/m)]	3.8	3.61
R/Q	[Ω]	126.8	133.7
G	[Ω]	277	283.6
R/Q·G	[Ω·Ω]	35124	37917

Figure 9: Weakly coupled two 8-cell structures based on RE shape.
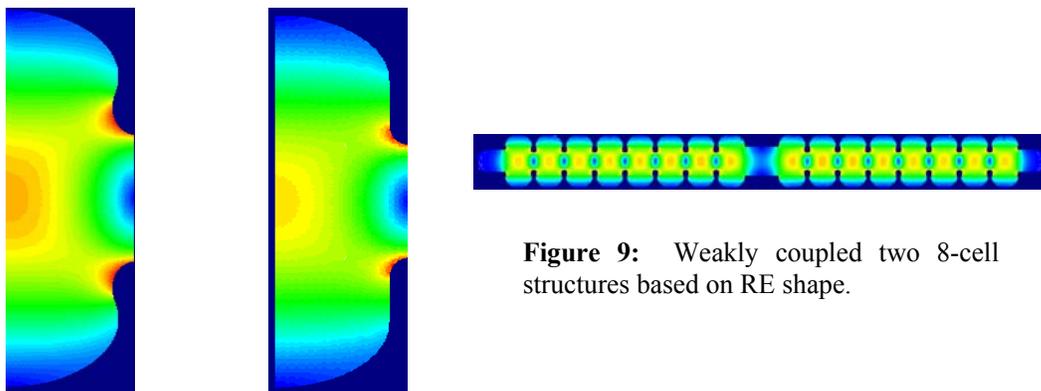
Figure 8: The RE inner cell (left) and LL inner cell (right) proposed for the ILC cavity.

3.10.3 Multi-Cell Structures

The investment costs reduction and the machine filling factor (a ration of the active length to the total machine length) lead to operation of multi-cell rather than single-cell cavities. The only exceptions are the single-cell B-factory cavities. They operate at very high currents with no energy recovery in circular accelerators. Thus power capability of input couplers and the required HOM damping allow for the single-cell design only.

There are three limitations in the number of cells in a superconducting structure:

- Field flatness of the accelerating mode
- Trapping of HOMs
- Power capability of the input coupler

We will briefly discuss two first limitations. Sensitivity of the accelerating field-to-cell frequency errors in the individual cells is an issue when structures operate at gradients just below the ultimate limit for niobium. In this case the cell having the most stored energy limits the performance of a whole multi-cell cavity, when others operate well below the limit. This reduces the acceleration efficiency.

The figure of merit for the field flatness sensitivity is the ratio:

$$a_{ff} = (N)^2/(\beta \cdot k_{cc})$$

where N is the number of cells. Lower a_{ff} means less sensitivity to the frequency errors and a smaller difference in E_{acc} amplitudes for a real multi-cell cavity. List of a_{ff} value for various multi-cell structures is shown in Table 4.

It is important to notice for future designs that even cavities with high a_{ff}, like the TESLA cavity, can be pre-tuned at room temperature and a field flatness better than 95% is preserved after all cleaning and assembly procedures. This was proven for more than 40 cavities installed at present in the TTF linac. Recently the RIA cavity which has the highest a_{ff} value was tuned successfully. Obviously there is a significant progress over the years in preserving the pre-tuning; therefore one can be less conservative in the future.

Table 4: Field Flatness Sensitivity Factor

Structure		N	a_{ff}
Original Cornell;	CEBAF 6 GeV	5	1489
High Gradient;	CEBAF 12GeV	7	2592
Low Loss;	CEBAF 12GeV	7	3288
TESLA		9	4091
SNS	$\beta = 0.61$	6	3883
SNS	$\beta = 0.81$	6	2924
RIA	$\beta = 0.47$	6	5040
RHIC		5	850

The second limitation in N is the HOM trapping. The phenomenon is due to differences in HOM frequencies of end- and inner-cells. A very helpful but limited remedy is to adjust end-cells and inner cells frequencies for both the accelerating and few chosen parasitic modes. This method has been first applied to TESLA cavities [1] to enhance damping of the third dipole passband which trapping was observed in the LEP structures.

The trapping problem was overcome in the RHIC 5-cell structure. Its end cells have very similar geometry to the inner cells. This is possible when irises are large and when the accelerating mode RF-parameters: (R/Q), E_{peak}/E_{acc} or B_{peak}/E_{acc} do not play the main part for the application. As it was already mentioned simulations showed that beam break-up threshold for that cavity is very high, which seems to be very exceptional for multi-cell structures. The other way to avoid trapping is to split long structures into subunits connected by short $\lambda/2$ interconnections (superstructure). For this configuration HOM couplers can be attached between subunits while the whole chain is fed by one input coupler and thus cost and filling advantages of long structures can be partially preserved.

3.10.4 Real Estate Gradient; End-cells and Interconnections

The real estate gradient is for long linear accelerators (ILC and XFEL linac) an important issue. Carefully achieved high gradients in accelerating cells should not be wasted by unnecessary space between structures and cryomodules. A good example can be the ILC accelerator. The TDR base line design foresees an interconnection between 9-cell structures of 283 mm. One may compress the interconnection to ~200 mm using a step in the interconnection as indicated in Fig. 10. The step-interconnection provides rather good decoupling for the accelerating mode and fixes standing wave pattern of monopole and dipole HOMs which have significant impedance (dipoles just above cut-off for the bigger diameter beam pipe). This makes their damping less sensitive to their frequency spread. The shorter interconnection demands a more compact design of a cold tuner or the utilization of a tuner similar to the one used for the weakly coupled structures [14]. In this case the tuner was attached at the helium vessel. Assuming that 30000 cavities will be installed in the ILC linac, the new interconnection will shorten the overall length by ~2.5 km. Again, further shortening is

possible when one uses weakly coupled structures. Every other interconnection is then $\lambda/2$ long (115 mm at 1.3 GHz) and the ILC accelerator is shorter by an additional 1.3 km. The benefit of total length reduction by ~4 km seems to be obvious and one should revise the end-cells and interconnection geometry for this machine.

Multi-cell cavity   Multi-cell cavity
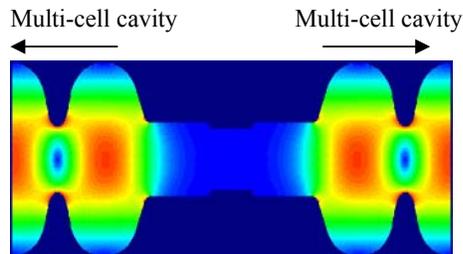
Figure 10: More compressed interconnection for the baseline design of the ILC accelerator.

3.10.5 Conclusions

The design of a standard cavity is a well understood process and only novel ideas demand sort of a "final tuning" to meet specifications coming from their applications. Some of them, still seen as a risky approach, e.g., weakly coupled pairs, will need more computer simulations and more experiments to proof further their RF properties and advantages.

Shape improvements can marginally push the performance of a cavity towards higher gradients, especially if one keeps in mind that the ultimate limitation of niobium is given by the critical magnetic field. However, an improvement of one of the inner cell parameters by a few percent—in this case the reduction of the peak magnetic surface field for a given accelerating gradient—degrades other parameters by more or less the same amount. Therefore it seems unlikely that one can make revolutionary improvements with elliptical cavity shapes presently in use. More can be expected from improved material purity, better surface preparation techniques and contamination-free assembly techniques.

3.10.6 Acknowledgements

3.10.7 References

1. Editors R. Brinkmann et al., "TESLA Technical Design Report," TESLA-Notes, 2001-23, March 2001.
2. L. Lilje, "State-of-the-Art SRF Cavity Performance," Proceedings of LINAC04, Lübeck, August 2004.

3. K. Saito, "Strategy for 50 MV/m," Presentation at TESLA Collaboration Meeting, DESY, Hamburg, April 2004.
4. J. Sekutowicz et al., "Low Loss Cavity for the 12 GeV CEBAF Upgrade," JLAB TN-02-023, June 2002.
5. E. Haebel et al., "Large or Small Iris Aperture in SC Multi-cell Cavities?" Proceedings of SRF1991, DESY, Hamburg, August 1991, p. 823.
6. P. Kneisel et al., "Performance of SC Storage Ring Cavities at 1500 MHz," *IEEE Trans. Magn.* **MAG-21**(2), 1985.
7. E. Haebel et al., "Cavity Shape Optimization for a Superconducting Linear Collider," HEACC, Vol. 2, Hamburg, 1992.
8. G. Ciovati et al., "An Improved Cavity Design for the CEBAF Upgrade," JLAB-TN 01-015, 2001.
9. P. Kneisel et al., "Superconducting Prototype Cavities for the Spallation Neutron Source (SNS) Project," Proceedings of EPAC2002, Paris, June 2002, p. 2247.
10. C.C. Compton et al., "Prototyping of a multi-cell superconducting cavity for acceleration of medium-velocity beams," submitted to *Phys. Rev. ST Accel. Beams*.
11. R. Calaga et al., "High Current Superconducting Cavities at RHIC," Proceedings of EPAC04, Lucerne, June 2004, p. 1120.
12. V. Shemelin et al., "The optimal shape of cells of a superconducting accelerating section," TESLA Note 2002-01, DESY.
13. J. Sekutowicz et al., "Design of a Low Loss SRF Cavity for the ILC," Proceedings of PAC2005, Knoxville, TN, May 2005, p. 3342.
14. J. Sekutowicz et al., "Test of two Nb superstructure prototypes," *Phys. Rev. ST Accel. Beams* **7**, 012002 (2004).

3.11 Testing the First 1300 MHz Reentrant Cavity

R.L. Geng, H. Padamsee, A. Seaman, J. Sears, V. Shemelin
Laboratory for Elementary Particle Physics,
Cornell University, Ithaca, NY 14853, USA
mail to: grl@mail.lns.cornell.edu

3.11.1 Abstract

We report the first test results of a superconducting niobium cavity of reentrant geometry, suitable for acceleration of β=1 charged particles in future superconducting machines such as a TeV scale superconducting linear collider. The reentrant geometry offers a reduced ratio of H_{pk}/E_{acc}. It hence has the potential to reach a higher accelerating gradient (E_{acc}) before the peak surface magnetic field (H_{pk}) hits the physical breakdown limit of superconductivity. A CW accelerating gradient of 44-45 MV/m was achieved at a peak surface magnetic field of 1683 Oe in a 1.3 GHz single-cell niobium cavity of reentrant geometry. As the critical RF magnetic field of niobium is still beyond 1683 Oe, further improvement in E_{acc} into the regime of 50 MV/m can be anticipated. New fabrication techniques were also adopted, such as half-cell post purification, half-cell electropolish and single-cell vertical electropolish.

3.11.2 Introduction

The accelerating gradient[5], E_{acc}, in RF superconducting niobium resonators has been raised remarkably in the past decades. In 1.3 GHz *single-cell* niobium cavities, an accelerating gradient in excess of 40 MV/m has been reliably achieved [1] with the best result being 42-43 MV/m [2].

The ultimate gradient limit E_{acc}^{max} for a given cavity geometry is set by breakdown of superconductivity when the peak magnetic field H_{pk} on the RF surface of a resonator reaches the critical RF magnetic field $H_{crit,RF}$,

$$E_{acc}^{max} = \frac{H_{crit,RF}}{H_{pk}/E_{acc}} \, . \tag{1}$$

$H_{crit,RF}$ is a material property and H_{pk}/E_{acc} is solely determined by the cavity geometry. The super-heating theory [3] predicts that $H_{crit,RF} = 1.2H_c$ for niobium at microwave frequencies, H_c being the DC thermodynamic critical field.

Despite the prediction of a $H_{crit,RF}$ value close to 2300 Oe at 2K, the maximum achieved experimental H_{pk} value is still below 1900 Oe. Over the past ten years, the 1.3-GHz niobium cavities in the 40-MV/m class were limited by quench at $H_{pk} = 1750 \pm 100$ Oe [4].

Advancing E_{acc} beyond the state-of-the-art can be realized through two avenues: (1) Develop new technologies for niobium material production and cavity surface processing so as to bring H_{pk} to the intrinsic limit $H_{crit,RF}$ of niobium or explore alternative material possessing a higher $H_{crit,RF}$, such as Nb_3Sn; (2) Reduce H_{pk}/E_{acc} by changing the cavity geometry.

The two approaches have different advantages: The first one has a higher potential premium; and the second one offers immediate benefit. Furthermore, these two approaches are totally independent and improvement realized through either one can be multiplied with that realized through the other. The present work has adopted the reducing H_{pk}/E_{acc} approach.

3.11.3 Reentrant Cavity and RF Optimization

The concept and RF optimization of reentrant cavity has been published in Ref. [5]. Here only a brief summary is given. Our optimization is referenced against the center-cell shape of the 1.3-GHz 9-cell TESLA cavity. Driven by the wakefield effect consideration, the bore hole diameter at iris is kept identical to that of the reference geometry (70 mm). This prerequisite has the following consequence: a reduced H_{pk}/E_{acc} is obtained only at the cost of an increased E_{pk}/E_{acc}. An elevated peak surface electric field (E_{pk}) in turn is disadvantageous in terms of field emission and voltage breakdown[6]. Nevertheless, there are convincing experimental data [6-8] to show that a

---

[5] The accelerating gradient is defined as the maximum voltage a β=1 particle can possibly gain during the transit of the resonator divided by the active length of the accelerating gap. The choice of the active gap length is not unique. In this paper, we take it as the half wavelength in vacuum of the microwave at the resonating frequency of the cavity.

[6] The conventional wisdom in cavity shape optimization is to reduce E_{pk}/E_{acc} for field emission concerns.

surface electric field of 100-200 MV/m imposes no fundamental limit to superconducting niobium.

The reentrant geometry we have chosen to evaluate experimentally is shown in Fig. 1. For comparison, the reference geometry of the original TESLA shape is given as well. Relevant RF parameters are compared in Table 1.
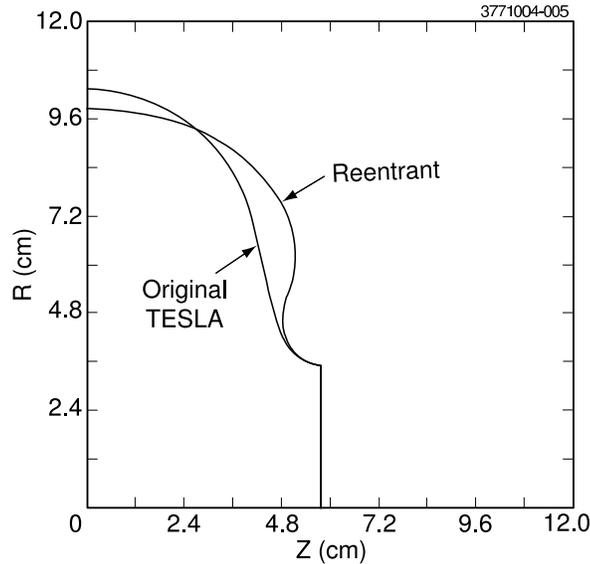
Figure 1: Half-cell contours of reentrant and original TESLA shape.

Table 1: RF parameters: reentrant vs. reference shape

Shape	$f[MHz]^{*}$	$\dfrac{H_{pk}}{E_{acc}}\left[\dfrac{Oe}{MV/m}\right]$	$\dfrac{E_{pk}}{E_{acc}}$	$k[\%]^{\dagger}$
Reentrant	1300	37.8	2.4	2.4
Original TESLA	1300	42.0	2.0	2.0

[*]Resonating frequency
[†]Cell-cell coupling factor

For understandable reasons, a single-cell cavity was fabricated for the first experimental evaluation of the concept. RF parameters of the single-cell cavity are slightly modified, as compared to that of the center cell of a multi-cell cavity, because of beam tubes. Ultimately, the calculated RF parameters of the single-cell reentrant cavity are given in Table 2.

Table 2: RF parameters of single-cell reentrant cavity

Frequency	1284	MHz
H_{pk}/E_{acc}	37.9	$\dfrac{Oe}{MV/m}$
E_{pk}/E_{acc}	2.2	--

3.11.4 Fabrication and Surface Treatment

The reentrant cavity was fabricated by using the regular method. Cups were formed by deep-drawing 3-mm-thick sheet material. The reentrant contour was obtained by multiple stamping steps using additional dies. Stacked cups with interleaving yttrium foils were heat treated in a furnace at 1200°C for four hours. The residual resistance ratio (RRR) was increased to about 500 from the starting value of 250. A layer of 20 μm was removed by chemical etch (BCP1:1:2) from both the inside and outside surfaces of the cups. Half-cells were joined to beam tubes (reactor grade niobium) by electron beam welding. The inner surfaces of half-cell/beam tube subassemblies were electropolished with a vertical setup [9], removing material by about 50 μm. The equator end of the subassemblies was immersed in BCP1:1:2 for five minutes. The final fabrication step was to join subassembly equators by electron beam welding (butt weld).

The surface preparation of the single-cell cavity, prior to each RF test, typically consists of chemical etch (BCP1:1:2 at temperatures below 10°C or vertical electropolish), followed by high-pressure water rinsing (pump pressure 1000-1200 psi), clean room assembly, and low temperature bake-out (90-120°C) under vacuum. Vertical electropolishing of a single-cell cavity (Fig. 2) is conceptually identical to that of a half-cell [9], except the fashion of acid agitation[7]. In any case, electropolish was performed in the continuous current oscillation mode.
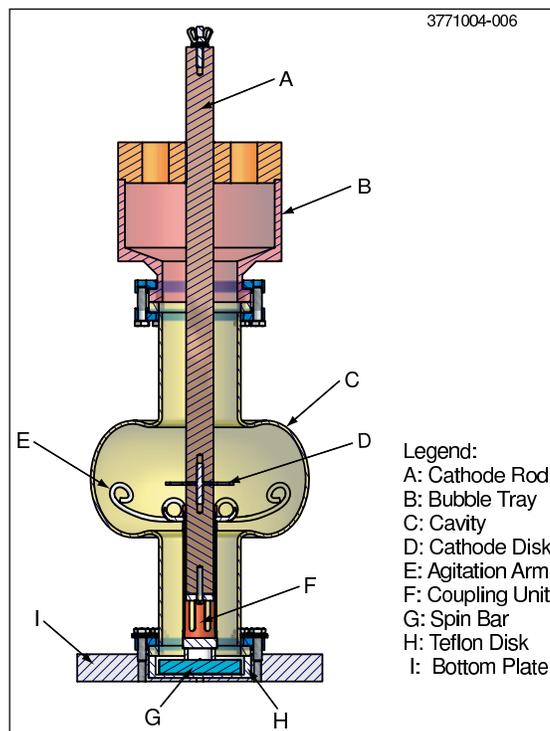
Figure 2: Vertical electropolish of a single-cell niobium cavity.

---

[7] For a half-cell, a magnetically driven spin bar alone provides sufficient agitation; whereas for a single-cell, acid agitation inside the cell must be provided directly by two flexible arms inserted into the cell space. The rotation movement of arms is provided by a coupled spin bar.

3.11.5 RF Test and Cavity Performance

RF tests were conducted at a nominal temperature of 2°K. Bremsstrahlung x-rays were monitored by a probe placed outside the liquid helium cryostat. The x-ray dose rate serves as an indicator for the intensity of field emission inside the cavity. $Q(E_{acc})$ curves were measured when the RF was operated in CW mode. RF processing (CW or pulsed) was applied often. Sometimes, gas helium processing was performed.

A summary of the results of the first eight RF tests is given in Table 3. After an accumulated surface removal of 18 μm by BCP1:1:2, an accelerating gradient of 27 MV/m was already reached during the second test at a Q_0 of 6×10^9. No field emission was observed. This result shows that gradients in excess of 25 MV/m can be obtained at a high Q_0 by performing heat treatment and primary electropolish at the half-cell stage. For large-scale cavity production, the fabrication cost can be saved appreciably if high temperature heat treatment and primary surface etch are done with half-cells.

The best result was obtained after the cavity was further electropolished (vertical electropolish and 50 μm surface removal) followed by additional etch with BCP1:1:2 (7 μm). Gas helium processing reduced field emission and boosted the accelerating gradient from 37 to 43 MV/m, a 16% gain. The highest gradient reached 44.4 MV/m at a Q_0 of 1×10^9 (Fig. 3) after the cavity was partially warmed up to an intermediate temperature (the exact value was not monitored). This corresponds to a peak surface magnetic field of 1683 Oe. A second gas helium processing somehow enhanced field emission. Nevertheless, it was able to re-establish the quench field at 44.3 MV/m despite the increased field emission. These data suggest that the high field quench is caused by the niobium material instead of field emission.

Table 3: Surface treatments after final equator welding and test results of the single-cell reentrant cavity

Test	Etch*	HPR†	Vacuum bake	E_{acc}^{m} **	$Q_0\left(E_{acc}^{m}\right)$	Limit	FE?	Comments
1	BCP 10μm	2 × 50 min	19 hr at 90 °C	25.0	5×10^9	Quench	Yes	
2	BCP 8μm	4 × 50 min	48 hr at 90 °C	27.1	6×10^9	Quench	No	
3	VEP 50μm‡	4 × 60 min	48 hr at 110 °C	26.9	7×10^8	Quench	Yes	
4	BCP 5μm	2 × 120 min	48 hr at 100 °C	18.4	2×10^8	Power	Yes	Test stand contaminated
5	BCP 2μm	2 × 60 min	--	37.1	8×10^8	Power	Yes	No bake out
6	--	--	54 hr at 100 °C	42.6	1×10^9	Power	Yes	After He processing
7	--	--	--	44.4	1×10^9	Quench	Yes	After partial warm up
8	--	--	--	44.3	8×10^8	Quench	Yes	After 2nd He processing

*   BCP 10μm = BCP1:1:2 etch to remove 10μm from both inside and outside surface
†   2 × 50 min = 2 cycles, 50 minutes each
**   Maximum E_{acc} achieved during test
‡   Single-cell vertical electropolish

A soft barrier was observed reproducibly at $E_{acc} \sim 25$ MV/m, in excellent agreement with calculated multipacting barrier (first order two-sided multipacting at equator [5]). It was easily processed through by exercising some RF processing. Similar multipacting barrier of comparable hardness is observable also in TESLA type single-cell cavities, as well as nine-cell cavities. Based on these results, it is expected that a multi-cell reentrant cavity will have also, but not be limited by, a soft multipacting barrier.

3.11.6 Conclusions

The results of these experiments demonstrate that the accelerating gradient can be improved by reducing the H_{pk} / E_{acc} ratio. Exploration in this direction is thus warranted. A new RF design has already shown that H_{pk} / E_{acc} can be further reduced to 35 Oe/(MV/m) by reducing the iris diameter to 60 mm.

The achieved 44.4 MV/m represents the highest accelerating gradient ever realized in a niobium RF resonator although field emission is strong. Q_0 remains $> 10^{10}$ up to $E_{acc} = 35$ MV/m. Further improvement into the regime of 50 MV/m can be anticipated by additional surface treatment.

The current optimization prerequisite of maintaining a large iris diameter results a penalizing higher E_{pk} / E_{acc}. Not surprisingly, excessive field emission was observed. But field emission was found to be not responsible for the gradient limit. The high peak surface electric field (~ 100 MV/m) on a broad area in CW mode is believed to impose no fundamental limit, but further tests are needed to carefully examine its effect.

These experiments also demonstrate that high-gradient (25 MV/m) cavities can be fabricated by doing high temperature post-purification heat treatment and primary chemical etch of RF surfaces at the half-cell stage. For large-scale production of niobium cavities, fabrication cost can be saved by using the half-cell method.
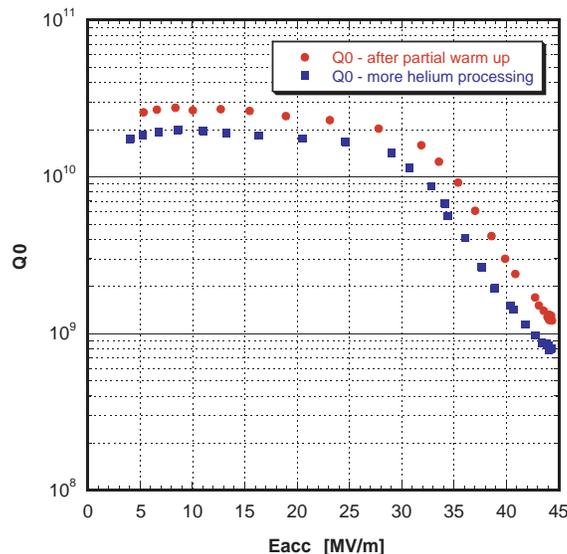
Figure 3: Dependence of the unloaded quality factor Q_0 on the accelerating gradient E_{acc} of the single-cell niobium cavity of reentrant geometry. Solid circle: after first helium processing and partial warm up. Solid square: after second helium processing.

3.11.7 Addition for ICFA Newsletter

Rapid progress has been made since the September 22-24, 2004 Pushing-Limit Workshop at ANL. A record gradient of 47 MV/m (pulsed) and 46 MV/m (CW) was achieved on November 16, 2004 by the first 1300 MHz reentrant cavity described in this report. The unloaded quality factor remained above 1×10^{10} at 1.9 K at the highest gradient with little field emission. These results were reported as a contributed oral presentation at the 2005 PAC held at Knoxville, TN, May 16-20, 2005.

In the meantime, another Cornell 1300 MHz reentrant cavity was sent to KEK for processing and evaluation. It reached 47 MV/m also in July of 2005 and further reached a new record gradient of 51-52 MV/m in September of 2005. These new results, along with others, will be reported in a KEK contribution to the coming EPAC.

3.11.8 Acknowledgments

We want to thank Joe Kirchgessner for consultation about the fabrication of the first reentrant cavity. Curtis Crawford demonstrated the first successful electropolish of a single-cell cavity with a vertical set-up, which was adapted to perform electropolish of the single-cell reentrant cavity. This work is supported by the National Science Foundation.

3.11.9 References

1. K. Saito, Proceedings of the 2003 Particle Accelerator Conference, Portland, OR, USA, 2003, p.462.
2. P. Kneisel et al., Proceedings of the Seventh Workshop on RF Superconductivity, Gif sur Yvette, France, B. Bonin (Ed.), 1995, p.449.
3. H. Padamsee, J. Knobloch, T. Hays, *RF Superconductivity for Accelerators*, John Wiley & Sons, Inc., 1998.
4. K. Saito, Private communication.
5. V. Shemelin, H. Padamsee, R.L. Geng, Nucl. Instrum. Methods A, **496** (2003) 1-7.
6. J. Graber et al., Nucl. Instrum. Methods. in Phys. Res. A, **350** (1994) 572-581.
7. J.R. Delayen, K.W. Shepard, Appl. Phys. Lett., **57** (1990) 514.
8. D. Moffat et al., Proceedings of the 4th Workshop on RF Superconductivity, KEK, Tsukuba, Japan, Y. Kojima (Ed.), 1990, p.445.
9. R.L. Geng et al., "Continuous current oscillation electropolishing and applications to half-cells," Proceedings of the 11th Workshop on RF Superconductivity, Lübeck-Travemünde, Germany, 2003 (http://srf2003.desy.de/).

4   Activity Reports

5   Workshop and Conference Reports

5.1   ICFA 38th Advanced Beam Dynamics and 9th Advanced & Novel Accelerators Joint Workshop on "Laser-Beam Interactions and Laser and Plasma Accelerators" —
4th LBI Workshop and 7th LPA Workshop jointly held in celebrating the United Nations International Year of Physics

W-Y. Pauchy Hwang
Department of Physics, National Taiwan University, Taipei, Taiwan
mail to: wyhwang@phys.ntu.edu.tw

Shin-ichi Kurokawa
Accelerator Laboratory, KEK, Tsukuba, Ibaraki, Japan
mail to: shin-ichi.kurokawa@kek.jp

5.1.1   Introduction

Until now the Laser-Beam Interactions Workshop (LBI) and Laser Plasma Accelerators Workshop (LPA) have been held independently. This time, we decided that the Fourth LBI and the Seventh LPA Workshops would be jointly held as the ICFA Workshop on Laser-Beam Interactions and Laser Plasma Accelerators for Celebrating the United Nations International Year of Physics. The workshop was held at the National Taiwan University in Taipei, Taiwan from December 12-16, 2005.

Recent advancements on ultra-intense and relativistic lasers and particle accelerators have inspired a broad range of applications to science and technology. On the technology side, one exciting development has been the laser and plasma based novel accelerators, with the promise of extending the energy of high energy accelerators far beyond what the conventional technology can provide. On the science side, the tremendous energy density provided by state-of-the-art laser and particle beams opens an exciting new window of opportunity for the investigations of frontier fundamental physics ranging from particle physics, nuclear physics, and condensed matter physics, to astrophysics.

This joint workshop focused on recent developments of the fundamental physics as well as the advanced accelerator technology based on ultra intense laser and particle beams. Inspired by the centenary celebration of Albert Einstein's magic year of 1905, new visions, novel concepts, and future prospects were emphasized in this meeting.

5.1.2   Committees

5.1.2.1   *International Advisory Committee*

F. Amiranoff (LULI, France)	W. Namkung (POSTECH, Korea)
I. Ben-Zvi (BNL, USA)	A. Noda (Kyoto U., Japan)
R. Bingham (RAL, UK)	P. P. Pashinin (IGP, Russia)
J. Chen (Peking U., China)	F. Pegoraro (Pisa, Italy)

P. Chen (SLAC, USA)
C. Joshi (UCLA, USA)
I..-S. Ko (PAL, Korea)
W. Leemans (LBNL, USA)
K. S. Liang (NSRRC, Taiwan)
C. S. Liu (NCU, Taiwan)
T. Mendonca (U. Lisbon, Portugal)
H. O. Moser (SSLS, Singapore)
G. Mourou (LOA, France)

M. Roth (Darmstadt, Germany)
F. Ruggiero (CERN, Switzerland)
V. C. Sahni (CAT, India)
P. Sprangle (NRL, USA)
T. Tajima (JAERI, Japan)
H. Takabe (Osaka, U., Japan)
M. Uesaka (U. Tokyo, Japan)
J. M. Vehn (MPI-G, Germany)
J. Zhang (IOP, China)

5.1.2.2 *International Program Committee*

S. Bulanov (IGP, Russia)
D. Giulietti (Pisa, Italy)
T. Hirose (Waseda U., Japan)
Y.-K. Ho (Fudan U., China)
Y. Hsiung (NTU, Taiwan)
Y.-C. Huang (NTHU, Taiwan)
W-Y. P. Hwang (NTU, Taiwan) Co-Chair
T. Katsouleas (USC, USA)
Y. Kitagawa (Osaka U., Japan)
S. Krishnagopal (CAT, India)
G. R. Kumar (TIFR. India)

S. Kurokawa (KEK, Japan) Co-Chair
M. Lontano (CNR, Italy)
V. Malka (LOA, France)
K. Nakajima (KEK, Japan)
J. S.-T. Ng (SLAC, USA)
P. Norreys (RAL, UK)
L. Schachter (IIT, Israel)
L. Silva (IST, Portugal)
H. Suk (KERI, Korea)
Y. Takahashi (UAH, USA)
A. Ting (NRL, USA)

5.1.2.3 *Local Organizing Committee*

P.-T. Chang (NTU, Taiwan)
S. Y. Chen (AS, Taiwan)
T. Chiueh (NTU, Taiwan)
Y. Hsiung (NTU, Taiwan)
K.-T. Hsu (NSRRC, Taiwan)
Y.-C. Huang (NTHU, Taiwan)

W-Y. P. Hwang (NTU, Taiwan) Co-Chair
S. Kurokawa (KEK, Japan) Co-Chair
K. Nakajima (KEK, Japan)
J. Wang (AS, Taiwan)
M. Z. Wang (NTU, Taiwan)
J.H.P. Wu (NTU, Taiwan)

5.1.3 Sponsorship

National Taiwan University
High Energy Accelerator Research Organization
National Science Council
Ministry of Education
National Synchrotron Radiation Research Center
International Committee for Future Accelerators
Asian Committee for Future Accelerators
Asia Pacific Center for Theoretical Physics
Electron Linear Accelerator Network

5.1.4 Conference Topics

The workshop addressed the most recent results and prospects on the following topics:

- Physics and applications of laser-beam and plasma interactions, including the generation of energetic particles, high-energy Gamma rays, short-pulse X-rays and Tera Herz radiations
- Laser applications for beam and plasma diagnoses, and beam cooling and handling
- Laser and plasma particle acceleration concepts and experiments including computer modeling of experiments
- Mono-energetic high quality particle beam generation in laser-plasma accelerators: mechanism, control and applications
- Over-GeV laser-plasma accelerator technology
- Extreme high-energy accelerator and collider concepts
- High energy density beam-plasma physics including Laboratory astrophysics
- High energy density astrophysics including ultrahigh energy cosmic ray acceleration, Gamma ray burst and Cosmic jet
- Fundamental physics related to laser and particle beams

5.1.5 Scientific Program

The workshop was programmed in the plenary sessions and the parallel working sessions. They were consisting of three groups:
- High quality electron beam generation and acceleration.
- X-ray, gamma-ray and Terahertz radiations and their applications.
- Proton/Ion/Positron generation and acceleration; Fundamental physics and Laboratory astrophysics.

6 Recent Doctorial Theses

6.1 Nonlinear Dynamics Study Including Vacuum Chamber

M. Attal

SESAME, C/O UNESCO Amman Office, Amman, Jordan

mail to: m.attal@unesco.org.jo

6.1.1 Introduction

In a storage ring the evaluation of the dynamic aperture taking into account the vacuum chamber limitation is more accurate and displays nonlinearity that could not be seen without vacuum chamber. As an example we present the dynamic aperture evaluations for SESAME during the optimization process of the bending magnet high order multipoles. The work has been carried out on SESAME optics 1 [1, 2] with β-tunes (Q_x=7.23, Q_z=5.19). The results have been crosschecked with two codes, BETA and TRACY, which gave similar results.

6.1.2   Vacuum Chamber Limitation

All the dynamic apertures are evaluated for chromaticity corrected to zero value in both planes with only 2 families of sextupoles. The on-momentum dynamic apertures, with and without chamber limitation, are shown in Fig. 1.
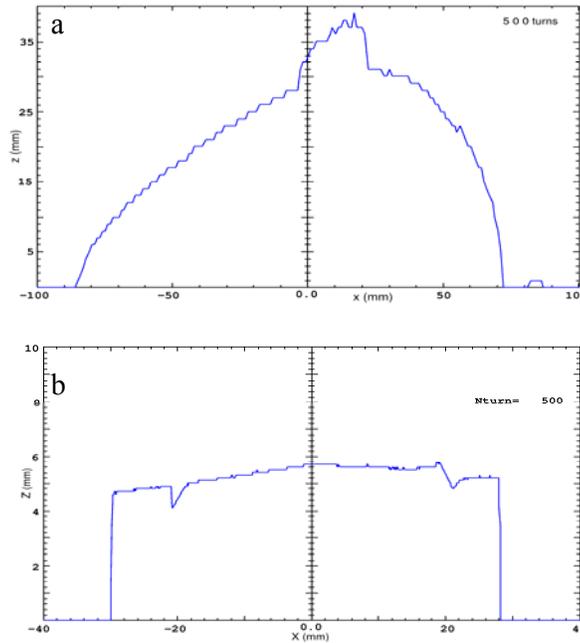
Figure 1: SESAME dynamic aperture without (a) and with (b) vacuum chamber.

The dynamic apertures are plotted in the middle of the *Long straight* ($\beta_x = 12.31$m and $\beta_z = 3.13$m, while $\beta_{xmax} = 12.807$m and $\beta_{zmax} = 21.35$m), and are obtained by tracking particles for 500 turns. The vacuum chamber apertures are $\Delta x = \pm 35$mm and $\Delta z = \pm 15$mm, while in the injection straight the horizontal aperture is limited, due to the thin septum position, to -30mm and + 35mm.

Figure 1b shows that the chamber-limited dynamic aperture is degrading at high vertical amplitudes especially in the left side and, moreover, has two clear vertical cuts at x = ~ ± 21mm. This is an indication of nonlinear motion that increases the particle oscillation amplitude until it gets lost on the chamber wall. This lost particle is considered stable by the tracking code in case of no chamber limitation due to the large oscillation space offered to it and so the nonlinearity could not be seen in Fig. 1.a.

This is proved by Fig. 2 which shows the vertical oscillation amplitudes versus x at vertical constant position z = 4.8mm. This graph has been obtained by tracking the particle from x = -30mm to 30mm in steps of 0.5mm at the above mentioned vertical amplitude. Then the vertical oscillation amplitude is drawn versus number of turns that was converted to x positions. The gradually increasing amplitude in the left half of the graph, explains the left hand side degradation, while the two drastic amplitude increases stand behind the two cuts.
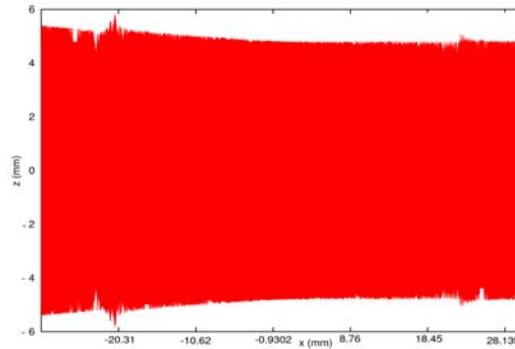
Figure 2: Vertical oscillations versus x at z = 4.8mm.

The nonlinearity seems to be not critically harmful and we can live with it since its destructive effect is at high vertical amplitudes. But its impact could be stronger due to some of the expected aberrations.

6.1.2.1   *Systematic High-Order Multipoles*

The pole profile of SESAME dipole has been optimized [3] by choosing the high order multipole configuration of smallest dynamic impact. The effect of the obtained multipole configuration on the on-momentum dynamic aperture, with and without vacuum chamber, is shown in Figure 3. Fig. 3a indicates that the dynamic aperture is still enough larger than the physical one (i.e. the chamber dimensions) and so the high order multipoles are tolerable, while Fig. 3b shows that the bending contents amplify the two cuts, seen in Fig. 1b, to a level that cannot be tolerated. Figure 4 shows the nonlinear vertical excursion of the particle due to the multipole effect.
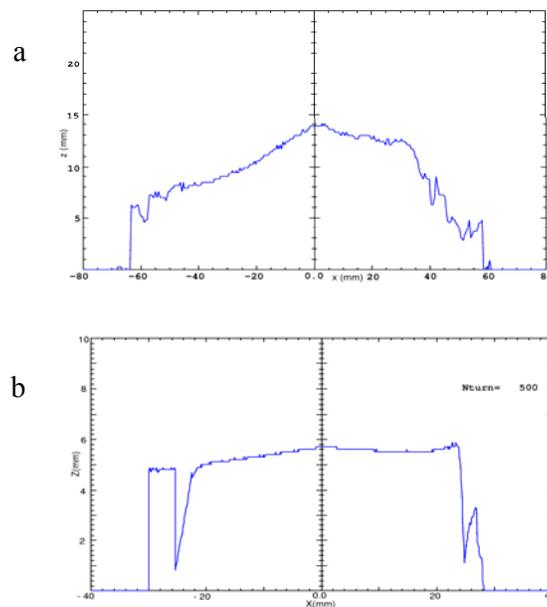
Figure 3: Dynamic aperture without (a) and with (b) vacuum chamber.
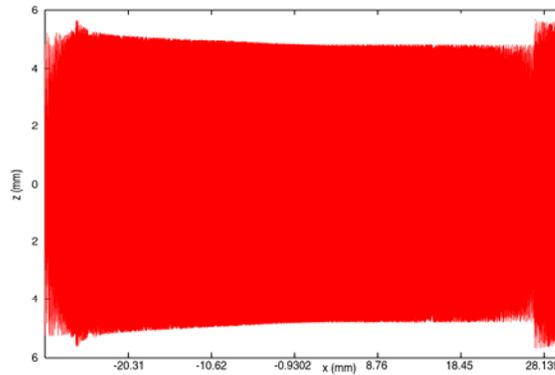
Figure 4: The multipole effect on the vertical oscillation amplitude at z = 4.8mm.

Eliminating these cuts by the sextupoles was not efficient. The change of the fractional part of the tune was a successful cure to solve the problem. Figure 5 shows the dynamic aperture after changing the tunes from ($Q_x = 7.23$, $Q_z = 5.19$) to ($Q_x = 7.21$, $Q_z = 5.185$).

As an explanation to what happened; the nonlinearity was a result of near systematic resonance effect, most probably the 5th order one that becomes stronger at higher oscillation amplitude for the particle. By changing the tune we put the working point on the 5th order resonance, which lose its power because the particle crosses it at zero amplitudes and moves away from it at higher amplitudes. Further studies on nonlinear dynamics are in progress with the Frequency Map Analysis.
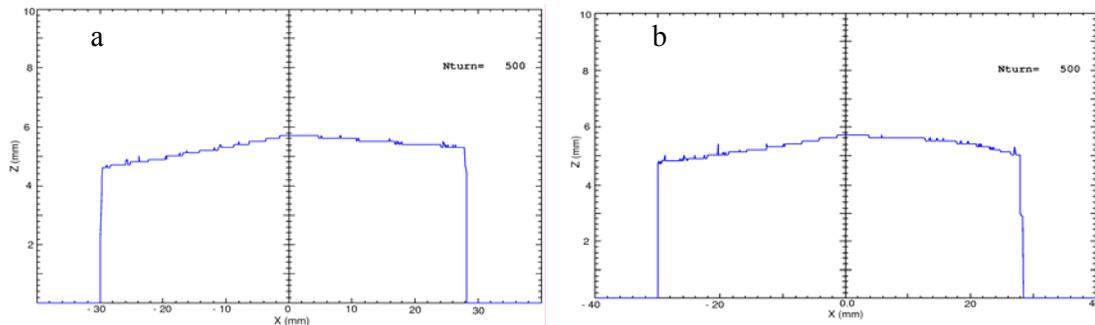
Figure 5: The dynamic aperture of modified tunes with vacuum chamber without (a) and with (b) bending higher order multipoles.

6.1.3 Conclusion

The dynamic aperture evaluation with the vacuum chamber limitations had the advantage of revealing a nonlinear region that was not seen in the case of standard dynamic aperture calculations. The tune modification enhanced the nonlinear dynamics and reduced its sensitivity to the field error effect. This result suggests also that it is more realistic to consider the chamber-limited dynamic aperture in the lifetime calculations.

6.1.4   References

1.   G. Vignola, M. Attal – SESAME Technical Note **O-1** – Dec. 2004.
2.   G. Vignola et al. - SESAME in Jordan, PAC 2005 Proceedings.
3.   S. Varnasseri – SESAME Technical Note **M-1** – Aug. 2005.

7   Forthcoming Beam Dynamics Events

7.1   The 37th Advanced Beam Dynamics Workshop: Future Light Sources

7.1.1   General Information

This is the second announcement for the ICFA workshop on Future Light Sources. The workshop will bring together experts working on the development and design of the various types of accelerator based light sources. Plenary talks will cover the scientific challenges in synchrotron radiation research and selected accelerator physics issues. Special topics will be discussed in dedicated working groups. For further information please see the attached program or visit http://fls2006.desy.de/.

We invite you to register for this workshop and are looking forward to welcome you in Hamburg.

7.1.2   Registration

Online registration is open: http://fls2006.desy.de/registration/index_eng.html. The deadline for early registration is 31 March 2006. Upon registration you will be asked to give your preferences for two working groups. Note that the invited speaker's registration is for invited plenary speakers only (see program).

7.1.3   Working Groups

Two days are devoted to working groups:
WG1:   Storage ring based synchrotron radiation sources
        Chair: K. Harkay (harkay@aps.anl.gov), A. Ropert (annick@esrf.fr)
WG2:   Energy Recovery Linac based synchrotron radiation sources
        Chair: G. Hoffstätter (hoff@mail.lepp.cornell.edu), S. Smith
        (S.L.Smith@dl.ac.uk)
WG3:   Free Electron Lasers
        Chair: Z. Huang (zrh@SLAC.Stanford.EDU), L. Serafini
        (luca.serafini@mi.infn.it)
WG4:   Low emittance electron guns
        Chair: W. Graves (wsgraves@mit.edu), M. Krasilnikov
        (mikhail.krasilnikov@desy.de), F. Stephan (frank.stephan@desy.de)

WG5:   Beam diagnostics and stability
        Chair: J. Byrd (JMByrd@lbl.gov), D. Nölle (dirk.noelle@desy.de)
WG6:   Insertion devices / New radiation source types (depending on participation)

Depending on participation working groups will run either one or two days. Please submit abstracts for oral presentations for the working group(s) of your interest as soon as possible to ensure efficient organization of the working groups. The deadline for abstract submission is 23 April 2006.

7.1.4   Poster Session

There will be a poster session to present new synchrotron radiation source projects in the planning or construction phase, as well as upgrade plans for existing facilities. Posters will be on display for the whole week and should be attended during two time slots (see program) to allow for questions and discussions.

A poster can have a maximum size of 841 mm $\times$ 1189 mm (33.1 in $\times$ 46.8 in, Din A0). Because of space limitations only one poster per project can be presented. Please submit abstracts for the poster session before 23 April 2006.

7.1.5   Publications

The workshop contributions will be published within the JACoW system. (http://www.jacow.org/) Papers should be in accordance to JACoW formatting rules as defined on the web page.

Plenary talk papers will have no page limit. Abstract submission is required until 23 April 2006, while the paper shall be uploaded until 19 May 2006.

The abstract submission deadline for working group presentations is 23 April 2006. Short term working group contributions during the workshop are welcome. For publication these contributions require a minimum of additional information: title, author, affiliation and a short abstract. The scientific secretaries of the working groups will assist authors in uploading this information.

Working group presentations can be accompanied with a three page paper. Such a paper should be uploaded by 19 May 2006 (the deadline for short term contributions is 1 July 2006).

In all cases presentations should be either uploaded prior to the workshop or handed to the scientific secretary before presentation. PowerPoint, Word, PDF or PS format will be accepted and converted into PDF format for presentation.

7.1.6   Summary of Presentation and Publication Options and Dates

		Plenary Talk	Working Group Announced	Working Group Short Term	Summary Talk	Project Poster
	Format	**Deadline**				
Abstract	JACOW	23 April 2006		19 May 2006		23 April 2006
Paper	Word, LaTeX	19 May 2006		1 July 2006		19 May 2006
Presen-tation	ppt, Word, pdf, ps Poster: 841 mm × 1189 mm (33.1 in × 46.8 in)	15 May 2006-19 May 2006			19 May 2006	15 May 2006 – 19 May 2006

7.2   The 39th ICFA Advanced Beam Dynamics Workshop: High Intensity High Brightness Hadron Beams—HB2006

7.2.1   General Information

The 39th ICFA Advanced Beam Dynamics Workshop, **"High Intensity High Brightness Hadron Beams, HB2006",** will be held at the EPOCHAL International Congress Center in Tsukuba City, Japan, near KEK on May 29-June 2, 2006. This Workshop is co-sponsored by KEK and JAEA (previously JAERI).

The themes of this workshop follow closely those of the previously held two workshops in the same series: ICFA-HB2002 (April 8-12, 2002 at Fermilab, USA) and ICFA-HB2004 (October 18-22, 2004, in Bensheim, Germany), which cover a wide range of issues associated with high intensity hadron beams. This time, however, since the commissioning of SNS will be already started by the time of the workshop and the construction of J-PARC linac will be nearly completed, more emphasis on J-PARC and SNS will be made as on-going major projects of the hadron machines.

The first and the last days are devoted to the plenary sessions for opening, reviews and working group summaries. The middle three days are dedicated to the working activities. Parallel invited sessions will be held in the morning for each topic and will be moved to the working sessions for the same topic in the afternoon. The working sessions will contain organized discussions as well as contributed papers, which will be selected from submitted abstracts by the session conveners. We encourage submission of contributed oral talks to be presented in the working sessions. Workshop proceedings containing all invited and contributed papers will be published on the JACoW web site, as well as its hard-copies and CDs will be published from KEK.

Details of the HB2006 Workshop appear on the web at http://hb2006.kek.jp/.

Please direct all the inquiries concerning this workshop to the e-mail address of the workshop secretariat; hb2006@kek.jp Your e-mail will be forwarded to the most appropriate personnel for your inquiry.

7.2.2 Scientific Program and Workshop Schedule

The first and the last days are devoted to the plenary sessions for opening, reviews and working group summaries. The middle three days are dedicated to the working activities. Two or three topics are picked up per day as the working subjects and a room will be allocated to each topic. Parallel invited sessions for those topics will be held in the morning and will be moved to the working sessions for the same topic in the afternoon. The working sessions will contain organized discussions as well as contributed papers, which will be selected from submitted abstracts by the session conveners. The J-PARC tour is planned in the afternoon of the last day. The Banquet will be held on Wednesday evening.

	Monday	Tuesday	Wednesday	Thursday	Friday
AM	Plenary	Invited Parallel	Invited Parallel	Invited Parallel	Plenary
PM	Plenary	Work Session	Work Session	Work Session	Tour

The subjects of the working groups and the session conveners are as follows:
A. Beam Instabilities and their cures
   Conveners: A. Burov (FNAL), F. Zimmermann (CERN).
B. Space-charge theory, simulations, and experiments
   Conveners: S. Cousineau (ORNL), I. Hofmann (GSI).
C. Beam diagnostics, collimation, injection/extraction and targetry
   Conveners: N. Mokhov (FNAL), M. Tomizawa (KEK), K. Wittenburg (DESY).
D. Beam cooling and intra-beam scattering
   Conveners: A. Fedotov (BNL), I. Meshkov (Dubna), J. Wei (BNL).
E. High intensity linacs / Proton drivers
   Conveners: W. Foster (FNAL), R. Garoby (CERN), B. Weng (BNL).
F. FFAG and other advanced accelerators and techniques
   Conveners: W. Chou (FNAL), S. Koscielniak (TRIUMF), Y. Mori (Kyoto Univ.).
G. Commissioning strategies and procedures
   Conveners: K. Hasegawa (JAEA), S. Henderson (ORNL), R. Schmidt (CERN).

7.2.3 Tentative List of Invited Talks in Plenary Session (Monday)

- Approach to a very high intensity beam at J-PARC by Y. Yamazaki (JAEA)
- Recent commissioning results of SNS by S. Henderson (ORNL)
- Review of progress in FFAG accelerators by Y. Mori (Kyoto Univ.)
- Comparison or survey of proton accelerators for high power applications by B. Weng (BNL)
- ISIS upgrade by D. Findlay (RAL)
- FAIR at GSI by a speaker to be decided
- Status and outlook of high intensity accelerator projects in China by J. Wei (BNL)
- BNL upgrade by W. Fischer (BNL)
- Beam intensity upgrade at Fermilab by Alberto Marchionni (FNAL) (to be confirmed)
- LHC status by R. Schmidt (CERN)

- CARE-HHH activities by F. Zimmermann (CERN)

The selection of invited talks for parallel sessions is now underway. The tentative list for the parallel invited talks will be published in the HB2006 web site (http://hb2006.kek.jp/) shortly.

7.2.4 Submission of Abstracts for Contributed Papers

We encourage submission of contributed oral talks to be presented in the working sessions. Due to time limitations in the working sessions, the acceptance of contributed oral papers is subject to approval by the session conveners. The authors selected for presentation of contributed papers will be notified as soon as possible. The abstracts are currently accepted on the HB2006 website (http://hb2006.kek.jp/). Further details can be found in the "Abstract Submission" page. The deadline for the abstract submission for contributed papers is March 17, 2006.

7.2.5 Workshop Proceedings

The ICFA Advanced Beam Dynamics Workshop series joined the JACoW in July 2005. Workshop proceedings containing all invited and contributed papers will be available on the JACoW web site, as well as its hard-copies and CDs will be published from KEK. Authors are requested to submit the paper in Postscript format (and other original files following the JACoW standard) and its camera-ready copy at the conference. Details for paper submission will be published on our website in due time.

7.2.6 Technical Tour

J-PARC site tour will be conducted on Friday afternoon. J-PARC site locates in a coastal village of Tokai, which is one hour drive from Tsukuba city. Bus transportation will be available between J-PARC site and the workshop site. As the J-PARC facility locates in a JAEA site, the participants are requested to provide information required to fill out their "visit proposal" for JAEA. Details will appear on our web site in due time.

7.2.7 Registration Fee

30,000 Yen (about 270 USD) for early registration
35,000 Yen (about 320 USD) for late registration

The banquet will be subsidized by companies and a local government. All the participants for the ICFA-HB2006 workshop are requested to make registration through our web site (http://hb2006.kek.jp/) before May 26, 2006. Online payment with a credit card is available on the website until May 12, 2006, after which only cash upon workshop will be accepted. Further details can be found in the "Registration" page on our website.

7.2.8 Workshop Site

The ICFA-HB2006 workshop is held at EPOCHAL international congress center (http://www.epochal.or.jp/english/index.html) in Tsukuba-city, Japan near KEK. The workshop site is a few minute walk from Tsukuba Center, where a bus center and a new

train station are located. The plenary sessions will be held at "Hall 200", and parallel and working sessions at "Meeting room 201" and "Meeting room 202". All the hall and meeting rooms is on the 2nd floor of the congress center.

7.2.9 Workshop Hotel

We have booked a number of rooms at two workshop hotels, "Okura Frontier Hotel Tsukuba Epochal" and "Okura Frontier Hotel Tsukuba". Their website is

http://www.okura-tsukuba.co.jp/english/index.html

The former locates just next to the workshop site, and the latter locates at the Tsukuba center which is a few minute walk from the workshop site. The secured number of rooms and their room types are listed in the "Accommodation" page on our website. All prices are for room rates per night including tax and service charge, but no breakfast. The internet access (wired LAN) is available from each room for free of charge. Please make your reservation through the reservation form on the hotel web site. Further details on the workshop discount rates and reservation procedure can be found in the "Accommodation" page on our website.

7.2.10 Social Events

- Welcome Reception on Monday Evening
  A welcome reception will be offered at the workshop site starting at 18:00. All the attendances and the accompanying persons are welcome.
- Banquet on Wednesday Evening
  The banquet on Wednesday evening will be a traditional Japanese feast at a nearby Japanese restaurant, Tsukuba Sansuitei, starting at 19:00. A shuttle bus service will be available between the workshop site and the restaurant. The banquet will be subsidized by companies and a local government.

7.2.11 Travel Information

Tsukuba is a suburban city of the Tokyo Metropolitan area locating 50 km northeast of downtown Tokyo, and 40 km northwest of Narita International Airport. We have an Airport Bus service between Tsukuba and Narita International Airport. We also have a new train service which connects Tsukuba to Akihabara in 45 minutes. The train, called "Tsukuba Express", started running in August, 2005, which greatly improved the transportation between Tsukuba and Tokyo. Both the workshop site and the workshop hotels locate in the walking distance from "Tsukuba Center", where the bus terminal and the new train station are locating. Details are available on our website.

7.2.12 Important Dates

March 17, 2006: Deadline of the submission of abstracts for contributed papers
Late March, 2006: Commencement of the paper submission
April 28, 2006: Deadline of the early registration
May 12, 2006: Deadline of the online payment of the registration fee

May 26, 2006: Deadline of the online registration

May 29 - June 2, 2006: HB2006 Workshop in Tsukuba

June 2, 2006: Deadline of the submission of papers for the invited and contributed oral papers

7.2.13 Members of the International Advisory Committee

Caterina Biscari (INFN)	Hitoshi Kobayashi (KEK)
Swapan Chattopadhyay (JLab)	Alessandra Lombardi (CERN)
Yanglai Cho (ANL)	Yoshiharu Mori (Kyoto U.)
Weiren Chou (FNAL)	Stephen Myers (CERN)
Jie Gao (IHEP)	Chris Prior (RAL)
David Gurd (ORNL)	Robert Ryne (LBL)
Ingo Hofmann (GSI)	Yuri Shatunov (BINP)
Stephen Holmes (FNAL)	Rainer Wanzenberg (DESY)
Roderich Keller (LANL)	Jie Wei (BNL)
In Soo Ko (PAL)	Yoshishige Yamazaki (JAEA)

7.2.14 Members of the Program Committee

Rick Baatman (TRIUMF)	Trevor Linnecar (CERN)
John Barnard (LLNL)	Robert Macek (LANL)
Oliver Boine-Frankenheim (GSI)	John Maidment (DESY)
Romuald Duperrier (CEA)	Nikolai Mokhov (FNAL)
Alexei Fedotov (BNL)	Akira Noda (Kyoto U.)
William Foster (FNAL)	Peter Ostroumov (ANL)
John Galambos (ORNL)	Deepak Raparia (BNL)
Roland Garoby (CERN)	Lenny Rivkin (PSI)
Stuart Henderson (ORNL)	Thomas Roser (BNL)
Norbert Holtkamp (ORNL)	Francesco Ruggiero (CERN)
Hideaki Hotchi (JAEA)	Ken Takayama (KEK)
Susumu Igarashi (KEK)	Masahito Tomizawa (KEK)
Ioanis Kourbanis (FNAL)	Bill Weng (BNL)
Jean-Michel Lagniel (CEA)	Frank Zimmermann (CERN)

7.2.15 Present Members of the Local Organizing Committee

Yong Ho Chin (yongho.chin@kek.jp): Co-chair

Hiroshi Yoshikawa (hiroshi.yoshikawa@j-parc.jp): Co-chair

Masanori Ikegami (masanori.ikegami@kek.jp): Vice-chair

Kazuo Hasegawa (hasegawa.kazuo@jaea.go.jp)

Hiroyuki Sako (sako.hiroyuki@jaea.go.jp): Electronic publication of proceedings

Rumiko Enjoji (rumiko.enjoji@kek.jp): Secretary

7.3   RuPAC 2006

7.3.1   Announcement

The XX Russian Accelerator Conference (RuPAC2006) will take place in Novosibirsk, Russia, September 10-14, 2006. The conference will be organized by
   • Budker Institute of Nuclear Physics
   • Russian Academy of Science
   • Federal Agency of Atomic Energy of the Russian Federation
   • Federal Agency of Science and Innovations of the Russian Federation
The format of the conference will be as usual: invited plenary talks, short oral contribution and poster section. The Conference provides a forum for exchange of new information and discussion in the area of acceleration science and engineering, particle beam physics, new accelerator designs, modernization of existing facilities, accelerator use for scientific purposes and applications.

7.3.2   Conference Topics

1. Modern trends in accelerator development.
2. Beam dynamics in accelerators and storage rings, cooling methods, new methods of acceleration.
3. High intensity cyclic and linear accelerators.
4. Heavy ions accelerators.
5. Synchrotron radiation sources and free-electron lasers.
6. Magnetic systems, power supply and vacuum systems for accelerators.
7. Superconducting accelerators and technology of cryogenics.
8. Accelerating structures and powerful electronics.
9. Control and diagnostic systems.
10. Ion sources, electron guns.
11. Accelerators for medical and industrial purposes.
12. Radiation problems in accelerators.

7.3.3   Regulations

Conference program will consist of review reports (40 min), oral presentations (20 min) and poster reports (poster size will be specified in the next circular). The working languages of the Conference are Russian and English. To include the report in the Conference program authors have to present an Abstract in English before April 15, 2006. The Program Committee will inform the authors about report reception and presentation method after the 1st of June 2006.

7.3.4   Proceedings

Report titles, abstracts and author list will be placed on the Conference web-site http://rupac2006.inp.nsk.su. The Book of Abstracts will not be published. The proceedings will be published in English in an electronic version on the web-site of Joint Accelerator Conferences Website (JACoW) http://www.jacow.org. Conference

participants will receive copies of the Book of Abstracts on CD-disks. The reports in English should be submitted to the Organizing Committee not later than on the first day of the Conference as a hard copy and an electronic version on a diskette 3.5" or CD-ROM. The on-line uploading through the Conference site is considered also. The pdf version of report should not exceed 300 kb. The electronic report copies have to be submitted in accordance with JACoW rules: http://www.jacow.org

7.3.5 Preliminary Registration

All participants of the Conference have to perform the procedure of preliminary registration on the Conference filling the accompanying Application form and sending it to the electron address rupac2006@inp.nsk.su or in on-line regime on the Conference web-site http://rupac2006.inp.nsk.su The registration in on-line regime is preferable. All participants of the Conference also have to perform the procedure of preliminary registration on the web-site of JACoW http://www.jacow.org/jacow/repository.html

7.3.6 Registration Fee

Registration Fee for foreign participants is 450 USD (preliminary) and covers Organizing Committee expenses, Conference Proceedings on CD-disk, participant bag, coffee/tea breaks, social program, welcome party, banquet and transportation from the airport or railway and back. It is planned to fix a special registration fee for participants from Russia taking into account the support of Russian Ministries (1000-1500 RUR preliminary).

7.3.7 Deadlines

March 30, 2006   Deadline for 2nd announcement
April 15, 2006   Deadline for sending of application forms and abstracts
June 1, 2006   the Organizing Committee informs participants about receiving and
                  the method of the report representation
June 15, 2006   Deadline for sending the information to the Organizing Committee
                  for visas execution.

7.3.8 Contact Persons

Vice-Chairman: Mr. Eugeny Levichev
                BINP SB RAS, Lavrentieva prosp. 11,
                Novosibirsk, Novosibirsk region, 630090
                RUSSIA
                Phone: 7 383 339 42 89
                Fax: 7 383 330 71 63
                e-mail: E.B.Levichev@inp.nsk.su
Scientific   Mr. Michael Petrichenkov
secretary   BINP SB RAS, Lavrentieva prosp. 11,
                Novosibirsk, Novosibirsk region, 630090
                RUSSIA
                e-mail: rupac2006@inp.nsk.su

Phone.: 7 383 339 46 34
Fax.: 7 383 330 71 63
Secretary   Mrs. Tatiana Rybitskaya
BINP SB RAS, Lavrentieva prosp. 11,
Novosibirsk, Novosibirsk region, 630090
RUSSIA
e-mail: tanij-r@mail.ru
Phone.: 7 383 339 54 35
Fax.: 7 383 330 71 63

8   Announcements of the Beam Dynamics Panel

8.1   ICFA Beam Dynamics Newsletter

8.1.1   Aim of the Newsletter

The ICFA Beam Dynamics Newsletter is intended as a channel for describing unsolved problems and highlighting important ongoing works, and not as a substitute for journal articles and conference proceedings that usually describe completed work. It is published by the ICFA Beam Dynamics Panel, one of whose missions is to encourage international collaboration in beam dynamics.

Normally it is published every April, August and December. The deadlines are 15 March, 15 July and 15 November, respectively.

8.1.2   Categories of Articles

The categories of articles in the newsletter are the following:

1. Announcements from the panel.

2. Reports of beam dynamics activity of a group.

3. Reports on workshops, meetings and other events related to beam dynamics.

4. Announcements of future beam dynamics-related international workshops and meetings.

5. Those who want to use newsletter to announce their workshops are welcome to do so. Articles should typically fit within half a page and include descriptions of the subject, date, place, Web site and other contact information.

6. Review of beam dynamics problems: This is a place to bring attention to unsolved problems and should not be used to report completed work. Clear and short highlights on the problem are encouraged.

7. Letters to the editor: a forum open to everyone. Anybody can express his/her opinion on the beam dynamics and related activities, by sending it to one of the

editors. The editors reserve the right to reject contributions they judge to be inappropriate, although they have rarely had cause to do so.

8. Editorial.

The editors may request an article following a recommendation by panel members. However anyone who wishes to submit an article is strongly encouraged to contact any Beam Dynamics Panel member before starting to write.

8.1.3 How to Prepare a Manuscript

Before starting to write, authors should download the template in Microsoft Word format from the Beam Dynamics Panel web site:

http://www-bd.fnal.gov/icfabd/news.html

It will be much easier to guarantee acceptance of the article if the template is used and the instructions included in it are respected. The template and instructions are expected to evolve with time so please make sure always to use the latest versions.

The final Microsoft Word file should be sent to one of the editors, preferably the issue editor, by email.

The editors regret that LaTeX files can no longer be accepted: a majority of contributors now prefer Word and we simply do not have the resources to make the conversions that would be needed. Contributions received in LaTeX will now be returned to the authors for re-formatting.

In cases where an article is composed entirely of straightforward prose (no equations, figures, tables, special symbols, etc.) contributions received in the form of plain text files may be accepted at the discretion of the issue editor.

Each article should include the title, authors' names, affiliations and e-mail addresses.

8.1.4 Distribution

A complete archive of issues of this newsletter from 1988 to the latest issue is available at

http://icfa-usa.jlab.org/archive/newsletter.shtml

This is now intended as the primary method of distribution of the newsletter.

Readers are encouraged to sign-up for electronic mailing list to ensure that they will hear immediately when a new issue is published.

The Panel's Web site provides access to the Newsletters, information about future and past workshops, and other information useful to accelerator physicists. There are links to pages of information of local interest for each of the three ICFA areas.

Printed copies of the ICFA Beam Dynamics Newsletters are also distributed (generally some time after the Web edition appears) through the following distributors:

Weiren Chou	chou@fnal.gov	North and South Americas
Rainer Wanzenberg	rainer.wanzenberg@desy.de	Europe* and Africa

Susumu Kamada   Susumu.Kamada@kek.jp   Asia** and Pacific

* Including former Soviet Union.

** For Mainland China, Jiu-Qing Wang (wangjq@mail.ihep.ac.cn) takes care of the distribution with Ms. Su Ping, Secretariat of PASC, P.O. Box 918, Beijing 100039, China.

To keep costs down (remember that the Panel has no budget of its own) readers are encouraged to use the Web as much as possible. In particular, if you receive a paper copy that you no longer require, please inform the appropriate distributor.

8.1.5   Regular Correspondents

The Beam Dynamics Newsletter particularly encourages contributions from smaller institutions and countries where the accelerator physics community is small. Since it is impossible for the editors and panel members to survey all beam dynamics activity worldwide, we have some Regular Correspondents. They are expected to find interesting activities and appropriate persons to report them and/or report them by themselves. We hope that we will have a "compact and complete" list covering all over the world eventually. The present Regular Correspondents are as follows:

Liu Lin   liu@ns.lnls.br   LNLS Brazil

S. Krishnagopal   skrishna@cat.ernet.in   RRCAT India

Sameen Ahmed Khan   rohelakhan@yahoo.com   MECIT Middle East and Africa

We are calling for more volunteers as *Regular Correspondents*.

8.2 ICFA Beam Dynamics Panel Members

Caterina Biscari	caterina.biscari@lnf.infn.it	LNF-INFN, Via E. Fermi 40, C.P. 13, Frascati, Italy
Yunhai Cai	yunhai@slac.stanford.edu	SLAC, 2575 Sand Hill Road, MS 26 Menlo Park, CA 94025, U.S.A.
Swapan Chattopadhyay	swapan@jlab.org	Jefferson Lab, 12000 Jefferson Avenue, Newport News, VA 23606, U.S.A.
Weiren Chou (Chair)	chou@fnal.gov	Fermilab, MS 220, P.O. Box 500, Batavia, IL 60510, U.S.A.
Yoshihiro Funakoshi	yoshihiro.funakoshi@kek.jp	KEK, 1-1 Oho, Tsukuba-shi, Ibaraki-ken, 305-0801, Japan
Miguel Furman	mafurman@lbl.gov	Center for Beam Physics, LBL, Building 71, R0259, 1 Cyclotron Road, Berkeley, CA 94720-8211, U.S.A.
Jie Gao	gaoj@ihep.ac.cn.	Institute for High Energy Physics, P.O. Box 918, Beijing 100039, China
Ingo Hofmann	i.hofmann@gsi.de	High Current Beam Physics, GSI Darmstadt, Planckstr. 1, 64291 Darmstadt, Germany
Sergei Ivanov	ivanov_s@mx.ihep.su	Institute for High Energy Physics, Protvino, Moscow Region, 142281 Russia
Kwang-Je Kim	kwangje@aps.anl.gov	Argonne Nat'l Lab, Advanced Photon Source, 9700 S. Cass Avenue, Bldg 401/C4265, Argonne, IL 60439, U.S.A.
In Soo Ko	isko@postech.ac.kr	Pohang Accelerator Lab, San 31, Hyoja-Dong, Pohang 790-784, South Korea
Alessandra Lombardi	Alessandra.Lombardi@cern.ch	CERN, CH-1211, Geneva 23, Switzerland
Yoshiharu Mori	mori@kl.rri.kyoto-u.ac.jp	Research Reactor Inst., Kyoto Univ. Kumatori, Osaka, 590-0494, Japan
Chris Prior	c.r.prior@rl.ac.uk	ASTeC Intense Beams Group, Rutherford Appleton Lab, Chilton, Didcot, Oxon OX11 0QX, U.K.
David Rice	dhr1@cornell.edu	Cornell Univ., 271 Wilson Laboratory, Ithaca, NY 14853-8001, U.S.A.
Yuri Shatunov	Yu.M.Shatunov@inp.nsk.su	Acad. Lavrentiev, prospect 11, 630090 Novosibirsk, Russia
Junji Urakawa	junji.urakawa@kek.jp	KEK, 1-1 Oho, Tsukuba-shi, Ibaraki-ken, 305-0801, Japan
Jie Wei	wei1@bnl.gov	BNL, Bldg. 911, Upton, NY 11973- 5000, U.S.A.
Jiu-Qing Wang	wangjq@mail.ihep.ac.cn	Institute for High Energy Physics, P.O. Box 918, 9-1, Beijing 100039, China
Rainer Wanzenberg	Rainer.wanzenberg@desy.de	DESY, Notkestrasse 85, 22603 Hamburg, Germany

The views expressed in this newsletter do not necessarily coincide with those of the editors. The individual authors are responsible for their text.